Control of Finite-Dimensional Quantum Systems Under Lindblad Dissipation

by

Darragh Patrick Rooney

A dissertation submitted in partial fulfillment
of the requirements for the degree of
Doctor of Philosophy
(Applied and Interdisciplinary Mathematics)
in The University of Michigan
2012

Doctoral Committee:

Professor Anthony M. Bloch, Chair
Professor Chitra Rangan
Professor Charles R. Doering
Professor Peter D. Miller
Professor Joseph P. Conlon

ACKNOWLEDGEMENTS

I would like to express my deepest gratitude for the opportunity to come to Michigan and complete my doctorate here. Ann Arbor is such a wonderful town and the Mathematics Department at the University of Michigan has been fantastic to me. My time here has been life-changing, and I will look back on this period of my life with utmost fondness.

I owe a tremendous debt to my advisor, Anthony Bloch. He has been patient with me. His door has always been open. He has provided me support and given me advice and guidance. He has been flexible and allowed me the independence I need to survive. Thank you, Tony.

I also owe special thanks to Chitra Rangan, my co-advisor, without whom I would not have even thought to apply to Michigan. Switching from physics to applied mathematics has been a great experience. I am still able to study my favorite subject in the world, but I also get exposed to a lot of other cool fields. Without you, I likely would have left academia, so I owe my academic career to you most of all.

Additionally, I thank my committee members Charlie Doering, Peter Miller and Joe Conlon. I know you have busy schedules and I am grateful to have you read my work.

My growth in Ann Arbor has been far more than just academic and professional. The people I have met and the friends I have made here I will remember for a long time. Thank you to all of those who passed through my life in Ann Arbor and

influenced me.

Last, but not certainly not least, to my parents. You don't always understand what I do or why I do it, but you've always supported me and wanted me to find my own way, as strange as it may be. I owe more to you than anyone else.

TABLE OF CONTENTS

LIST OF FIGURES

Figure

CHAPTER I

Introduction

The maturation of quantum physics in recent decades has seen a shift from the passive description of quantum phenomena to the active viewpoint of manipulation and engineering. Two broad areas of study, both taking root in the eighties, played a key role in this shift. Firstly, the promise of quantum computation [35], originally imagined by Feynman [18], has prompted a wide search for means to implement a quantum computer. A quantum computer, consisting of qubits (two-level quantum systems) instead of ordinary zero-one bits, would allow the implementation of algorithms that would be impractical on a classical computer. Despite considerable effort, experimental progress towards this end has been slow. Secondly, the development of the laser has given us a powerful and precise tool to manipulate chemical systems, and this has suggested the potential for coherent control of molecular reactions (Tannor and Rice [57, 42] as well as Shapiro and Brumer [47, 48] provided the foundation). "Coherent control" here means the use of quantum interferences to favor certain pathways in chemical reactions by shaping the attributes of the laser beam. The development and success of mathematical control theory as applied to classical systems (for example, in robotics and aeronautics), suggests the parallel study of quantum control, in which one determines what is mathematically possible

to do to, and with, quantum systems.

Controlling quantum systems when they are exposed to an environment has proven to be a thorny problem. There are of course issues with how to model the interaction with the environment and what assumptions to use. Even after pinning down a model, however, the mathematics is generally much more challenging. In particular, the theory of closed systems relies heavily on the unitary group of evolution operators. The group structure is generally spoiled by exposing the system to the environment, and one is left with only a semi-group structure. This thesis considers a common model for open systems called the Lindblad equation and addresses the question of controllability under this model.

Before diving into original work, this introduction will discuss (1) basic notions of controllability, (2) the main results for control of closed quantum systems, (3) the dynamics of open quantum systems, particularly Lindbladian systems, and (4) an example of a physical quantum control system, the trapped ion.

1.1 Notions of controllability

There are four general questions that one can ask about controlling the evolution of dynamical systems:

1. Can we get there? (controllability)
2. How do we get there? (trajectory planning)
3. What is the best way to get there? (optimal control)
4. How do we stay there? (stabilization)

The first three questions fall under the study of open-loop control, in which no observation or measurement need be included in the control process. The fourth

question involves closed-loop control, as it requires a feedback mechanism. While very interesting questions arise in the study of closed-loop quantum control (because the measurement postulate, which is not even fully understood in epistemic terms, plays a fundamental role), this thesis does not consider research in this direction (see [32] and [8] for references).

Furthermore, the second question above is often subsumed as a particular optimal control question in the quantum setting. The payoff functional is often defined to be the overlap of the final state with a target state: $J = |\langle\psi_f|\psi_{target}\rangle|^2$. Trajectory planning is then reduced to the problem of attaining a payoff of one. A lot of work has gone into quantum optimal control: Peirce *et al.* [37] and Tannor *et al.* f[56] were seminal works. Zhu and Rabitz [61] laid out a numerical algorithm for control of closed systems. Rangan and Bucksbaum [41] and later Palao and Kosloff [36] connected optimal quantum control with quantum computation. Khaneja, Brockett and Glaser [23, 24] considered time optimal control in the context of spin systems. Carlini *et al.* studied the time optimal control of mixed systems under Lindblad dissipation, and Xu *et al.* [59] considered control under non-Markovian dissipation. Tannor, Sklarz, Bartana and Khaneja [55, 49] studied the laser cooling problem. Sugny and co-workers studied optimal control of pure systems in [53] and control of mixed systems in [52, 54].

While questions of optimality are important, this work deals primarily with the first question, namely whether attaining a target state from an initial state is even possible. Two notions of controllability will dominate the analysis: global controllability and small-time local controllability. First, we establish the general notion of a control system [17]:

Definition I.1. A *control system* is a quadruple $(\mathcal{M}, \mathrm{T}, \mathcal{U}, \Theta)$. $\mathcal{M}$ is the state space,

and is often a differentiable manifold. T is the time set − while discrete-time control systems exist, this work presumes that $\mathrm{T} = [0, \infty)$. $\mathcal{U}$ is the set of control functions, which map from T to some control set U. These functions will be assumed to be piecewise continuous. Finally, Θ is the transition function which maps the initial state to final states: $\Theta : \mathcal{M} \times \mathrm{T} \times \mathrm{T} \times \mathcal{U} \to \mathcal{M}$. That is, given an initial state, initial time, final time, and control function, Θ produces a final state. For continuous-time control systems, Θ is usually defined implicitly using a differential equation.

One can define an equivalence relation on $\mathcal{M}$: $m_1 \sim m_2$ if and only if there exists a control function $u_{12} \in \mathcal{U}$ that steers m_1 to m_2 in finite time, and a control function u_{21} that steers m_2 to m_1. By definition, this relation satisfies the symmetry property. It is reflexive since any state is steered to itself in zero time. It is transitive only if we assume the following closure property of $\mathcal{U}$: if $u_1(t), u_2(t) \in \mathcal{U}$, then, for any $0 \leq a \leq b$, $\theta(a-t)u_1(t)+\theta(b-t)u_2(t-b)$ is also in $\mathcal{U}$, where $\theta(t)$ is the step function. In this way, we can turn control functions off and on. If we assume this property, $\sim$ is an equivalence relation and partitions $\mathcal{M}$ into equivalence classes.

Definition I.2. A subset $\mathcal{M}'$ of $\mathcal{M}$ is *globally controllable* (GC) if it is a subset of such an equivalence class. $\mathcal{M}'$ is *maximally globally controllable* (MGC) if it is identical to an equivalence class.

While it is *a priori* possible to have many sets that are maximally globally controllable, in the systems we consider such a set is typically unique (neglecting singleton sets of course). Note that global controllability imposes no condition on the time to transition between states. The following stronger notion of controllability takes this into account:

Definition I.3. Let $R_t(m)$ be the set of states reachable from state m in time t or

less. A control system is small-time locally controllable (STLC) at a state m if and only if, for any $t > 0$, m is in the interior of $R_t(m)$.

Essentially, if one has STLC, one may reach nearby states in short times. If one has GC but not STLC, one may be able to reach nearby states but only using circuitous routes.

1.2 Control of closed systems

While much work has gone into developing the theory of quantum control, the large majority of progress has been with respect to closed quantum systems. Mathematically, these systems are cleaner because of the group structure that unitary dynamics provides. Thus, the seminal work of Jurdjevic and Sussmann [22], as well as Brockett [10, 11] on controllability of Lie groups can be applied, as introduced by Ramakrishna, Rabitz *et al.* [39]. The time-evolution operators for open systems, on the other hand, form only a semi-group. But before discussing the dynamics of open systems, we present a quick survey of the control of closed systems.

The state space of a closed quantum system is a complex projective Hilbert space $\mathcal{H}$. Throughout this work, we will assume this Hilbert space is finite-dimensional. Typically, we consider a state to be a vector in the non-projective space with norm one. To preserve norm, the evolution between two distinct times is described by a unitary operator $U(t_1, t_2)$

$$U(t_1, t_2) \left|\psi(t_1)\right\rangle = \left|\psi(t_2)\right\rangle$$

where the bra-ket notation defines $|\psi\rangle$ to be a vector and $\langle\psi|$ to be its algebraic dual. The differential version of this evolution is the Schrödinger equation:

$$\frac{d}{dt}\left|\psi(t)\right\rangle = -iH(t)\left|\psi(t)\right\rangle$$

where $H(t)$ is Hermitian and called the Hamiltonian operator, and $\frac{d}{dt}U(t,t_1) = -iH(t)U(t,t_1)$. In the control perspective, the control functions often appear as part of the Hamiltonian: $H(t,u(t)) = H_0 + \Sigma u_i(t)H_i$, and U is some subset of $\mathbb{R}^n$. Henceforth, the time dependence shall be suppressed and the Hamiltonian will be abbreviated $H(u)$.

The preceding formulation is known as the Schrödinger picture. An alternate formulation, known as the Heisenberg picture, considers states to be stationary and makes operators dynamical. In this picture, the unitary evolution operator, as well as the Hamiltonian, carry over, and the dynamical equations for an arbitrary operator $A(t)$ are

$$A(t_2) = U^\dagger(t_1,t_2)A(t_1)U(t_1,t_2)$$
$$\frac{d}{dt}A(t) = [-iA(t), H(t)].$$

When one wants to consider ensembles of states (*i.e.* quantum statistics), as well as open systems, the density operator picture is introduced. The density operator ρ corresponding to a single state $|\psi(t)\rangle$, is the rank-one operator $|\psi(t)\rangle\langle\psi(t)|$. An ensemble of such orthogonal states is a linear combination of such operators $\sum_i p_i|\psi_i(t)\rangle\langle\psi_i(t)|$, where $\sum_i p_i = 1$. Any ensemble can be represented by a positive-semidefinite density operator with trace one, and the probability that a system is in state $|\psi_i(t)\rangle$ is $\langle\psi_i(t)|\rho|\psi_i(t)\rangle$.

There are various measures of purity, which measures how close a density operator is to a single quantum state, but the most common is: $P_2(\rho) = \sqrt{\mathrm{Tr}(\rho^2)}$. For an n-dimensional system, $P_2(\rho) \in [\frac{1}{n}, 1]$, where the operator with minimal purity is unique: $P_2(\frac{1}{n}I) = \frac{1}{n}$. The latter state is known as the completely mixed state.

The extension of the Schrödinger equation to density operators is the von Neu-

mann equation:

$$\frac{d}{dt}\rho(t) = [-iH(u), \rho(t)]\,.$$

Note this equation preserves rank and purity.

D'Alessandro [15, 1] has specified some notions of controllability that relate to these evolution equations. *Operator controllability* is defined as the condition that, for any unitary operator U_f acting on $\mathcal{H}$, there exist a (finite) time T and admissible control(s) $u(t)$ such that the solution to the evolution equation specifies $U(T,0) = U_f$. A weaker notion of controllability relates to the Schrödinger equation: *pure state controllability* is the condition that, for any pair of initial and final states $|\psi_i\rangle$ and $|\psi_f\rangle$, there exist a time T and admissible control(s) $u(t)$ such that the Schrödinger equation, using the initial condition $|\psi(0)\rangle = |\psi_i\rangle$, gives $|\psi(T)\rangle = |\psi_f\rangle$.[1]

D'Alessandro adds a third notion: *density matrix controllability* is the condition that given any two *unitarily equivalent*[2] density matrices ρ_i and ρ_f, there exist a time T and control(s) $u(t)$ such that $\rho(0) = \rho_i$ under the von-Neumann equation is steered to $\rho(T) = \rho_f$. This is only a useful definition for closed systems, however, since open systems involve non-unitary dynamics. One can show that operator and density matrix controllability are equivalent, whereas pure state controllability may be satisfied even when the stronger conditions are not.

In finite dimensions, the dynamics occurs on a compact Lie group. The compactness is essential in what follows: one can directly apply established classical results for control over spheres [11] to quantum systems. The standard procedure to determine controllability on a compact Lie group is to evaluate the *dynamical Lie algebra*. First

[1] D'Alessandro defines pure state controllability as controllability on the non-projective Hilbert space, as distinguished from *equivalent state controllability*, which applies to the projective space. Using theory of Lie groups and algebras, however, one can show that either notion implies the other.

[2] that is, there exists a unitary U such that $\rho_f = U\rho_i U^\dagger$

one chooses a basis for the linear space $\text{span}_{u\in \text{U}}\{-iH(u)\}$. For a bilinear[3] system, this basis can be $\{-iH_0, -iH_1...\}$. The dynamical Lie algebra $\mathcal{L}$ is then just the Lie algebra generated by this basis set. This Lie algebra can be calculated iteratively by taking commutators of increasing depth, a procedure which clearly must terminate for a finite dimensional system (although it may be tedious for high dimensions). One then uses the following theorem [15] to determine controllability:

Theorem I.4. *An n-dimensional quantum control system is operator controllable if and only if* $\mathcal{L} = \mathfrak{u}(n)$ *or* $\mathcal{L} = \mathfrak{su}(n)$.

A simple dimension count suffices to decide whether this criterion is satisfied: $\dim(\mathcal{L})$ must be n^2 or $n^2 - 1$.

For a system to be pure state controllable, it suffices that the Lie group $e^{\mathcal{L}}$ is transitive on the complex sphere $S^{n-1}_{\mathbb{C}}$. Results from Lie group theory can be used to prove the following theorem[15].

Theorem I.5. *An n-dimensional quantum control system is pure state controllable if and only one of the following conditions holds:*

1. *The system is operator controllable.*
2. $\mathcal{L}$ *is conjugate to the symplectic Lie algebra* $\mathfrak{sp}(\frac{n}{2})$.
3. $\mathcal{L} = span\{iId\} \oplus \bar{\mathcal{L}}$, *where* $\bar{\mathcal{L}}$ *is conjugate to* $\mathfrak{sp}(\frac{n}{2})$.

Once the reachable set has been determined (that is, the Lie group $e^{\mathcal{L}}$ which contains all operators $U(t, 0)$ that can be achieved in finite time), one can use the following proposition [15].

[3]Bilinear in this case means the system is linear in both the control variables, as well as the state, so that $\frac{d}{dt}|\psi\rangle = -i(H_0 + \sum_k u_k H_k)|\psi\rangle$.

Proposition I.6. *If $e^{\mathcal{L}}$ is a compact Lie group, whose algebra is generated by a set $\{A_1, A_2...\}$, then any element of the group may be expressed as a* finite *product of exponentials $e^{A_i t_i}$.*

This means any operator that is reachable can be reached using a *finite* sequence of piecewise constant controls. Determining the order in which the generators should be applied, and for how long, may not be straightforward. Also, a practical concern for quantum control is that piecewise constant control functions may involve very high frequency components, corresponding to transitions between widely separated energy levels that have been neglected in the modelling process.

1.3 Lindblad dissipation

Downplaying the influence of the environment is not an option if quantum control theory is to be useful with respect to interesting applications. Fighting decoherence (that is, the tendency of the environment to destroy quantum coherences) has long been recognized as the primary barrier to building a practical quantum computer: while quantum computations have been performed for a very small number of qubits, the influence of the environment grows with size, and neutralizing this influence is necessary to scale these computations up into those of practical use. Similarly, modelling the control of chemical reactions as a closed system is also unrealistic. Many reactions take place in solution and can be very sensitive to temperature. Indeed, biomolecules such as proteins require a solvent and a narrow temperature range to function as they do.

As mentioned, in studying open quantum systems, there is much work in choosing how to model the environment, before the mathematics can be studied. The most general dynamical equation incorporating the environment is an integro-differential

equation called the Nakajima-Zwanzig (NZ) equation [9]. Essentially, if there is coupling between system and environment, the dynamics of the system depends on the state of the environment and the entanglement between system and environment. Both of these are affected by the history of the system, so an integro-differential equation is required.

For simplification purposes, one often makes the two following assumptions, which allow us to work with a differential equation instead:

1. The dynamics is Markovian. That is, the evolution of the system at time t_1 depends on $\rho(t_1)$ and not on its past history.

2. The dynamics is time-invariant.

If these two conditions are met, one has what is called Lindblad dissipation. This work only considers this type of open system dynamics.

A derivation of the Lindblad and Lindblad-Kossakowski equations, which describe Lindblad dissipation, can be found in [9]. Lindblad's work can be found in [30], although Gorini, Kossakowski and Sudarshan concurrently studied the finite-dimensional case in [20, 19]. I will present here a derivation based on Preskill's notes [38] that relies on Kraus operators. This derivation is slightly less rigorous but will be helpful for the interpretational framework that will be presented in the following chapter.

A superoperator $\$(\cdot)$ is a completely positive[4] map from the set of density operators to itself: $\$: \rho \to \rho'$. In particular, the time-evolution of a density operator is described by a superoperator $\$_{t_1,t_2}(\rho(t_1)) = \rho(t_2)$. It can be shown [35] that any

[4] $\$ is completely positive if it is positive and if $I_k \otimes \$ is positive for all k. In other words, the map is still physical when a non-interacting environment is introduced.

superoperator has an operator-sum representation:

$$\$(\rho) = \sum_j M_j \rho M_j^\dagger$$

where the M_j's are called Kraus operators. For the superoperator to be trace-preserving, the Kraus operators must satisfy the normalization condition $\sum_j M_j^\dagger M_j = I$. Note that if there is only one Kraus operator, it must be unitary, so the single-operator case describes the dynamics of a closed system, while open systems require more than one operator. The operator sum-representation is also not unique; however, any two such representations can be connected by a unitary operation on the space of matrices: $M_j^{(2)} = \sum_k u_{jk} M_k^{(1)}$, with $\sum_j u_{ik}\bar{u}_{jk} = \delta_{ij}$.

Now consider a density operator at time $t + \delta t$. The assumption of Markovicity means it is completely determined by $\rho(t)$. We can write it as

$$\rho(t+\delta t) = \$_{t,t+\delta t}(\rho(t)) = \rho(t) + O(\delta t) = M_0 \rho(t) M_0^\dagger + \sum_{j=1,2\ldots} M_j \rho(t) M_j^\dagger$$

where $M_0 = I + O(\delta t)$, and $M_j = L_j\sqrt{\delta t} + o(\sqrt{\delta t})$ for $j \geq 1$. We must satisfy the normalization condition, so we write $M_0 = I + (-iH + K)\delta t + o(\delta t)$, where H and K are Hermitian. We then have

$$\sum_{j=0,1\ldots} M_j^\dagger M_j = I + 2K\delta t + \sum_{j=1,2\ldots} L_j^\dagger L_j \delta t + o(\delta t).$$

It is clear that $K = -\frac{1}{2}\sum_{j=1,2\ldots} L_j^\dagger L_j$. Note that we are treating H, K and the L_j's as constant matrices, which follows from the time-homogeneity assumption.

By taking $\delta t \to 0$, we can turn the operator-sum representation into a differential equation, known as the Lindblad equation:[5]

$$\frac{d\rho}{dt} = [-iH, \rho] + \sum_{j=1,2\ldots} \left(L_j \rho L_j^\dagger - \frac{1}{2}\{L_j^\dagger L_j, \rho\} \right). \tag{1.1}$$

[5]Throughout this thesis, square brackets indicate a commutator, and curly braces an anti-commutator: $[A, B] := AB - BA$ and $\{A, B\} := AB + BA$.

The operator H is the total Hamiltonian, but it may not be identical to the system Hamiltonian. There may be a contribution from the system-environment coupling. The operators L_j are known as Lindblad operators, or jump operators. Note we have not imposed any upper bound on the number of Lindblad operators, but for a finite-dimensional system, any Lindblad equation can be written with at most $N^2 - 1$ traceless operators that are orthogonal to each other (with respect to the Hilbert-Schmidt inner product $(A, B) = tr(A^\dagger B)$).

To see this, we introduce the Lindblad-Kossakowski equation. Pick a basis $\{l_k : k = 0, 1, 2 \ldots N^2 - 1\}$ for the N^2-dimensional space of operators on the Hilbert space that (1) is orthonormal to the Hilbert-Schmidt inner product and (2) has $l_0 = \frac{1}{\sqrt{N}} I$, with the remaining l_k's traceless. If $L_j = \sum_k a_{jk} l_k$, then

$$L_j \rho L_j^\dagger - \frac{1}{2}\{L_j^\dagger L_j, \rho\} = [\frac{1}{\sqrt{N}} \sum_{k=1,2\ldots} \frac{1}{2}(a_{j0}\bar{a}_{jk} l_k^\dagger - a_{jk}\bar{a}_{j0} l_k), \rho]$$

$$+ \sum_{k,l=1,2\ldots} a_{jk}\bar{a}_{jl} \left(l_k \rho l_l^\dagger - \frac{1}{2}\{l_l^\dagger l_k, \rho\} \right).$$

The first term just adds to the total Hamiltonian, and the second gives a non-diagonal version of the dissipative term in the Lindblad equation. The $a_{jk}\bar{a}_{jl}$'s form a (rank-one) positive-semidefinite matrix of coefficients. When the contributions of all Lindblad operators are summed, their corresponding matrices will combine to also give a positive-semidefinite matrix A, with entries $A_{kl} = \sum_j a_{jk}\bar{a}_{jl}$, which is called the Gorini-Kossakowski-Sudarshan (GKS) matrix. We can now write down the Lindblad-Kossakowski equation:

$$\frac{d\rho}{dt} = [-iH, \rho] + \sum_{j,k=1}^{N^2-1} A_{jk} \left(l_j \rho l_k^\dagger - \frac{1}{2}\{l_k^\dagger l_j, \rho\} \right).$$

Note that the H may be different than in the first version of the Lindblad equation, as some of the L_j's could have components in the l_0 direction.

Since A is positive-semidefinite, it may be diagonalized. Its eigenvalues will be non-negative and it has an orthonormal eigenbasis. It follows that any Lindblad equation can be written in diagonal form:

$$\frac{d\rho}{dt} = [-iH, \rho] + \sum_{j=1}^{M \leq N^2-1} \left(L_j \rho L_j^\dagger - \frac{1}{2}\{L_j^\dagger L_j, \rho\} \right).$$

We now have a different set of M Lindblad operators $\{L_j\}$; they are the eigenvectors (in the space of operators) of A corresponding to its M non-zero eigenvalues, with norm equal to the square root of its eigenvalue. Note that these Lindblad operators, besides being mutually orthogonal, are traceless, as the non-traceless parts can always be absorbed into the total Hamiltonian. Henceforth, we will refer to both this "diagonal" version, as well as (1.1), as the Lindblad equation. If we require orthogonality of the Lindblad operators, we shall say so. For all versions, the superoperator $\mathcal{L}_D(\rho)$ will be used to abbreviate the dissipative term.

Lindblad superoperators can be characterized as *unital* or *non-unital*. $\mathcal{L}_D(\rho)$ is unital if $\mathcal{L}_D(I) = 0$ (in other words, the completely mixed state is stationary). In terms of the Lindblad operators, the superoperator is unital if and only if all Lindblad operators are Hermitian, since $\mathcal{L}_D(I) = \sum_k [L_k, L_k^\dagger]$. In terms of the GKS matrix, the superoperator is unital if and only if the GKS matrix is symmetric. It follows that the space of unital systems has dimension $\frac{n(n+1)}{2}$, while the space of all Lindblad systems has dimension n^2.

Control of Lindblad systems typically presumes that control variables only appear in the Hamiltonian piece. There has been work towards engineering quantum decoherence, particularly Markovian decoherence [45, 31, 2], that has been experimentally supported [3] recently. This thesis however will presume that the Lindblad operators are not engineered (or changing in time).

1.4 Physical example: the trapped ion

An example of a physical system that captures various features of interest is the trapped ion system (see Wineland and co-workers [58, 27] for an overview). Cirac and Zoller [14] proposed this system as a possible platform for quantum computation. The ion itself is a finite-dimensional system: Cirac and Zoller proposed a three-level system, although Monroe *et al.* showed that only two levels are necessary [33]. These finite dimensions are internal degrees of freedom, *e.g.* electron or nuclear spin. An ion can be cooled in a trap, so that there is an external vibrational degree of freedom, which can be modelled as a linear harmonic oscillator. The system Hamiltonian is given by:

$$H_{sys} = H_{ion} + H_{trap} = \left(\frac{1}{2}E_0\sigma_z\right) \otimes Id + Id \otimes \left(\nu a^\dagger a\right).$$

Here, the Hilbert space is a direct product of a two-level system with the infinite-dimensional harmonic oscillator Hilbert space. The annihilation and creation operators for the oscillator are $a = \sum_{j=0}^{\infty} \sqrt{j+1}|j\rangle\langle j+1|$ and $a^\dagger = \sum_{j=0}^{\infty} \sqrt{j+1}|j+1\rangle\langle j|$, so that $a^\dagger a = \sum_{j=0}^{\infty} j|j\rangle\langle j|$. E_0 is the energy-level separation between the internal states of the ion, and ν is the separation between the oscillator states. To distinguish states of the ion, we shall designate σ_z above as $|\uparrow\rangle\langle\uparrow| - |\downarrow\rangle\langle\downarrow|$, so that $|n = 0, 1 \cdots\rangle$ represent oscillator states.

The ion can be controlled by addressing it with a laser (for a quantum computer with multiple ions, each ion can be addressed by a separate laser). One can use two traveling-waves, in the direction of the vibrational motion:

$$H_{int} = (\lambda\sigma_+ + \lambda^*\sigma_-) \otimes \mathcal{E}(t)$$

$$\mathcal{E}(t) = \mathcal{E}_c(t)e^{ik_c x}e^{-i\omega_c t} + \mathcal{E}_r(t)e^{ik_r x}e^{-i\omega_r t} + h.c.$$

where *h.c.* denotes the Hermitian conjugate of the preceding terms, λ is the coupling strength and $\mathcal{E}(t)$ is the electromagnetic field. The frequencies are tuned so that the so-called *carrier frequency* $\omega_c = E_0$ and the *red-sideband frequency* $\omega_r = E_0 - \nu$. The position operator for a harmonic oscillator is $x = \frac{1}{\sqrt{2m\omega_r}}(a + a^\dagger)$, so if we define $\eta_i := \frac{\omega_i}{c\sqrt{2m\omega_r}}$, which are called the Lamb-Dicke parameters, we have

$$\mathcal{E}(t) = \mathcal{E}_c(t)e^{i\eta_c(a+a^\dagger)}e^{-i\omega_c t} + \mathcal{E}_r(t)e^{i\eta_r(a+a^\dagger)}e^{-i\omega_r t} + h.c.$$

Now if one transforms into the interaction picture (*i.e.* using a time-dependent basis), where $|\psi\rangle = e^{-iH_{sys}t}|\psi\rangle_I$, the interaction Hamiltonian can be written, after using a rotating-wave approximation [25],

$$H_{int} = \lambda\sigma_+ \otimes \left(\mathcal{E}_c(t)e^{-\eta_c(ae^{-i\nu t}+a^\dagger e^{i\nu t})} + \mathcal{E}_r(t)e^{-\eta_r(ae^{-i\nu t}+a^\dagger e^{i\nu t})}\right) + h.c.$$

Furthermore, ν is typically much larger than the magnitude of the interaction Hamiltonian, so the interaction Hamiltonian can be approximated as [25]:

$$\begin{aligned} H_{int} &= \sigma_+ \otimes \left(\sum_{n=0}^{\infty} c_n(t)|n\rangle\langle n| + r_n(t)|n\rangle\langle n+1|\right) + h.c. \\ c_n(t) &= \lambda\mathcal{E}_c(t)e^{-\eta_c^2/2}L_n^{(0)}(\eta_c^2) \\ r_n(t) &= \lambda\mathcal{E}_r(t)\frac{i\eta_r}{\sqrt{n+1}}e^{-\eta_r^2/2}L_n^{(1)}(\eta_r^2) \end{aligned}$$

where $L_n^{(m)}(\cdot)$ are the generalized Laguerre polynomials.

We now have an infinite-dimensional system (see figure 1.1 for a schematic), subject to two control fields. $\mathcal{E}_c(t)$ and $\mathcal{E}_r(t)$ are the control functions. Law and Eberly [26, 25] (see also Yuan and Lloyd [60]) provided a scheme to steer an arbitrary initial finite superposition of states (*i.e.* in the energy-eigenbasis, only a finite number of components are non-zero) to an arbitrary final finite superposition. Bloch, Brockett and Rangan [4] extended this by providing criteria by which any infinite-dimensional

system has this property, a result they call the Finite Controllability Theorem. One can steer an arbitrary superposition to the ground state $|\downarrow, 0\rangle$ by alternating the carrier and red-sideband fields. A state with the top populated component $|\uparrow, n\rangle$ can be steered using the carrier frequency to one with top populated component $|\downarrow, n\rangle$. Similarly, if the top populated component is $|\downarrow, n\rangle$, the red-sideband frequency can be used to depopulate the top component, so that the new top component is $|\uparrow, n-1\rangle$. Once the ground state is reached, the process of sequential application of fields can be reversed to attain an arbitrary final (finite) superposition.

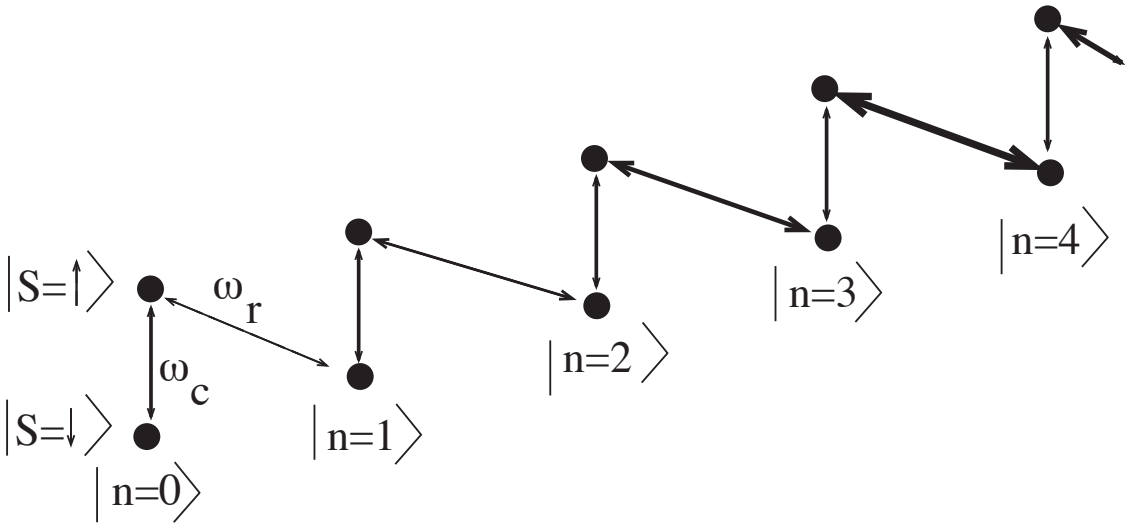

Figure 1.1: Schematic of a spin-half particle coupled to a harmonic oscillator, subject to control fields with the carrier and red-sideband frequencies.

This thesis considers only finite-dimensional systems, however, and in fact the trapped ion can be made effectively finite [40]. The trap strength can be tuned to manipulate the Lamb-Dicke parameters η_c and η_r, and if either η_c^2 or η_r^2 corresponds to a root of $L_n^{(0)}$ or $L_n^{(1)}$, respectively, that transition is turned off. For example, if $L_n^{(0)}(\eta_c^2) = 0$, then a $(2n+1)$-dimensional Hilbert space is sequestered from higher levels, in the sense that a superposition of the states $\{|\downarrow, m\rangle : m \leq n\} \cup \{|\uparrow, m\rangle : m < n\}$ can only be steered to other superpositions of these states. This "finitized"

trapped ion is controllable, so we may consider it as a model system for controllable quantum systems of arbitrary finite dimension.

The central question that this thesis tackles is: how much controllability do we retain if such a system is subject to Lindblad dissipation? One mechanism of dissipation is the eigenstate jump, which is modelled with the Lindblad operator $\sqrt{\gamma_{s_1 s_2 n_1 n_2}}|s_1, n_1\rangle\langle s_2, n_2|$. Under such an operator, the state $|s_2 n_2\rangle$ will jump to the state $|s_1 n_1\rangle$ at a rate $\gamma_{s_1 n_1 s_2 n_2}$. For example, a state $|\uparrow, n\rangle$ may spontaneously emit a photon of frequency ω_c, thereby jumping to the state $|\downarrow, n\rangle$. Conversely, a state $|\downarrow, n\rangle$ may absorb a photon of frequency ω_c and jump to the state $|\uparrow, n\rangle$.

Much of the research in this thesis is inspired by the work of Tannor and co-workers [55, 49] who studied laser cooling of atoms. "Cooling" in this sense meant driving a mixed state, in the presence of spontaneous emission, to the (pure) ground state. It was noted that, without emission, the purity could not be increased. While the Hamiltonian control could not *directly* influence purity, it could be used to steer the system to states where the emission process was optimized. This idea will recur throughout this thesis: Hamiltonian control fields, in the absence of dissipation, can only steer density operators along a unitary orbit. Only through dissipation can the system transition between orbits, thereby changing purity. The question is: how do we steer *along* the orbit so that this motion *between* orbits is to our liking?

Previous work of my adviser Anthony Bloch has also motivated me. His work with Brockett and Ratiu [5] as well as with Krishnaprasad, Marsden and Ratiu [6] used nonlinear double bracket terms as a way of modeling dissipation. In certain instances, for example when the Lindblad operators are Hermitian, the dissipation superoperator in the Lindblad equation can be written as a sum of (linear) double brackets. In Bloch and Rojo [7], the control of squeezed quantum states was studied,

including the case where the system is exposed to an an infinite bath of oscillators.

Other important work that contributed to my thinking include that of Solomon and Schirmer, who studied Lindblad dissipation and control on finite-dimensional systems [50, 51]. Dirr, Helmke and co-workers [16] studied control of finite-dimensional Lindblad systems using a Lie-semigroup structure. Li and Khaneja [28, 29] also studied finite-dimensional quantum control involving ensembles of Bloch balls.

1.5 Overview of thesis

With preliminaries out of the way, we now lay out the results of this thesis. The second chapter covers our analysis of the two-dimensional case. We begin with a classification of possible Lindblad operators, and then proceed to the first main result: how to isolate the dynamics between unitary orbits from the dynamics along unitary orbits. This results in a new control system, consisting of a one-dimensional ODE and a control set homeomorphic to S^1. We proceed to analyze the controllability of this system, and this analysis allows us to classify the purifiable systems in two dimensions. This work has been submitted for publication and can be found on the ArXiV [43].

Chapters three and four consider three-dimensional systems. We proceed with isolating the inter-orbit dynamics and come up with differential equations. As the control set is more complicated than for two dimensions, we instead consider a reduced control set consisting of just six controls. This leads to some interesting analysis of both small-time local controllablility and global controllability. In particular, we discover some beautiful combinatorial formulas that describe certain points on the set of STLC.

The final chapter lays out what we can generalize to arbitrary finite dimensions.

In particular, we are able to write down differential equations that describe the inter-orbit dynamics. Moreover, we are able to generalize the small-time local controllability result. We are also able to show that our first combinatorial formula result holds for arbitrary dimension.

This thesis proceeds from two to three to higher dimensions for pedagogical reasons. The two-dimensional case is fairly well developed, and the set of density matrices can be visualized as a closed ball in $\mathbb{R}^2$. The three-dimensional case is considerably more challenging. The set of density matrices is not easy to visualize as it is eight-dimensional. The set of unitary orbits however can be visualized as a closed subset of $\mathbb{R}^2$. This allows us to use some visual intuition in our proofs. Proceeding to higher dimensions, we see a lot of the results closely follow the three-dimensional case, although here we have to work more abstractly in some of our proofs.

CHAPTER II

Two-Dimensional Systems

2.1 Interpretation of Lindblad operators

It would be helpful to have a more intuitive interpretation of a given Lindblad operator, and we begin by providing one for the $n = 2$ case. We will do this by considering what a Lindblad operator L does to an arbitrary pure state $|\psi\rangle$. In a short time interval δt, this pure state becomes $M_0|\psi\rangle\langle\psi|M_0^\dagger + M_1|\psi\rangle\langle\psi|M_1^\dagger$, which is a mixture of two pure states. So we can think of the pure state as branching into one of two states at every given time. M_1 is just the Lindblad operator L times $\sqrt{\delta t}$, and we can think of the second term as representing a jump to a state $\frac{1}{\sqrt{\langle\psi|L^\dagger L|\psi\rangle}}L|\psi\rangle$ with probability $\langle\psi|L^\dagger L|\psi\rangle\delta t$. It is considered a "jump" because the destination state does *not* tend to the original state as $\delta t \to 0$. With probability $1 - \langle\psi|L^\dagger L|\psi\rangle\delta t$, there is no jump, but that does not mean the state is stationary. We have $M_0 = I - \frac{1}{2}L^\dagger L\delta t$, which means the branch that has stayed behind may still drift (we use the word "drift" to emphasize the fact that the distance between the old and new states is of order δt).

Since we are dealing with two-dimensional traceless operators, the Lindblad operator must fall into one of three cases:

1. Its only eigenvalue is zero.

2. It has two distinct eigenvalues $\pm\lambda$, and its eigenvectors are orthogonal.

3. It has two distinct eigenvalues $\pm\lambda$, and its eigenvectors are not orthogonal.

2.1.1 Case 1: the degenerate Lindblad operator

Neglecting the trivial case of a Lindblad operator that is the zero operator, we are left with the case of an operator with a one-dimensional eigenspace. Such a Lindblad operator can be written $L = \sqrt{\gamma}|a\rangle\langle b|$, where $|a\rangle$ and $|b\rangle$ form an orthogonal basis for the Hilbert space. This means that the destination of the jump is always $|a\rangle$, and the probability a state $|\psi\rangle = c_a|a\rangle + c_b|b\rangle$ jumps to $|a\rangle$ is $\gamma|c_b|^2\delta t$. As for the drifting branch, $M_0 = I - \frac{1}{2}L^\dagger L\delta t = I - \frac{\gamma}{2}|b\rangle\langle b|\delta t$, which can become a differential equation of an un-normalized vector:

$$\frac{d}{dt}|\psi\rangle = -\frac{\gamma}{2}\left(|b\rangle\langle b|\right)|\psi\rangle.$$

which has the general solution $|\psi\rangle = c_a(0)|a\rangle + c_b(0)e^{-\gamma t/2}|b\rangle$. The norm of this un-normalized vector is the square root of the probability the state is still in the drift branch. The normalized vector clearly tends to $|a\rangle$ over time, unless the initial state is $|b\rangle$, in which case the drifting branch is stationary. There are two possibilities then:

1. If the initial pure state is $|b\rangle$, the drift branch is stationary, but there is a constant probability rate of jumping, γ, as time progresses. The overall state is in a mixture of $|a\rangle$ and $|b\rangle$, with the respective fractions being $1-e^{-\gamma t}$ and $e^{-\gamma t}$.

2. If the initial pure state is anything other than $|b\rangle$, the state drifts toward $|a\rangle$:

   $$\frac{c_a(0)|a\rangle + c_b(0)e^{-\gamma t/2}|b\rangle}{\sqrt{|c_a(0)|^2 + |c_b(0)|^2 e^{-\gamma t}}}.$$

   with a positive, but decreasing, probability rate of jumping ahead to $|a\rangle$, $\gamma\frac{|c_b(0)|^2 e^{-\gamma t}}{|c_a(0)|^2+|c_b(0)|^2 e^{-\gamma t}}$.

This type of Lindblad operator is used to describe spontaneous emission of a photon by an excited state, in which case $|b\rangle$ is the excited state and $|a\rangle$ is the ground state. Conversely, it can also describe absorption of a photon, where $|b\rangle$ is now the ground state and $|a\rangle$ is the excited state. We will refer to this process as a "population jump", since a jump results in a state completely populating $|a\rangle$ and de-populating $|b\rangle$.

2.1.2 Case 2: orthogonal eigenvectors

If the eigenvalues of L are non-zero, they must have opposite sign since L is traceless. Furthermore, we can choose them to be real: multiplying a Lindblad operator by an overall phase does not change the Lindblad equation. If $|a\rangle$ and $|b\rangle$ are the orthogonal eigenvectors, the Lindblad operator can be written $\sqrt{\gamma}(|a\rangle\langle a| - |b\rangle\langle b|)$, where $\pm\sqrt{\gamma}$ are the eigenvalues. This Lindblad operator will send an arbitrary pure state $c_a|a\rangle + c_b|b\rangle$ to the pure state $c_a|a\rangle - c_b|b\rangle$ with probability $\gamma\delta t$. In other words, the amplitudes with respect to the eigenbasis of L do not change, but the relative phase jumps by π. Because the eigenvectors are orthogonal, $L^\dagger L$ is a multiple of the identity, which means that the drifting branch is actually stationary: $M_0 = (1 - \frac{\gamma}{2}\delta t)I$. Therefore, a system that starts in the state $c_a|a\rangle + c_b|b\rangle$ will always be in a mixture of that state and $c_a|a\rangle - c_b|b\rangle$ (since each state is the jump destination of the other, and there is no drift). The relative populations (of the states $c_a|a\rangle \pm c_b|b\rangle$) are $\frac{1 \pm e^{-\gamma t}}{2}$, so as $t \to \infty$, this will become a fifty-fifty mixture.

This type of dissipation is often called "de-phasing", since the populations in states $|a\rangle$ and $|b\rangle$ do not change, but a coherent super-position of two states with well-defined phase evolves into an incoherent mixture where the phase is completely random. We will refer to this process as a "balanced phase jump", since it results in back-and-forth jumping between two states of opposite phase.

2.1.3 Case 3: non-orthogonal eigenvectors

If the eigenvectors are not orthogonal, so that $\alpha e^{i\beta} := \langle a|b\rangle \neq 0$, then $L = \frac{\sqrt{\gamma}}{1-\alpha^2}(|a\rangle\langle a| - |b\rangle\langle b| - \alpha e^{i\beta}|a\rangle\langle b| + \alpha e^{-i\beta}|b\rangle\langle a|)$. As before, this sends an arbitrary superposition $c_a|a\rangle + c_b|b\rangle$ to its phase-flipped partner $c_a|a\rangle - c_b|b\rangle$, and vice versa, with probability $\gamma\delta t$. Unlike the $\alpha = 0$ case, however, the drifting branch is *not* stationary, since $L^\dagger L$ is not a multiple of the identity. The evolution of ρ is more complicated in this case, as the phase jump destination changes as the drifting branch migrates, and each state in this migration generally has a different phase partner. There is a unique pair of phase-flipped partners that do not drift: $|\pm\rangle := \frac{1}{\sqrt{2}}(|a\rangle \pm e^{-i\beta}|b\rangle)$, which are the eigenvectors of $L^\dagger L$. If the initial pure state is one of these two, there is back-and-forth jumping, and the state relaxes to a mixture with fractions $\frac{1}{2} \mp \frac{\alpha}{1+\alpha^2}$. In general, an initial density matrix (in the $|\pm\rangle$ basis)

$$\begin{pmatrix} \frac{1+z_0}{2} & \frac{x_0 - iy_0}{2} \\ \frac{x_0 + iy_0}{2} & \frac{1-z_0}{2} \end{pmatrix}$$

will evolve as

$$\begin{pmatrix} \frac{1}{2} - \frac{\alpha}{1+\alpha^2} & 0 \\ 0 & \frac{1}{2} + \frac{\alpha}{1+\alpha^2} \end{pmatrix}$$

$$+ \begin{pmatrix} e^{-2\gamma(1+\alpha^2)t/(1-\alpha^2)}(\frac{z}{2} + \frac{\alpha}{1+\alpha^2}) & \frac{x_0}{2}e^{-2\gamma\alpha^2 t/(1-\alpha^2)} - \frac{iy_0}{2}e^{-2\gamma t/(1-\alpha^2)} \\ \frac{x_0}{2}e^{-2\gamma\alpha^2 t/(1-\alpha^2)} + \frac{iy_0}{2}e^{-2\gamma t/(1-\alpha^2)} & e^{-2\gamma(1+\alpha^2)t/(1-\alpha^2)}(-\frac{z}{2} - \frac{\alpha}{1-\alpha^2}) \end{pmatrix}$$

which relaxes to the same asymptotic mixture as before.

We will refer to this process as an "unbalanced phase jump", since the Lindblad operator flips the phases, but the drift disrupts the see-saw jumping between all but one phase-flipped pair.

2.1.4 Cholesky decomposition of Lindblad dissipation

Every Lindblad dissipation can be described uniquely by three orthogonal Lindblad operators, but since orthogonality of operators does not have an immediate intuitive interpretation, this decomposition is not necessarily the most appropriate. A different factorization of a positive-(semi)definite matrix is the Cholesky decomposition $A = RR^\dagger$, where R is lower-triangular. If A has full rank, this decomposition is unique. If A has rank m less than the full rank, R is unique if one demands only the first m columns are non-zero. In this description, we have m Lindblad operators corresponding to the m non-zero columns of R. Since $A_{jk} = \sum_l r_{jl}\bar{r}_{kl}$, the Lindblad-Kossakowski equation becomes

$$\begin{aligned}\frac{d\rho}{dt} &= [-iH,\rho] + \sum_{j,k=1}^{m} A_{jk}\left(l_j\rho l_k^\dagger - \frac{1}{2}\{l_k^\dagger l_j,\rho\}\right)\\ &= [-iH,\rho] + \sum_{j,k,l=1}^{m} r_{jl}\bar{r}_{kl}\left(l_j\rho l_k^\dagger - \frac{1}{2}\{l_k^\dagger l_j,\rho\}\right)\\ &= [-iH,\rho] + \sum_{l=1}^{m}\left(L_l^C\rho L_l^{C\dagger} - \frac{1}{2}\{L_l^{C\dagger}L_l^C,\rho\}\right).\end{aligned}$$

where $L_l^C = \sum_j r_{jl}l_j$ are the new Lindblad operators, where the lth operator has at most $n^2 - l$ components.

Note that the Cholesky decomposition is basis-dependent: we must choose which directions we want to "have the most zeros". The reason for using the Cholesky decomposition is to privilege certain operators, and in our case we wish to privilege the three operators with the most intuitive use to physicists: (1) the de-phasing operator in the energy eigenbasis, also known as the z Pauli matrix σ_z, and (2) the raising and lowering operators $\sigma_\pm$:

$$\sigma_z = \begin{pmatrix} 1 & 0 \\ 0 & -1 \end{pmatrix} \quad \sigma_+ = \begin{pmatrix} 0 & 1 \\ 0 & 0 \end{pmatrix} \quad \sigma_- = \begin{pmatrix} 0 & 0 \\ 1 & 0 \end{pmatrix}.$$

The lowering operator can describe spontaneous emission, where an excited state spontaneously emits a photon and drops to the ground state. The raising operator can describe stimulated absorption, where a ground state is excited by absorbing a photon. The de-phasing operator describes the loss of coherence between the energy eigenstates.

If we use the order above, for the case of full rank we have decomposed the dissipation into three processes:

1. L_3^C can only have a component in the σ_- direction, so it must correspond to a population jump from the excited state to ground state, akin to spontaneous emission.

2. L_2^C must have a component in the σ_+ direction. If there is no component in the σ_- direction, this corresponds to a population jump from the ground state to the excited state. If there is a σ_- component, we have a phase jump. The fact that there is no σ_z component means this phase jump is relative to a basis of states with equal energy and opposite phase, *i.e.* $|a, b\rangle = c_1|0\rangle \pm c_2|1\rangle$.

3. L_1^C must have a component in the σ_z direction, and may or may not have components in the other directions. This operator can describe any of the cases not covered by L_2^C and L_3^C: it may be a population jump to any non-energy eigenstate, or it may be a phase-jump relative to two states that aren't of equal energy and opposite phase.

If the rank m is less than full, the dissipation is described by a selection of m processes among these three possibilities.

2.2 Projection of dynamics

Having discussed the uncontrolled aspects of two-dimensional Lindblad dissipation, we now want to investigate controlling such systems. In quantum control theory, the control variables typically appear in the Hamiltonian operator − the dissipation piece is considered "external". Unfortunately, this type of control can only move the system along unitary orbits: ρ at any time t is $U(t)\rho(0)U^\dagger(t)$. Moreover, the unitary orbits of ρ correspond one-to-one to the possible spectra of ρ, so the spectrum is invariant under non-dissipative dynamics. This is unfortunate since it restricts us to controlling only $N-1$ of the possible N^2-1 directions, and in particular it prevents us from controlling the mixture fractions (the eigenvalues of ρ) and the purity $\sqrt{tr(\rho^2)} = \sum \lambda_j^2$. To move between unitary orbits, we need the dissipative dynamics.

With this in mind, we would like to isolate the dynamics between orbits from the overall dynamics. First, let's derive the overall dynamics on the Bloch ball. The density operator can be written in terms of the Pauli matrices: $\rho = \frac{1}{2}(I + \sum_{j=x,y,z} n_j\sigma_j)$, where the n_j's are the coordinates on the Bloch ball, and the x and y Pauli matrices are $\sigma_x = \sigma_+ + \sigma_-$ and $\sigma_y = -i\sigma_+ + i\sigma_-$. We will assume we have unbounded Hamiltonian control in all directions: $H = \sum u_j\sigma_j$, where $u_j \in \mathbb{R}$. Adding multiples of the identity to the Hamiltonian does not change the dynamics, so we can set the trace to zero. Also, we neglect the drift Hamiltonian, since it only shifts u_z by half the energy level separation. Substituting these expressions into the Lindblad-Kossakowski equation (where we use the Pauli matrices times $\frac{1}{\sqrt{2}}$ as our basis), we get

$$\frac{1}{2}\sum_j \frac{dn_j}{dt}\sigma_j = \sum_{j,k}[-iu_j\sigma_j, \frac{1}{2}n_k\sigma_k] + \frac{1}{4}\sum_{jk} a_{jk}[\sigma_j, \sigma_k] + \frac{1}{4}\sum_{jkl} a_{jk}n_l(\sigma_j\sigma_l\sigma_k - \frac{1}{2}\{\sigma_k\sigma_j, \sigma_l\})$$

$$= \sum_{jk} (\frac{-i}{2} u_j n_k + \frac{1}{4} a_{jk})[\sigma_j, \sigma_k] + \frac{1}{4} \sum_{jkl} a_{jk} n_l (\sigma_j \sigma_l \sigma_k - \frac{1}{2} \{\sigma_k \sigma_j, \sigma_l\}).$$

The Pauli matrices obey the relations

$$[\sigma_j, \sigma_k] = 2i \sum_l \epsilon_l \sigma_l$$

$$\{\sigma_j, \sigma_k\} = 2\delta_{jk} I$$

$$\sigma_j \sigma_l \sigma_k - \frac{1}{2} \{\sigma_k \sigma_j, \sigma_l\} = \delta_{kl} \sigma_j + \delta_{jl} \sigma_k - 2\delta_{jk} \sigma_l.$$

Using these relations, the Lindblad-Kossakowski equation above becomes

$$\frac{1}{2} \sum_l \frac{dn_l}{dt} \sigma_l = \sum_{j,k,l} \epsilon_{jkl} u_j n_k \sigma_l + \sum_{j,k,l} \frac{1}{2} i a_{jk} \epsilon_{jkl} \sigma_l + \frac{1}{4} \sum_{jl} (a_{jl} (n_j \sigma_l + n_l \sigma_j) - 2a_{jj} n_l \sigma_l).$$

If we define $b_l = \sum i a_{jk} \epsilon_{jkl}$, and $a^S_{jk} = \frac{a_{jk} + a_{kj}}{2}$, we have

$$\sum_l \frac{dn_l}{dt} \sigma_l = 2 \sum_{j,k,l} \epsilon_{jkl} u_j n_k \sigma_l + \sum_l b_l \sigma_l + \sum_{jl} (a^S_{jl} n_j \sigma_l - a^S_{jj} n_l \sigma_l).$$

In vector notation, we can write:

$$\frac{d\vec{n}}{dt} = \vec{b} + \vec{u} \times \vec{n} + (A^S - tr(A^S) I) \vec{n}. \tag{2.1}$$

where A^S is the matrix with elements a^S_{ij}.

Now we want to decompose this equation into dynamics along and between unitary orbits. For a given Bloch vector $\vec{n}$, the density matrix is $\rho = \frac{1}{2}(I + \sum n_j \sigma_j)$. ρ has the eigenvalues $\frac{1 \pm r}{2}$, where $r := |\vec{n}|$ and eigenvectors

$$|\psi_\pm\rangle := \sqrt{\frac{1 + n_z}{2}} |1\rangle + \sqrt{\frac{1 - n_z}{2}} e^{n_x + i n_y} |2\rangle.$$

Note the spectra correspond one-to-one with the values of r, the Bloch radius. It follows that the unitary orbits are concentric spheres, except for the completely

mixed state, which corresponds to the point $r = 0$. So we can parametrize the orbits by r, which lives on the closed interval $[0, 1]$, and characterize the motion along orbits with the unit vector $\hat{n} = \vec{n}/r$. We must be careful with respect to the innermost orbit however. The unit vector $\hat{n}$ is not defined there, which means that the differential equations which we will derive for r and $\hat{n}$ will have solutions that exist for finite times (those solutions correspond to trajectories of ρ that pass through the completely mixed state).

Since $r^2 = \vec{n} \cdot \vec{n}$, we have $2r\frac{dr}{dt} = 2\vec{n} \cdot \frac{d\vec{n}}{dt}$ and therefore $\frac{dr}{dt} = \hat{n} \cdot \frac{d\vec{n}}{dt}$. So,

$$\frac{dr}{dt} = \hat{n} \cdot \vec{b} + \hat{n} \cdot (\vec{u} \times \vec{n}) + \hat{n} \cdot (A^S - tr(A^S)I)\vec{n}.$$

The middle term vanishes, the first term is constant in r and the third is linear in r. We can write

$$\frac{dr}{dt} = \hat{n} \cdot \vec{b} + r(\hat{n} \cdot (A^S\hat{n}) - tr(A^S)). \tag{2.2}$$

To find the ODE for $\hat{n}$, we use $\vec{n} = r\hat{n}$, which gives $\frac{d\hat{n}}{dt} = \frac{1}{r}(\frac{d\vec{n}}{dt} - \frac{dr}{dt}\hat{n})$. So we get

$$\frac{d\hat{n}}{dt} = 2\vec{u} \times \hat{n} + \frac{1}{r}(\vec{b} - (\vec{b} \cdot \hat{n})\hat{n}) + (A^S - \hat{n} \cdot (A^S\hat{n}))\hat{n}. \tag{2.3}$$

Our goal here is to view equation (2.2) as a control ODE where $\hat{n}$ is the control. This view requires that we have full control over $\hat{n}$, and we claim that we do, in terms specified by the following lemma.

Lemma II.1. *Let S be the sphere centered at the origin with radius one, let B be the associated closed ball, and let B^* be the closed ball with the origin removed. Let $\hat{n}(t)$ be a piecewise differentiable function from a time interval $[0, T]$ into S such that the corresponding solution $r(t)$ of equation (2.2) is contained in the interval $(0, 1]$. Then there are piecewise continuous control functions $u_x(t)$, $u_y(t)$ and $u_z(t)$ such that equation (2.1) has the piecewise differentiable solution $\vec{n}(t) = r(t)\hat{n}(t)$ on B^*.*

Proof. First re-write equation (2.3):

$$\vec{u} \times \hat{n} = \frac{1}{2}\left(\frac{d\hat{n}}{dt} - \frac{1}{r}(\vec{b} - (\vec{b}\cdot\hat{n})\hat{n}) - (A^S - \hat{n}\cdot(A^S\hat{n}))\hat{n}\right).$$

Any equation of the form $\vec{x}\times\vec{a} = \vec{b}$, where $\vec{a}\cdot\vec{b} = 0$, has solution $\vec{x} = \vec{a}\times\vec{b}$. It follows that we can choose the controls to be

$$\begin{aligned}\vec{u}(t) &= \hat{n}\times\frac{1}{2}\left(\frac{d\hat{n}}{dt} - \frac{1}{r}(\vec{b} - (\vec{b}\cdot\hat{n})\hat{n}) - (A^S - \hat{n}\cdot(A^S\hat{n}))\hat{n}\right)\\ &= \frac{1}{2}\left(\hat{n}(t)\times\dot{\hat{n}} - \frac{1}{r(t)}\hat{n}(t)\times\vec{b} - \hat{n}(t)\times(A^S\hat{n}(t))\right).\end{aligned}$$

Since $\hat{n}(t)$, $\dot{\hat{n}}(t)$ and $r(t)$ are piecewise continuous, so is $\vec{u}(t)$. □

Note that the prescription for $\vec{u}(t)$ is unbounded as $r \to 0$ because of the middle term. This is because the system cannot approach the completely mixed state from any direction: when $\vec{n} = \vec{0}$, $\frac{d\vec{n}}{dt}$ is fixed to be $\vec{b}$ regardless of the controls $\vec{u}(t)$.

We finish this section by writing down an alternate version of (2.2) in terms of the eigenvalues of A^S, which allows us to specify a given system in terms of six real parameters. Let $a_1 \geq a_2 \geq a_3$ be the eigenvalues of A^S. Let $\{b_j : j = 1,2,3\}$ and $\{n_j : j = 1,2,3\}$ be the components of $\vec{b}$ and $\vec{n}$ relative to the intrinsic axes of A^S (whereas the subscripts x, y and z denote the components relative to the eigenvectors of the Pauli matrices). This gives

$$\frac{dr}{dt} = \sum_{j=1}^{3} b_j n_j - r\sum_{j=1}^{3} a_j(1-n_j^2). \tag{2.4}$$

The six parameters obey the following inequality, which arises from the positive semi-definiteness of A:

$$a_1 b_1^2 + a_2 b_2^2 + a_3 b_3^2 \leq 4a_1a_2a_3. \tag{2.5}$$

The positive semi-definiteness of A also ensures the positive semi-definiteness of A^S, so we also have $a_1, a_2.a_3 \geq 0$.

2.3 Controllability analysis

To analyze controllability of (2.4), we look at the functions $f_M(r)$ and $f_m(r)$, which give the maximum and minimum attainable values of $\dot{r}$ for a given $r \in (0, 1]$. It is clear that (2.4) is controllable on a closed subinterval of $(0, 1)$ if $f_M > 0$ and $f_m < 0$ everywhere on the subinterval. To steer between two points r_i and r_f, we choose our controls so that $\dot{r}(r) = f_M(r)$ if $r_i < r_f$, or $\dot{r}(r) = f_m(r)$ if $r_i > r_f$.

Some properties of f_M and f_m can be gleaned from inspection of the differential equation, which we collect into a proposition:

Proposition II.2. *If* $f_M(r) := \sup\{\dot{r}(r)\}$ *and* $f_m(r) := \inf\{\dot{r}(r)\}$,

1. f_M *and* f_m *are non-increasing.*
2. $\lim_{r\to 0+} f_M(r) = |\vec{b}|$ *and* $\lim_{r\to 0+} f_m(r) = -|\vec{b}|$.
3. $f_M(1) \leq 0$.
4. $f_m(r) \leq 0$ *for all* r *and system parameters.* $f_m(r) = 0$ *for* $r > 0$ *only for the trivial case where* $a_1 = 0$ *(which requires that all* a_j*'s and* b_j*'s are zero).*
5. *If* $\vec{b}$ *has non-zero magnitude,* $f_M(r)$ *has an isolated intercept* $r_T \in (0, 1]$.

Proof. 1. If a control vector $\hat{n}^*$ achieves the maximum $\dot{r}$ at $r = r^*$, then choosing that control for all $r < r^*$ can only achieve a larger or equal $\dot{r}$, since the coefficient of r in the differential equation, $\sum_{j=1}^{3} a_j(1 - n_j^2)$, must be non-negative. Similarly, if a control $\vec{n}^*$ achieves the minimum at $r = r^*$, then choosing that control for all $r > r^*$ can only achieve a smaller or equal $\dot{r}$. Furthermore, if a_1 and a_2 are positive, the coefficient of r cannot be made zero, so in this case, we can strengthen "non-increasing" to "decreasing".

2. As $r \to 0+$, the linear term in (2.4) can be neglected, and we must extremize $\vec{b} \cdot \vec{n}$. The range of this is clearly $[-|\vec{b}|, |\vec{b}|]$.

3. Since r cannot exceed one, $\dot{r}|_{r=1} \leq 0$.

4. Non-positivity follows from 1. and 2. If $a_1 > 0$, $\dot{r}$ can be always made negative by choosing $\vec{n} = \langle 0, 0, 1 \rangle$.

5. Non-zero $\vec{b}$ implies that at a_1 and a_2 are positive, which means that f_M is strictly decreasing on $(0, 1)$. This, together with 2. and 3. imply the existence of r_T.

□

Corollary II.3. *If $\vec{b}$ is nonzero, there is an interval $(0, r_T)$, which we call a* trap*, inside of which the system is controllable. Outside of the trap, on $[r_T, 1]$, the system is one-way controllable; that is, r_i can be steered to r_f in finite time if and only if $r_f \leq r_i$.*

Proof. The statements in the proposition imply that $f_m(r) < 0 < f_M(r)$ on $(0, r_T)$, in which case we can steer r_i to $r_f \geq r_i$ by choosing the control that satisfies $\dot{r} = f_M(r_f)$ provided $r_f < r_T$. Conversely, to steer r_i to $r_f \leq r_i$, we can choose the control that satisfies $\dot{r} = f_m(r_f)$. On the interval $[r_T, 1]$, $f_M(r) \leq 0$, so r_i cannot be steered to $r_f > r_i$, but can be steered to $r_f < r_i$ by choosing the control that satisfies $\dot{r} = f_m(r_i)$, which must be negative. □

In the case that $|\vec{b}| = 0$, there is no trap: $\dot{r} \leq 0$ for all r, and in fact we can say that

$$-r(a_1 + a_2) \leq \dot{r} \leq -r(a_2 + a_3) \tag{2.6}$$

where we can achieve the upper and lower bounds by choosing $\vec{n}$ to be $\langle \pm 1, 0, 0 \rangle$ and $\langle 0, 0, \pm 1 \rangle$, respectively. In the case that $a_2 = a_3 = 0$, the decay of r may be halted,

but otherwise r will decay exponentially to zero at a rate above or equal to $a_2 + a_3$. It is evident, then, that the presence of an asymmetric part in the dissipative term (represented by $\vec{b}$) significantly enhances the possibility of control.

In order to calculate f_M and f_m for a given r, we can use the method of Lagrange multipliers. In some cases, we can solve the resulting equations analytically, but in general one must find the roots of a sixth-order polynomial, so we must resort to numerics. Before considering the general case, we will look at a particular case that can be treated analytically. We consider the possibility that a two-level system can undergo one of two population jumps represented by the raising and lowering operators σ_+ and σ_- at rates α_+ and α_-, respectively. If one constructs the Lindblad equation using this scenario, and expresses it in the basis of the Pauli matrices, one finds that $a_1 = a_2 = \frac{|\alpha_+ - \alpha_-|}{2}$, $a_3 = 0$, $b_1 = b_2 = 0$ and $b_3 = \alpha_+ - \alpha_-$. The fact that $\vec{b}$ has only one non-zero component simplifies the equations so that we can treat the system analytically.

If we apply the method of Lagrange multipliers to the right-hand side of (2.4) and set $b_1 = b_2 = 0$ and $a_1 = a_2$, we get

$$\begin{aligned} 2ra_1n_1 &= 2\lambda n_1 \\ 2ra_1n_2 &= 2\lambda n_2 \\ b_3 &= 2\lambda n_3 \\ n_1^2 + n_2^2 + n_3^2 &= 1 \end{aligned}$$

where λ is the Lagrange multiplier. This has the following solutions:

$$\hat{n} = \langle 0, 0, \pm 1 \rangle \tag{2.7}$$

$$\hat{n} = \left\langle n_1, n_2, \frac{b_3}{2a_1 r} \right\rangle \tag{2.8}$$

where n_1 and n_2 in (2.8) can be any pair that satisfies the normalization condition. Solutions (2.8) do not exist for all r, since the magnitude of n_3 must not exceed one. They exist only on $[\frac{|b_3|}{2a_1}, 1]$. To determine which solutions correspond to f_M and f_m, we substitute back into (2.4). Solutions (2.7) give

$$\dot{r} = \pm|b_3| - 2a_1 r \tag{2.9}$$

and solutions (2.8) give

$$\dot{r} = \frac{|b_3|^2}{4a_1 r} - ra_1. \tag{2.10}$$

We can easily conclude that $f_m(r) = -|b_3| - 2a_1 r$. Furthermore, $f_M(r) = |b_3| - 2a_1 r$ on the interval $(0, \frac{|b_3|}{2a_1})$, where solution (2.8) does not exist. Where it does exist, however,

$$\frac{|b_3|^2}{4a_1 r} - ra_1 \geq |b_3| - 2a_1 r \tag{2.11}$$

and this inequality is saturated only where (2.9) and (2.10) touch. It happens that r_T in this case coincides with this touching point, *i.e.* $r_T = \frac{|b_3|}{2a_1}$. This is not a general phenomenon, however: if $a_3 > 0$, the touching point and the trap radius would not coincide. Fig. 2.1 depicts these solutions for $a_1 = a_2 = 10$ and $b_3 = 12$.

More generally, one can perform this analytical treatment in the following cases: (1) if $\vec{b}$ has one non-zero component, (2) if $\vec{b}$ has two non-zero components, and the corresponding a_j's are equal, and (3) $\vec{b}$ has three non-zero components, and $a_1 = a_2 = a_3$. If the system does not fall into any of those three categories, Lagrange multipliers lead to either a fourth-degree polynomial in λ (technically solvable, but inordinately messy) or a sixth-degree polynomial (generally not solvable). The fourth-degree polynomial arises in the cases (1) $\vec{b}$ has two non-zero components but corresponding a_j's are not equal and (2) $\vec{b}$ has three non-zero components and $a_1 = a_2 > a_3$ or

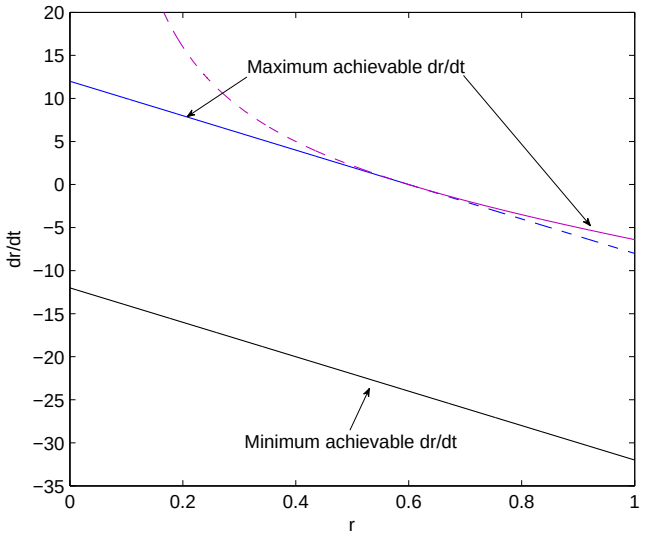

Figure 2.1: Maximum and minimum achievable dr/dt vs. r for a case that can be solved analytically. System parameters: $a_1 = a_2 = 10$, $a_3 = 0$, $b_1 = b_2 = 0$, $b_3 = 12$. Solid lines represent f_M and f_m. Blue and purple indicate solutions (2.7) and (2.8), respectively. Dotted lines indicate where these solutions do not coincide with f_M.

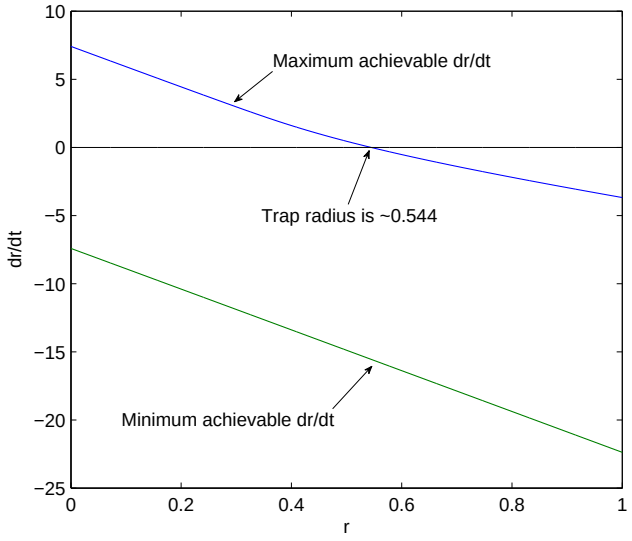

Figure 2.2: Maximum and minimum achievable dr/dt vs. r for a case that must be solved numerically. The trap radius is where the maximum achievable dr/dt passes from positive to negative. System parameters: $a_1 = 10$, $a_2 = 5$, $a_3 = 0.3$, $b_1 = 0.15\sqrt{0.6}$, $b_2 = 0.9$, $b_3 = 3\sqrt{6}$

$a_1 > a_2 = a_3$. The sixth-degree polynomial arises if $\vec{b}$ has three non-zero components and $a_1 > a_2 > a_3$.

In those cases, we can find the real roots of the polynomial numerically. Then we can compute the corresponding values of $\dot{r}$, choose the maximum and minimum values, and assign the values to f_M and f_m. In fig. 2.2, f_M and f_m are shown for a particular system that required solving a sixth-order polynomial. We have computed the curves for 10,000 points apiece. r_T can be found by numerically interpolating f_M. For the case depicted in fig. 2.2, r_T was computed to be 0.544387876644064 (to machine precision).

2.4 Purifiable systems

An important goal in quantum control is purification: the process of steering a mixed state to a pure state, which can be characterized by a purity $tr(\rho^2) = 1$. Alternatively, a system is pure if the leading eigenvalue is one, with remaining eigenvalues being zero. In terms of the above analysis, we say a system is *purifiable* if and only if the trap radius $r_T = 1$. In other words, the function $f_M(r)$ has an isolated intercept at $r = 1$. This section is devoted to proving the following theorem, which characterizes the possible purifiable systems.

Theorem II.4. *A two-level Lindblad system is purifiable if and only if it can be described as one of the following:*

- *A population jump*
- *An unbalanced phase jump*
- *A population jump and any number of phase jumps between the destination of the population jump and other states*

- *Any number of phase jumps that share a common eigenvector*

Proof. We are required to show two things to prove a system is purifiable: $f_M(1) = 0$, and $a_2 > 0$. $a_2 \geq 0$. The latter ensures that f_M is strictly decreasing rather than constant in r. When combined with the former condition, this implies that f_M is positive for all $r < 1$, and therefore controllable.

We will make use of the following lemma:

Lemma II.5. *$\dot{r} = 0$ at $r = 1$ if and only the system is in a state that is an eigenvector of all contributing Lindblad operators.*

Proof. Write the Bloch radius $r = \lambda_+ - \lambda_-$, where $\lambda_+ \geq \lambda_-$ are the eigenvalues of ρ. We have

$$\begin{aligned}
\dot{\lambda_j} &= \langle \dot{\psi_j}|\rho|\psi_j\rangle + \langle\psi_j|\rho|\dot{\psi_j}\rangle + \langle\psi_j|\dot{\rho}|\psi_j\rangle \\
&= \lambda_j(\langle \dot{\psi_j}|\psi_j\rangle + \langle\psi_j|\dot{\psi_+}\rangle) + \langle\psi_j|\dot{\rho}|\psi_j\rangle \\
&= \lambda_j \frac{d}{dt}(\langle\psi_j|\psi_j\rangle) + \langle\psi_j|[-iH,\rho]|\psi_j\rangle + \langle\psi_j|\mathcal{L}_D(\rho)|\psi_j\rangle \\
&= \langle\psi_j|\mathcal{L}_D(\rho)|\psi_j\rangle. \qquad (2.12)
\end{aligned}$$

In the last step, we have used the fact $[-iH, \rho]$ is skew-Hermitian and thus its diagonal elements are zero.

Now, if the dissipation is characterized by a collection of Lindblad operators $\{L_j\}$'s, which are not necessarily orthogonal, we can use (1.1) to specify $\mathcal{L}_D(\rho)$:

$$\begin{aligned}
\frac{dr}{dt} = \sum_j \Bigg(&\langle\psi_+|L_j\rho L_j^\dagger|\psi_+\rangle - \frac{1}{2}\langle\psi_+|L_j^\dagger L_j\rho|\psi_+\rangle - \frac{1}{2}\langle\psi_+|\rho L_j^\dagger L_j|\psi_+\rangle \\
&-\langle\psi_-|L_j\rho L_j^\dagger|\psi_-\rangle + \frac{1}{2}\langle\psi_-|L_j^\dagger L_j\rho|\psi_-\rangle + \frac{1}{2}\langle\psi_-|\rho L_j^\dagger L_j|\psi_-\rangle\Bigg).
\end{aligned}$$

We are interested in $\dot{r}$ when $r = 1$, so insert $\rho = |\psi_+\rangle\langle\psi_+|$. We get

(2.13)
$$\frac{dr}{dt} = \sum_j \left(\langle\psi_+|L_j|\psi_+\rangle\langle\psi_+|L_j^\dagger|\psi_+\rangle - \langle\psi_+|L_j^\dagger L_j|\psi_+\rangle - \langle\psi_-|L_j|\psi_+\rangle\langle\psi_+|L_j^\dagger|\psi_-\rangle \right).$$

If we insert the identity operator between $L_j^\dagger$ and L_j in the middle term, we get the expression

$$\frac{dr}{dt} = -2\sum_j |\langle\psi_-|L_j|\psi_+\rangle|^2.$$

For $\dot{r}$ to vanish, we need $|\langle\psi_-|L_j|\psi_+\rangle|^2$ to vanish for each L_j. This is only possible however if $|\psi_+\rangle$ is an eigenvector of each L_j, since otherwise $L_j|\psi_+\rangle$ would have some component in the $|\psi_-\rangle$ direction. This proves the lemma. □

It follows from the lemma that a system is purifiable only if all contributing Lindblad operators share a common eigenvector, or else $f_M(1)$ will be strictly negative. This is only a necessary condition however and not a sufficient one, since the condition implies only that $f_M(1) = 0$. We also require that $a_2 > 0$. So consider the case $a_2 = 0$. This implies that a_3 and $\vec{b}$ are also zero (due to (2.5)), so that A has only one non-zero entry in its natural basis. We claim that A in this form corresponds to a balanced phase jump. It is a rank-one real positive matrix, and therefore can be written $A = \sum_{ij=x,y,z} m_i m_j$ for some real 3-vector $\vec{m}$. When one diagonalizes the Lindblad equation, however, only a single Lindblad operator $L = \sum_{j=x,y,z} m_j \sigma_j$ remains. This operator is Hermitian and therefore must have two distinct, orthogonal eigenvectors. Such an operator describes a balanced phase jump.

In other words, as long as the system obeys the terms of the lemma, and does not consist of a single balanced phase jump operator, the system is purifiable. The first two cases in the theorem cover the remaining possible single-operator cases. The

remaining two cases can be seen by noting that two population jumps cannot share eigenvectors, since they have only one (we consider two operators that are multiples of each other to be essentially one process). The third case covers the possibility of one population jump: its eigenvector is its destination state, and that eigenvector must be shared with the other phase jumps. The fourth case in the theorem covers the possibility of no population jumps but more than one phase jump. Note that the phase jumps in the third and fourth cases do not need to be unbalanced. □

CHAPTER III

Three-Dimensional Systems

3.1 Projection of the three-dimensional Lindblad equation

Generalizing results from the two-dimensional case is not as straightforward as one would hope. There are several features that do not carry over to three or higher dimensions:

· The boundary of $\mathcal{D}_n$, the set of density matrices for an n-dimensional Hilbert space, is not the set of pure states in the same way that the set of pure states is the boundary of the Bloch ball. $\mathcal{D}_n$ has (real) dimension n^2-1, so its boundary must have dimension n^2-2. The set of pure states, however, is a $(2n-2)$-dimensional manifold.

· The Bloch vector may be defined for three dimensions: $r_j = \mathrm{Tr}(\rho\lambda_j^{GM})$, where the λ_j^{GM}'s are the Gell-Mann matrices. A similar formula applies for higher dimensions, with the Gell-Mann matrices being replaced by some orthonormal basis of $sl(n,\mathbb{C})$. The generalized Bloch vector must lie within a closed ball, as in two dimensions: $\sqrt{\sum r_j^2} \leq 1$. However, this ball includes vectors that do *not* correspond to physical density matrices. $\mathcal{D}_n$ is homeomorphic to a *proper* closed subset of the ball for $n \geq 3$.

· In two dimensions, the rate of optimal purity increase/decrease could be written

as a function of purity. In higher dimensions, there are distinct orbits with equal purity. In order to increase purity, it may be necessary to steer along an isopurity set (or first decrease purity) before finding an orbit where purity can be increased.

The first step is to understand the decomposition of $\mathcal{D}_3$ into its unitary orbits (much of what follows is inspired by Schirmer *et al.* [44]). The set of orbits can be indexed by the eigenvalues of ρ: $\lambda_1 \geq \lambda_2 \geq \lambda_3 = (1 - \lambda_1 - \lambda_2) \geq 0$. We can map the set of orbits to a compact subset of $\mathbb{R}^2$, $\mathcal{T}_3 : \mathcal{D}_3 \to \mathbb{R}^2$, $\vec{x} = \mathcal{T}_3(\rho) := (x_1, x_2)^T$:

$$\begin{aligned} x_1 &= \lambda_1 - \lambda_2 \\ x_2 &= \tfrac{1}{\sqrt{3}}(\lambda_1 + \lambda_2 - 2\lambda_3) = \tfrac{1}{\sqrt{3}}(1 - 3\lambda_3) \end{aligned} \quad . \tag{3.1}$$

This mapping has the advantage of matching two of the components of the Bloch vector when ρ is diagonal with decreasing elements, in which case $x_1 = r_3$ and $x_2 = r_8$. This mimics the $n = 2$ treatment: when the 2-dimensional density matrix was diagonal, r matched the third component of the Bloch vector.

The image of this mapping is a 2-simplex. The three vertices are:

- $(x_1, x_2) = (1, \frac{1}{\sqrt{3}})$ corresponding to $(\lambda_1, \lambda_2, \lambda_3) = (1, 0, 0)$. This point corresponds to the orbit of pure states, which is a four-dimensional manifold.

- $(x_1, x_2) = (0, \frac{1}{\sqrt{3}})$ corresponding to $(\lambda_1, \lambda_2, \lambda_3) = (\frac{1}{2}, \frac{1}{2}, 0)$. This point corresponds to the orbit of states that are completely mixed in a two-dimensional subspace, but do not populate the third orthogonal direction. It is also a four-dimensional manifold.

- $(x, y) = (0, 0)$ corresponding to $(\lambda_1, \lambda_2, \lambda_3) = (\frac{1}{3}, \frac{1}{3}, \frac{1}{3})$. This point corresponds to the completely mixed state, which is a zero-dimensional manifold.

As for the edges of the simplex:

· the vertical leg consists of orbits with $\lambda_1 = \lambda_2$, so that there is equal mixing between the two most populated eigenstates. Each orbit, except for that of $(0, 0)$, is a four-dimensional manifold.

· the hypotenuse consists of orbits with $\lambda_2 = \lambda_3$, so that there is equal mixing between the two least populated eigenstates. Each orbit, except for that of $(0, 0)$, is a four-dimensional manifold.

· the top horizontal leg consists of orbits with $\lambda_3 = 0$, so that there are only two populated eigenstates. Apart from its endpoints, each orbit is a six-dimensional manifold.

All interior points correspond to orbits that have distinct non-zero eigenvalues: $\lambda_1 > \lambda_2 > \lambda_3 > 0$. Each of these orbits is a six-dimensional manifold (note that the dimensionality of these orbits is determined by the multiplicity of the eigenvalues).

It will be of some use to consider an enlarged space, where instead of considering the set of unitary orbits, which corresponds to the set of *unordered* triples of eigenvalues, we look at the set of *ordered* triples of eigenvalues. In this case, the image of the mapping is an equilateral triangle, plus interior, with vertices $(1, \sqrt{3})$, $(-1, \sqrt{3})$ and $(0, -\frac{2}{\sqrt{3}})$, which correspond to the spectra $(1, 0, 0)$, $(0, 1, 0)$ and $(0, 0, 1)$. This simplex contains six copies of the previous simplex, corresponding to the six permutations of the eigenvalues. The original and extended simplices will henceforth be referred to as T_3 and T_3^E, respectively. They are shown in fig. 3.1.

To each point in T_3 and T_3^E belongs an orbit. The six-dimensional orbit is a complete flag manifold. Each point on the orbit is a complete flag $0 \subset \text{span}(|\psi_1\rangle) \subset \text{span}(|\psi_1\rangle, |\psi_2\rangle) \subset \text{span}(|\psi_1\rangle, |\psi_2\rangle, |\psi_3\rangle)$, where $|\psi_j\rangle$ is an eigenvector of ρ corresponding to λ_j. Let $\mathcal{V}_3$ be the set of such flags. The four-dimensional orbit is

composed of partial flags: $0 \subset \text{span}(|\psi_1\rangle) \subset \text{span}(|\psi_1\rangle, |\psi_2\rangle, |\psi_3\rangle)$ if $\lambda_2 = \lambda_3$ and $0 \subset \text{span}(|\psi_1\rangle, |\psi_2\rangle) \subset \text{span}(|\psi_1\rangle, |\psi_2\rangle, |\psi_3\rangle)$ if $\lambda_1 = \lambda_2$. Henceforth, $flg(|\psi_1\rangle, |\psi_2\rangle, |\psi_3\rangle)$ denotes the complete flag generated by the vectors in its argument.

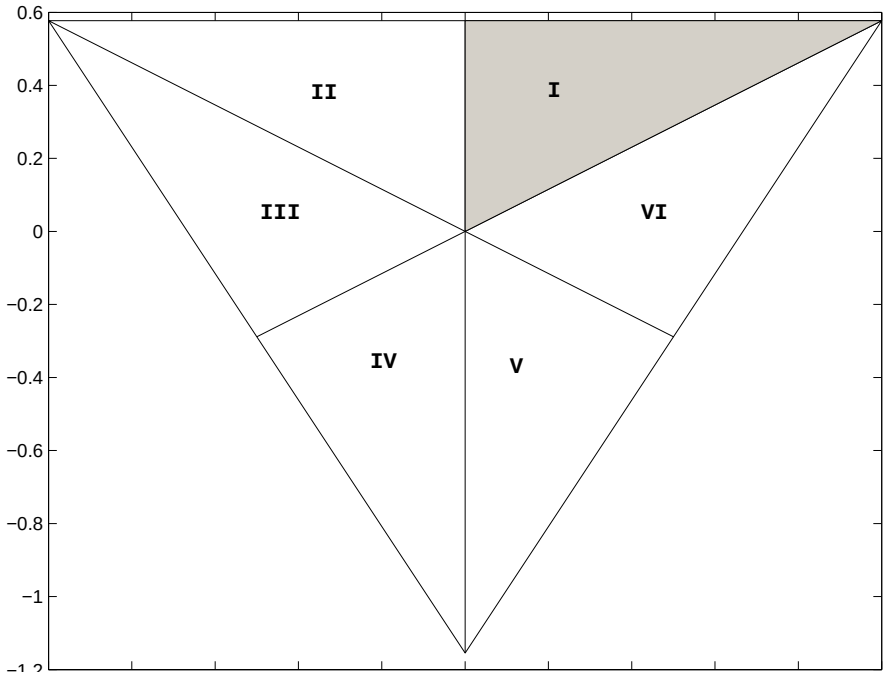

Figure 3.1: T_3^E. The shaded region is T_3. The central point corresponds to the completely mixed state and the three vertices correspond to the orbit of pure states. The "sextants" have been numbered for future reference.

The next step is to find differential equations for $\vec{x}$. The calculation in (2.12) is valid for all dimensions, so we have

$$\begin{aligned} \dot{x}_1 &= \langle\psi_1|\mathcal{L}_D(\rho)|\psi_1\rangle - \langle\psi_2|\mathcal{L}_D(\rho)|\psi_2\rangle \\ \dot{x}_2 &= -\sqrt{3}\langle\psi_3|\mathcal{L}_D(\rho)|\psi_3\rangle \end{aligned} \quad . \tag{3.2}$$

Now we can write

$$\rho = \frac{1}{3}I + \frac{x_1}{2}(|\psi_1\rangle\langle\psi_1| - |\psi_2\rangle\langle\psi_2|) + \frac{x_2}{2\sqrt{3}}(I - 3|\psi_3\rangle\langle\psi_3|).$$

Inserting this into (3.2), we get

$$\dot{x}_1 = \frac{1}{3}\sum_k(\langle\psi_1|[L_k, L_k^\dagger]|\psi_1\rangle - \langle\psi_2|[L_k, L_k^\dagger]|\psi_2\rangle)$$
$$+ \frac{x_1}{2}\sum_k(\langle\psi_1|L_k|\psi_1\rangle\langle\psi_1|L_k^\dagger|\psi_1\rangle + \langle\psi_2|L_k|\psi_2\rangle\langle\psi_2|L_k^\dagger|\psi_2\rangle$$
$$- \langle\psi_1|L_k|\psi_2\rangle\langle\psi_2|L_k^\dagger|\psi_1\rangle - \langle\psi_2|L_k|\psi_1\rangle\langle\psi_1|L_k^\dagger|\psi_2\rangle - \langle\psi_1|L_k^\dagger L_k|\psi_1\rangle - \langle\psi_2|L_k^\dagger L_k|\psi_2\rangle)$$
$$+ \frac{x_2}{2\sqrt{3}}\sum_k(\langle\psi_1|[L_k, L_k^\dagger]|\psi_1\rangle - \langle\psi_2|[L_k, L_k^\dagger]|\psi_2\rangle$$
$$- 3\langle\psi_1|L_k|\psi_3\rangle\langle\psi_3|L_k^\dagger|\psi_1\rangle + 3\langle\psi_2|L_k|\psi_3\rangle\langle\psi_3|L_k^\dagger|\psi_2\rangle)$$

$$\dot{x}_2 = -\frac{1}{\sqrt{3}}\sum_k\langle\psi_3|[L_k, L_k^\dagger]|\psi_3\rangle - \frac{\sqrt{3}}{2}x_1\sum_k(\langle\psi_3|L_k|\psi_1\rangle\langle\psi_1|L_k^\dagger|\psi_3\rangle - \langle\psi_3|L_k|\psi_2\rangle\langle\psi_2|L_k^\dagger|\psi_3\rangle)$$
$$- x_2\sum_k(\langle\psi_3|[L_k, L_k^\dagger]|\psi_3\rangle - 3\langle\psi_3|L_k|\psi_3\rangle\langle\psi_3|L_k^\dagger|\psi_3\rangle + 3\langle\psi_3|L_k^\dagger L_k|\psi_3\rangle).$$

If one inserts $I = \sum_j |\psi_j\rangle\langle\psi_j|$ between Lindblad operators, and abbreviates $w_{ij} = \sum_k |\langle\psi_i|L_k|\psi_j\rangle|^2$, we get the following system of differential equations:

(3.3)

$$\dot{x}_1 = \frac{1}{3}(2w_{12} - 2w_{21} + w_{13} - w_{23} + w_{32} - w_{31})$$
$$- \frac{x_1}{2}(2w_{12} + 2w_{21} + w_{32} + w_{31}) - \frac{x_2}{2\sqrt{3}}(2w_{21} - 2w_{12} + 2w_{13} - 2w_{23} + w_{31} - w_{32})$$
$$\dot{x}_2 = \frac{1}{\sqrt{3}}(w_{13} + w_{23} - w_{32} - w_{31}) - \frac{\sqrt{3}x_1}{2}(w_{31} - w_{32}) - \frac{x_2}{2}(2w_{13} + 2w_{23} + w_{31} + w_{32}).$$

Let $W_3 \subset \mathbb{R}^6$ be the image of the map $\mathcal{W} : \mathcal{V}_3 \to \mathbb{R}^6$, such that $\mathcal{W}(flg(|\psi_1\rangle, |\psi_2\rangle, |\psi_3\rangle)) = \vec{w} := (w_{12}, w_{21}, w_{23}, w_{32}, w_{31}, w_{13})$. If $\vec{w}$ is held constant, (3.3) is an affine differential equation:

$$\dot{\vec{x}} = \vec{b}(\vec{w}) - A(\vec{w})\vec{x} =: \mathcal{F}(\vec{x}, \vec{w}). \tag{3.4}$$

We can sum up the situation as follows:

$$\mathcal{D}_3 \subset T_3 \times \mathcal{V}_3 \subset T_3^E \times \mathcal{V}_3$$
$$T_3^E \times \mathcal{V}_3 \xrightarrow{Id \times \mathcal{W}} T_3^E \times W_3 \xrightarrow{\mathcal{F}} TT_3^E.$$

The first inclusion in the first line is not proper however, because on the boundary of T_3, multiple complete flags map to the same density matrix.

The control aspect of these differential equations must be clearly defined. Ultimately, we wish to control the state space $\mathcal{D}_3$ with Hamiltonians taking values in the control set $SU(3)$. To do this, we want to "pull back" to one of the state spaces T_3 or T_3^E, using the control set of the flags $\mathcal{V}_3$. These control problems are not quite equivalent, however. In the interior of T_3, which we will denote T_3^o, each orbit is homeomorphic to $\mathcal{V}_3$. On the boundary of T_3, however, some orbits have dimension 4 or 0. As in the two-dimensional case, we will make the assumption that we have sufficient control of the Hamiltonian piece of the Lindblad equation that we may choose the position along the orbit on an arbitrarily short timescale. But because the orbits along part of the boundary of T_3 lose dimensionality, we lose control there. For example, at the completely mixed state, we have no control: $\dot{\rho} = \frac{1}{3}\sum_k [L_k, L_k^\dagger]$, and there is no dependence on the structure of the Hamiltonian. Similarly, whenever two eigenvalues cross, we may choose the eigenvector with the distinct eigenvalue, but we do not have the ability to choose a basis of the degenerate sector. The choice of the former, but not the latter, restricts us to a four-dimensional manifold, rather than a six-dimensional one.

With this in mind, we modify our objective somewhat. Instead of controllability over $\mathcal{D}_3$, we seek controllability over $\mathcal{D}_3^o$, the set of density matrices with distinct, non-zero eigenvalues. To do this we look for controllability on T_3^E using controls

found in $\mathcal{V}_3$.The intersection of the controllable sets with T_3^o can then be used to infer controllability on $\mathcal{D}_3^o$. To make this precise, let us state the following theorem:

Theorem III.1. *Let $\mathcal{U}$ be a maximally globally controllable open subset of T_3^E, where the control functions are piecewise-differentiable function taking values in $\mathcal{V}_3$. Let $\vec{x}_1$ and $\vec{x}_2$ be in $\mathcal{U} \cap T_3^o$. The trajectory between them may exit (and re-enter) T_3^o. Then any density matrix $\rho_1 \in \mathcal{T}_3^{-1}(\vec{x}_1)$ may be steered arbitrarily close to $\rho_2 \in \mathcal{T}_3^{-1}(\vec{x}_2)$.*

Proof. We start with a trajectory $\vec{x}^E(t)$ through T_3^E which is effected by the trajectory through $\mathcal{V}_3$ defined by the vector trajectories $\{|\psi_i^E\rangle(t)\}$. $\vec{x}^E(t)$ may exit and re-enter T_3, but we can alway find a trajectory that does not exit by permuting the vectors. Any piece of the trajectory that is in sextants II through VI can be transformed by applying elements of the symmetric group S_3. For example, a trajectory piece in sextant II that starts at $\vec{x}(t_a)$ and finishes at $\vec{x}(t_b)$ can be reflected across the x_2 axis into sextant I by exchanging $|\psi_1^E\rangle(t)$ and $|\psi_2^E\rangle(t)$, which in turn exchanges w_{12} with w_{21}, w_{31} with w_{32} and w_{13} with w_{23}. It can be checked that this sends $\dot{x}_1$ to -$\dot{x}_1$ and fixes $\dot{x}_2$. So a trajectory starting at $(-x_1(t_a), x_2(t_a))$ will finish at $(-x_1(t_b), x_2(t_b))$ using these permuted controls. Similarly, we can take care of sextants III through VI by exchanging indices 1 and 3 (sextant IV), exchanging indices 2 and 3 (sextant VI), cycling 1 to 2 to 3 to 1 (sextant III) and cycling 1 to 3 to 2 to 1 (sextant V). Using this procedure, we have a new trajectory $\vec{x}(t)$, using different controls $flg(\{|\psi_i(t)\rangle\})$, that is now entirely contained in T_3.

The next problem is the sections of the trajectory that lie on the boundary of T_3. Here we will resort to the fact that under (3.3), two nearby points will stay nearby:

$$\begin{aligned}\frac{d}{dt}||\vec{x}_a - \vec{x}_b||^2 &= 2(\vec{x}_a - \vec{x}_b) \cdot (\dot{\vec{x}}_a - \dot{\vec{x}}_b) \\ &= -2(\vec{x}_a - \vec{x}_b)A(\vec{w})(\vec{x}_a - \vec{x}_b).\end{aligned}$$

Since $A(\vec{w})$ can only have eigenvalues with non-negative real part (see chapter four), this derivative must be non-positive. Therefore, even though $\vec{x}(t)$ may contain points on the boundary of T_3, we can find a nearby trajectory $\vec{x}^o(t)$ that does not. If $\vec{x}(t)$ hits the boundary at time t_i, we can deal with this by removing a gap from the control function: for $t \geq t_i - \delta t$, let $|\psi_i(t)\rangle = |\psi_i(t+\delta t)\rangle$. The new trajectory will stay within a distance $||\vec{x}(t_i) - \vec{x}(t_i - \delta t)||$. Note that if $\vec{x}(t)$ travels along the boundary for a time period longer than zero, the new trajectory will not hit the boundary during that time. That would require $||\vec{x}_{new} - \vec{x}_{old}|| = 0$, which cannot happen for a time-varying affine system. Of course, the new trajectory may hit the boundary at different times than the old, but we can always repeat the process.

So we have a trajectory $\vec{x}^o(t)$ that is controlled by $flg(\{|\psi_i(t)\rangle\})$. Now we want to show there is a Hamiltonian trajectory that effects the flag trajectory, and it turns out we have an explicit formula. The diagonal elements in the $\{|\psi_i(t)\rangle\}$ basis can be taken to be zero, and the off-diagonal elements are

$$\langle\psi_j|H|\psi_k\rangle = \frac{\lambda_j\langle\dot{\psi_j}|\psi_k\rangle + \lambda_k\langle\psi_j|\dot{\psi_k}\rangle - \langle\psi_j|\mathcal{L}_D(\rho)|\psi_k\rangle}{i(\lambda_j - \lambda_k)}.$$

Notice the formula is only defined for distinct λ_j, which of course is not a surprise. To show this formula works, we can decompose the time-derivative of ρ into the time-derivatives of its eigenvalues and eigenvectors (which only works when there are distinct eigenvalues), and work backwards by using our Hamiltonian formula to reconstruct the Lindblad equation:

$$\begin{aligned}
\dot{\rho} &= \sum_j \dot{\lambda_j}|\psi_j\rangle\langle\psi_j| + \sum_j \lambda_j(|\dot{\psi_j}\rangle\langle\psi_j| + |\psi_j\rangle\langle\dot{\psi_j}|) \\
&= \sum_j \langle\psi_j|\mathcal{L}_D(\rho)|\psi_j\rangle|\psi_j\rangle\langle\psi_j| + \sum_{j,k} \lambda_j(|\psi_k\rangle\langle\psi_k|\dot{\psi_j}\rangle\langle\psi_j| + |\psi_j\rangle\langle\dot{\psi_j}|\psi_k\rangle\langle\psi_k|) \\
&= \mathcal{L}_D(\rho) + \sum_{j\neq k}(\lambda_k\langle\psi_j|\dot{\psi_k}\rangle|\psi_j\rangle\langle\psi_k| + \lambda_j\langle\dot{\psi_j}|\psi_k\rangle|\psi_j\rangle\langle\psi_k| - \langle\psi_j|\mathcal{L}_D(\rho)|\psi_k\rangle|\psi_j\rangle\langle\psi_k|)
\end{aligned}$$

$$= \mathcal{L}_D(\rho) + \sum_{j\neq k} \frac{\lambda_j \langle\dot{\psi}_j|\psi_k\rangle|\psi_j\rangle\langle\psi_k| + \lambda_k\langle\psi_j|\dot{\psi}_k\rangle|\psi_j\rangle\langle\psi_k| - \langle\psi_j|\mathcal{L}_D(\rho)|\psi_k\rangle|\psi_j\rangle\langle\psi_k|}{i(\lambda_j - \lambda_k)} i(\lambda_j - \lambda_k)$$

$$= \mathcal{L}_D(\rho) + \sum_{j\neq k} \langle\psi_j|H|\psi_k\rangle|\psi_j\rangle\langle\psi_k| i(\lambda_j - \lambda_k)$$

$$= \mathcal{L}_D(\rho) + \sum_{j\neq k;l} [-i\langle\psi_j|H|\psi_k\rangle|\psi_j\rangle\langle\psi_k|, \lambda_l|\psi_l\rangle\langle\psi_l|]$$

$$= \mathcal{L}_D(\rho) + [-iH, \rho].$$

Going from the second to third line, we've use the fact that $\langle\dot{\psi}_j|\psi_j\rangle + \langle\psi_j|\dot{\psi}_j\rangle = 0$.

We now have shown that we can steer a density matrix unitarily equivalent to ρ_1 arbitrarily close to a density matrix unitarily equivalent to ρ_2. Let these unitary equivalent matrices be ρ_1' and ρ_2'. They are determined by the initial and final points of $flg\{|\psi_j(t)\rangle\}$. To steer ρ_1 to ρ_2, we want to "book-end" the trajectory prescribed by $\vec{x}^o(t)$ by two fast unitary transformations. These will not connect precisely, but we can show that the error is quite manageable. In summary, we will quickly drive ρ_1 to $\bar{\rho}_1'$ which is near ρ_1', then steer $\bar{\rho}_1'$ to $\bar{\rho}_2'$ which is near ρ_2', and finally quickly drive $\bar{\rho}_2'$ to $\bar{\rho}_2$, which hopefully will be near ρ_2. Let the transit times be Δt_1 and Δt_2 for the fast transitions, and T for $\vec{x}^o(t)$. Let $\rho_j' = e^{-iH_j}\rho_j e^{iH_j}$, so that any Hamiltonian of the form $\frac{H_j}{\Delta t_j}$ can connect the two. We have

$$\begin{aligned}
||\bar{\rho}_2 - \rho_2|| =& ||\rho_1 + \int_0^{\Delta t_1} [-i\frac{H_1}{\Delta t_1}, \rho]dt + \int_0^{\Delta t_1} \mathcal{L}_D(\rho)dt + \int_{\Delta t_1}^{\Delta t_1+T} [-iH, \rho]dt \\
&+ \int_{\Delta t_1}^{\Delta t_1+T} \mathcal{L}_D(\rho)dt + \int_{\Delta t_1+T}^{\Delta t_1+T+\Delta t_2} [-i\frac{H_2}{\Delta t_2}, \rho]dt + \int_{\Delta t_1+T}^{\Delta t_1+T+\Delta t_2} \mathcal{L}_D(\rho)dt - \rho_2|| \\
=& ||\rho_1' + \int_0^{\Delta t_1} \mathcal{L}_D(\rho)dt + \int_{\Delta t_1}^{\Delta t_1+T} [-iH, \rho]dt + \int_{\Delta t_1}^{\Delta t_1+T} \mathcal{L}_D(\rho)dt \\
&+ \int_{\Delta t_1+T}^{\Delta t_1+T+\Delta t_2} [-i\frac{H_2}{\Delta t_2}, \rho]dt + \int_{\Delta t_1+T}^{\Delta t_1+T+\Delta t_2} \mathcal{L}_D(\rho)dt - \rho_2|| \\
=& ||\rho_2' + \int_0^{\Delta t_1} \mathcal{L}_D(\rho)dt + \int_{\Delta t_1+T}^{\Delta t_1+T+\Delta t_2} [-i\frac{H_2}{\Delta t_2}, \rho]dt \\
&+ \int_{\Delta t_1+T}^{\Delta t_1+T+\Delta t_2} \mathcal{L}_D(\rho)dt - \rho_2||
\end{aligned}$$

$$
\begin{aligned}
&= || \int_0^{\Delta t_1} \mathcal{L}_D(\rho) dt + \int_{\Delta t_1 + T}^{\Delta t_1 + T + \Delta t_2} \mathcal{L}_D(\rho) dt || \\
&\leq (\Delta t_1 + \Delta t_2) \cdot \sup_{\rho \in \mathcal{D}_3} ||\mathcal{L}_D(\rho)|| \\
&\leq (\Delta t_1 + \Delta t_2) \cdot \sup_{\rho \in \mathcal{D}_3} \sum_k (||L_k \rho L_k^\dagger|| + || - \frac{1}{2}\{L_k^\dagger L_k, \rho\}||) \\
&\leq (\Delta t_1 + \Delta t_2) \cdot 2 \sum_k ||L_k||^2.
\end{aligned}
$$

Note that the preceding technically only applies if $\vec{x}^E(t)$ and $\vec{x}^o(t)$ coincide, but the modifications to include the other case are straightforward. □

The preceding theorem covers global controllability, but the concept of small-time local controllability will be covered more in this thesis. While STLC is a stronger condition, this theorem is much less involved:

Theorem III.2. *If one has STLC at a point $\vec{x}_0 \in T_3^o$, then one has STLC at any density matrix $\rho_0 \in \mathcal{T}_3^{-1}(\vec{x}_0)$.*

Proof. A point is STLC if one can generate a set of tangent vectors in its tangent space whose convex cone is the entire tangent space (see chapter four). The tangent space at ρ_0 is the product of the tangent space at $\vec{x}_0$ with the tangent space of the unitary orbit at ρ_0. Vectors in the latter are generated by the Hamiltonians, and since we've assumed we can generate any Hamiltonian, and we've assumed STLC at $\vec{x}_0$, STLC at ρ_0 follows. □

Henceforth, we will look for controllability over open subsets of T_3^E where our control set is taken to be $\mathcal{V}_3$, even on the points where eigenvalues cross, with the understanding that we will later restrict to T_3^o.

3.2 Using a discrete control set

The procedure used in the previous chapter for the two-dimensional case could in principle be used for three dimensions. Our controls can be written in terms of three Bloch vectors $\vec{m}$, $\vec{n}$ and $\vec{p}$:

$$
\begin{aligned}
|\psi_1\rangle &= \sqrt{\frac{1+m_1}{2}}|1\rangle + \frac{m_2+im_3}{\sqrt{2(1+m_1)}}\left(\sqrt{\frac{1+n_1}{2}}|2\rangle + \frac{n_2+in_3}{\sqrt{2(1+n_1)}}|3\rangle\right)\\
|\psi_2'\rangle &= -\sqrt{\frac{1-m_1}{2}}|1\rangle + \frac{m_2+im_3}{\sqrt{2(1-m_1)}}\left(\sqrt{\frac{1+n_1}{2}}|2\rangle + \frac{n_2+in_3}{\sqrt{2(1+n_1)}}|3\rangle\right)\\
|\psi_3'\rangle &= -\sqrt{\frac{1-n_1}{2}}|2\rangle + \frac{n_2+in_3}{\sqrt{2(1-n_1)}}|3\rangle\\
|\psi_2\rangle &= \sqrt{\frac{1+p_1}{2}}|\psi_2'\rangle + \frac{p_2+ip_3}{\sqrt{2(1+p_1)}}|\psi_3'\rangle\\
|\psi_3\rangle &= -\sqrt{\frac{1-p_1}{2}}|\psi_2'\rangle + \frac{p_2+ip_3}{\sqrt{2(1-p_1)}}|\psi_3'\rangle.
\end{aligned}
$$

where $\sum m_j^2 = \sum n_j^2 = \sum p_j^2 = 1$. The six coefficients w_{jk} could be computed in terms of the nine components and the elements of the Lindblad operators. If the Lindblad operators are broken down according to the GKS matrix, which has 64 real components, one would need to compute $6 \times 64 = 384$ different expressions, which may or may not be polynomials. Given co-ordinates (x_1, x_2), we can then ask what tangent vectors $(\dot{x}_1, \dot{x}_2)$ we can achieve in a given direction. This would yield four constraints (three for the Bloch vectors, one to constrain the direction) to optimize the quantity $\dot{x_1}^2 + \dot{x_2}^2$. The method of Lagrange multipliers would yield thirteen equations in terms of thirteen variables (four multipliers and three Bloch vectors).

Instead of tackling such a daunting mess of algebra, we will consider a less ambitious problem. To motivate this, we will return to the two-dimensional case. In general, optimizing $\dot{r}$ at the left endpoints $r = 0$ is much easier than for $r > 0$. There, $\dot{r} = \vec{b} \cdot \hat{n}$, and clearly the optimal values are $\pm|\vec{b}|$ and these are achieved by

the two controls $\hat{n} = \pm\vec{b}/|\vec{b}|$. One can then easily compute the size of the globally controllable set using only those two controls: $r_T^R = \frac{|\vec{b}|^3}{tr(A)|\vec{b}|^2 - \sum_j a_j b_j^2}$, where the superscript R denotes "pertaining to the reduced control set". $f_M^R(r) = |\vec{b}|(1 - \frac{r}{r_T^R})$ and $f_m^R(r) = |\vec{b}|(-1 - \frac{r}{r_T^R})$. The difference between them is $2|\vec{b}|$, which is independent of r. Fig. 3.2 shows a typical comparison of f_m and f_M with f_m^R and f_M^R. The globally controllable set is reduced, but not by more than 25%. Note the latter pair are the linearizations of the former about $r = 0$. This is true in general, and we will now show this.

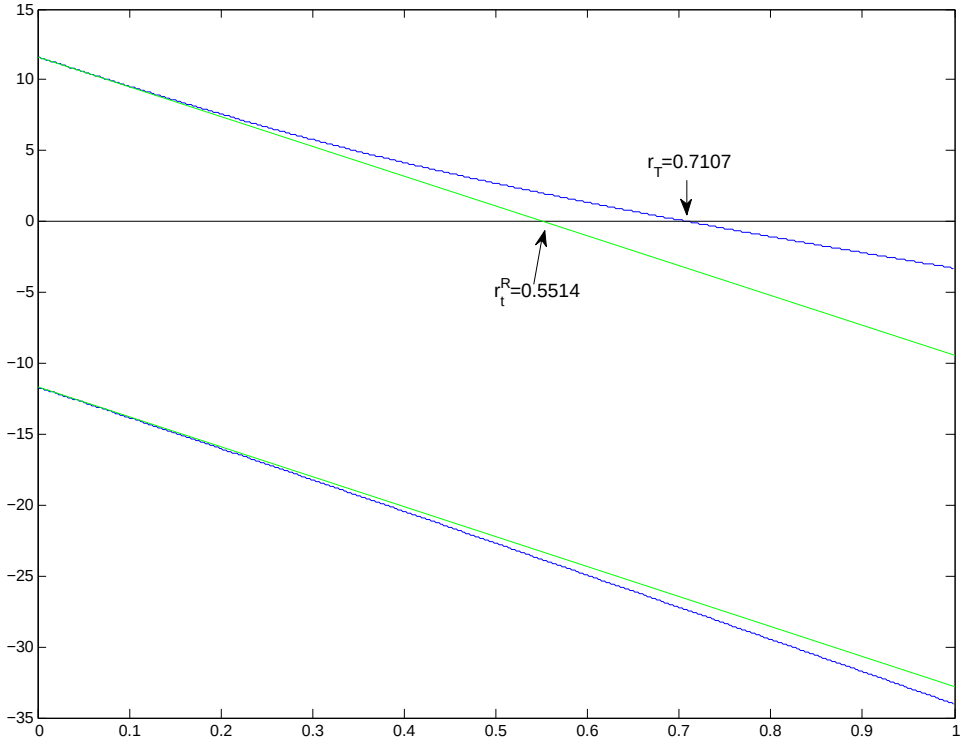

Figure 3.2: f_M^R and f_m^R are shown (in green) for a two-dimensional system with $a_1 = 15$, $a_2 = 8$, $a_3 = 1$, $b_1 = 3.7101$, $b_2 = 2.9331$, $b_3 = 10.6537$. f_M and f_m are shown in blue for contrast.

Proposition III.3. *For the control system described in (2.2),*

$$f_M'(r) = f_m'(r) = -\frac{|\vec{b}|}{r_T^R}.$$

Proof. Let $r = \delta r$ be small. Using Lagrange multipliers on equation (2.2), we get

$b_j + 2\delta r a_j n_j = 2\lambda n_j$. This yields $n_j = \frac{b_j}{2(\lambda - \delta r a_j)} \simeq \frac{b_j}{2\lambda}(1 + \frac{\delta r a_j}{\lambda})$. Substituting into the normalization constraint $\sum n_j^2 = 1$, and re-arranging, we get the cubic polynomial:

$$4\lambda^3 - |\vec{b}|^2\lambda - 2\delta r \sum a_j b_j^2 = 0.$$

For $\delta r = 0$, the roots are $\lambda = 0, \pm\frac{|\vec{b}|}{2}$. Linearizing the cubic polynomial about those points, we find the perturbed roots are $\lambda = -2\delta r \frac{\sum a_j b_j^2}{|\vec{b}|^2}, \pm\frac{|\vec{b}|}{2} + \delta r \frac{\sum a_j b_j^2}{|\vec{b}|^2}$. The first root leads to n_j's that are unbounded, so we can neglect it. The other two give, to first order, $n_j = \pm\frac{b_j}{|\vec{b}|}(1 \pm 2\delta r(\frac{a_j}{|\vec{b}|} - \frac{\sum a_k b_k^2}{|\vec{b}|^3}))$. And in turn, $\sum_j b_j n_j = \pm|\vec{b}|$. There is no linear term in the latter expression, which means, for small δr, $\dot{r} = \pm|\vec{b}| + \delta r \sum a_j(\frac{b_j}{|\vec{b}|} - 1)$. This, however, is just f_M^R and f_m^R, so we are done. □

So at least for two dimensions, trimming our control set from a sphere to a pair allows us to greatly simplify the mathematics, while still retaining a significant portion of the globally controllable set. The simplicity is due to the fact that, regardless of dimension, the Lindblad term reduces nicely when the density matrix is completely mixed: $\mathcal{L}_D(\frac{1}{n}I) = \frac{1}{n}\sum_k [L_k, L_k^\dagger]$. In three dimensions, we can precisely describe $\mathcal{F}(\vec{0}, W_3)$, the set of tangent vectors $\dot{\vec{x}}$ we can achieve when $\vec{x} = (0, 0)$. We lay this out in the following proposition:

Proposition III.4. *Consider the differential equations (3.3). Let* $\{|\Lambda_j\rangle, j = 1, 2, 3\}$ *be the eigenvectors of the operator* $\sum_k \frac{1}{3}[L_k, L_k^\dagger]$*, with eigenvalues* λ_j^{LC}*. Assume the eigenvalues are indexed in descending order, and since the Lindblad operators are traceless, they must sum to zero. If the eigenvalues are distinct,* $\mathcal{F}(\vec{0}, W_3)$ *is bounded by the hexagon with vertices*

$$(\pm(\lambda_1^{LC} - \lambda_2^{LC}), \sqrt{3}(\lambda_1^{LC} + \lambda_2^{LC}))$$

$$(\pm(\lambda_1^{LC} - \lambda_3^{LC}), \sqrt{3}(\lambda_1^{LC} + \lambda_3^{LC}))$$

$$(\pm(\lambda_2^{LC} - \lambda_3^{LC}), \sqrt{3}(\lambda_2^{LC} + \lambda_3^{LC})).$$

This is a tight bound: every point on the hexagon can be achieved. The six vertices are achieved by setting $\{|\psi_j\rangle\}$ to one of the six permutations of $\{|\Lambda_j\rangle\}$.

If there is a double eigenvalue, the vertices converge so that the hexagon becomes a triangle. If there is triple multiplicity, all eigenvalues are zero, which means the system is unital, and the hexagon is now just the zero point.

Proof. First, $\dot{x}_2 = -\sqrt{3}\langle\psi_3|\mathcal{L}_D(\frac{1}{3}I)|\psi_3\rangle$. Since $\lambda_3^{LC} \leq \langle\psi_3|\mathcal{L}_D(\frac{1}{3}I)|\psi_3\rangle \leq \lambda_1^{LC}$, we have the bounds

$$-\sqrt{3}\lambda_1^{LC} = -\sqrt{3}(\lambda_2^{LC} + \lambda_3^{LC}) \leq \dot{x}_2 \leq -\sqrt{3}\lambda_3^{LC} = -\sqrt{3}(\lambda_1^{LC} + \lambda_2^{LC}).$$

These bounds are saturated when $|\psi_3\rangle = |\Lambda_1\rangle$ and $|\Lambda_3\rangle$, respectively.

If we choose $|\psi_3\rangle = |\Lambda_3\rangle$, $|\psi_1\rangle$ and $|\psi_2\rangle$ must be orthogonal superpositions of $|\Lambda_1\rangle$ and $|\Lambda_2\rangle$. In fact if $|\psi_1\rangle = \cos(\frac{\phi}{2})|\Lambda_1\rangle + e^{i\theta}\sin(\frac{\phi}{2})|\Lambda_2\rangle$ and $|\psi_2\rangle = -\sin(\frac{\phi}{2})|\Lambda_1\rangle + e^{i\theta}\cos(\frac{\phi}{2})|\Lambda_2\rangle$, we have

$$\dot{x} = \langle\psi_1|\mathcal{L}_D(\frac{1}{3}I)|\psi_1\rangle - \langle\psi_2|\mathcal{L}_D(\frac{1}{3}I)|\psi_2\rangle = \cos(\phi)(\lambda_1^{LC} - \lambda_2^{LC}).$$

This traces out the top, horizontal edge of the hexagon, and we can do the same for the bottom by choosing $|\psi_3\rangle = |\Lambda_1\rangle$. The remaining four edges can be treated by noting they always have the slopes $\pm\sqrt{3}$. It follows that the quantities $\dot{x}_2 \pm \sqrt{3}\dot{x}_1$ have constant bounds in the same way $\dot{x}_1$ and $\dot{x}_2$ do. □

Figure 3.3 shows some examples. The hexagon is regular when $\lambda_2^{LC} = 0$, so that $\lambda_1^{LC} = -\lambda_3^{LC}$, which is shown in the upper left frame. The upper right shows what happens for $\lambda_2^{LC} > 0$: the hexagon is no longer regular but there is still a non-trivial group of symmetries. Namely, there are three reflections and two rotations that leave it invariant, so that the symmetry group is the symmetric group S_3. This is natural,

considering one moves between vertices of the hexagon by permuting the eigenbasis $\{|\psi_j\rangle\}$.

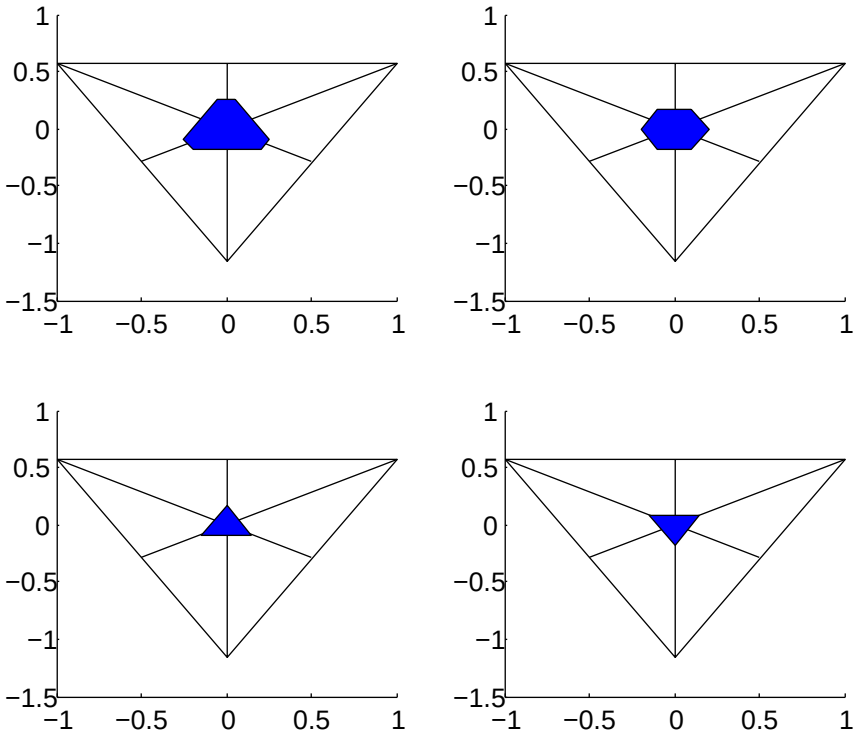

Figure 3.3: Possible $\mathcal{F}(\vec{0}, W_3)$ for various $\mathcal{L}_D(\rho)$. The sets are superimposed on T_3^E. The spectra for $\mathcal{L}_D(\frac{1}{3}I)$ are: $\{0.1, 0.05, -0.15\}$ (upper left), $\{0.1, 0, -0.1\}$ (upper right), $\{0.05, 0.05, -0.1\}$ (lower left), $\{0.1, -0.05, -0.05\}$ (lower right)

The next chapter will consider the problem of controlling the state space T_3^E using the discrete control set $\{flg(\{|\Lambda_{\sigma(j)}\rangle) : j = 1, 2, 3\} : \sigma \in S_3\}$. Our results however will hold for *any* set of six permuted flags. We will refer to the system with the control set $\{flg(\{|\psi_{\sigma(j)}\rangle) : j = 1, 2, 3, \sigma \in S_3\}$, where $\{|\psi_{\sigma(j)}\rangle) : j = 1, 2, 3\}$ is any eigenbasis, as the $\mathcal{V}_3^R$-control problem. We will finish this chapter with a proposition on the symmetry properties of this reduced problem. Let W_3^R be the image of $\mathcal{V}_3^R$ under $\mathcal{W}$. We are essentially considering six vector fields on T_3^E, $\mathcal{F}(\cdot, \vec{w})$, where $\vec{w}$ is one of the six elements of W_3^R. One can generate all six vector fields from one by using rotations and reflections:

Proposition III.5. *Let* $\vec{w}^0 = \mathcal{W}(flg(|\Lambda_1\rangle, |\Lambda_2\rangle, |\Lambda_3\rangle))$*, the element of* W_3 *corresponding to the vertex of* $\mathcal{F}(\vec{0}, W_3)$ *in* T_3*. This control leads to the vector field* $\dot{\vec{x}} = \vec{b}(\vec{w}^0) - A(\vec{w}^0)\vec{x} =: \vec{b}_0 - A_0\vec{x} =: V_0(\vec{x})$*. Define the reflection matrices about the interior lines of* T_3^E *(*$x_1 = 0$ *and* $x_1 = \pm\sqrt{3}x_2$*):*

$$R_1 = \begin{pmatrix} -1 & 0 \\ 0 & 1 \end{pmatrix} \qquad R_2 = \begin{pmatrix} 1/2 & \sqrt{3}/2 \\ \sqrt{3}/2 & -1/2 \end{pmatrix} \qquad R_3 = \begin{pmatrix} 1/2 & -\sqrt{3}/2 \\ -\sqrt{3}/2 & -1/2 \end{pmatrix}.$$

and let $R_0 := I$*,* $R_4 := R_3R_1$ *and* $R_5 := R_3R_2$*,* i.e. *the rotation matrices by angles of* 0*,* $2\pi/3$ *and* $4\pi/3$*. These matrices form a representation of the symmetric group* S_3*. Then the remaining vector fields generated by the five remaining elements of* W_3 *can be written* $V_j(\vec{x}) = R_j\vec{b}_R - (R_jA_RR_j^{-1})\vec{x}$*,* $j = 1 \ldots 5$*.*

Proof. We will prove the case for $V_2(\vec{x})$, as all the remaining cases would proceed in a similar fashion. One finds $V_2(\vec{x})$ from $V_I(\vec{x})$ by exchanging $|\psi_2\rangle$ and $|\psi_3\rangle$. Taking (3.3) and exchanging the indices 2 and 3, we get

$$\begin{aligned}
\dot{x}_1 &= \tfrac{1}{3}(2w^0_{13} - 2w^0_{31} + w^0_{12} - w^0_{32} + w^0_{23} - w^0_{21}) \\
&\quad -\tfrac{x_1}{2}(2w^0_{13} + 2w^0_{31} + w^0_{23} + w^0_{21}) - \tfrac{x_2}{2\sqrt{3}}(2w^0_{31} - 2w^0_{13} + 2w^0_{12} - 2w^0_{32} + w^0_{21} - w^0_{23}) \\
\dot{x}_2 &= \tfrac{1}{\sqrt{3}}(w^0_{12} + w^0_{32} - w^0_{23} - w^0_{21}) - \tfrac{\sqrt{3}x_1}{2}(w^0_{21} - w^0_{23}) - \tfrac{x_2}{2}(2w^0_{12} + 2w^0_{32} + w^0_{21} + w^0_{23}).
\end{aligned}$$

On the other hand,

$$\begin{aligned}
R_2\vec{b}_0 &= \begin{pmatrix} 1/2 & \sqrt{3}/2 \\ \sqrt{3}/2 & -1/2 \end{pmatrix} \begin{pmatrix} \frac{2}{3}w^0_{12} - \frac{2}{3}w^0_{21} + \frac{1}{3}w^0_{13} - \frac{1}{3}w^0_{23} + \frac{1}{3}w^0_{32} - \frac{1}{3}w^0_{31}) \\ \frac{1}{\sqrt{3}}w^0_{13} + \frac{1}{\sqrt{3}}w^0_{23} - \frac{1}{\sqrt{3}}w^0_{32} - \frac{1}{\sqrt{3}}w^0_{31}) \end{pmatrix} \\
&= \begin{pmatrix} \frac{1}{3}w^0_{12} - \frac{1}{3}w^0_{21} + \frac{2}{3}w^0_{13} - \frac{1}{3}w^0_{23} - \frac{2}{3}w^0_{32} - \frac{1}{3}w^0_{31}) \\ \frac{1}{\sqrt{3}}w^0_{12} - \frac{1}{\sqrt{3}}w^0_{21} - \frac{1}{\sqrt{3}}w^0_{23} + \frac{1}{\sqrt{3}}w^0_{32}) \end{pmatrix}.
\end{aligned}$$

Also,

$$R_2A_0R_2^{-1} = \begin{pmatrix} \frac{1}{2} & \frac{\sqrt{3}}{2} \\ \frac{\sqrt{3}}{2} & -\frac{1}{2} \end{pmatrix} \times$$

$$\begin{pmatrix} \frac{1}{2}(2w_{12}^0+2w_{21}^0+w_{31}^0+w_{32}^0) & \frac{1}{2\sqrt{3}}(2w_{21}^0-2w_{12}^0+2w_{13}^0-2w_{23}^0+w_{31}^0+w_{32}^0) \\ \frac{\sqrt{3}}{2}(w_{31}^0-w_{32}^0) & \frac{1}{2}(2w_{13}^0+2w_{23}^0+w_{31}^0-w_{32}^0) \end{pmatrix} \begin{pmatrix} \frac{1}{2} & \frac{\sqrt{3}}{2} \\ \frac{\sqrt{3}}{2} & -\frac{1}{2} \end{pmatrix}$$

$$= \begin{pmatrix} \frac{1}{2}(2w_{31}^0+2w_{13}^0+w_{21}^0+w_{23}^0) & \frac{1}{2\sqrt{3}}(2w_{12}^0+2w_{31}^0-2w_{32}^0-2w_{13}^0+w_{21}^0-w_{23}^0) \\ \frac{\sqrt{3}}{2}(w_{21}^0-w_{23}^0) & \frac{1}{2}(2w_{12}^0+2w_{32}^0+w_{21}^0+w_{23}^0) \end{pmatrix}.$$

The two components of $R_2\vec{b}_0$ and the four components of $R_2A_0R_2^{-1}$ match the components in (3.5), so we are done. □

CHAPTER IV

Control of Three-Dimensional Systems using the Discrete Control Set

4.1 Small-time local controllability

For the $\mathcal{V}_3^R$ control system, we can specify a condition for STLC in terms of convex cones. The convex cone generated by a collection of vectors is the set of all linear combinations of those vectors with non-negative coefficients.

Proposition IV.1. *T_3^E is STLC at a point $\vec{x}_0$ if the cone generated by the vector fields $\{V_j(\vec{x}_0)\}$ is $\mathbb{R}^2$. Equivalently, if we partition the interval $[0, 2\pi]$ by considering the angular separations of angularly adjacent vectors, then the system is STLC at $\vec{x}_0$ iff the largest angular separation is strictly less than π.*

Proof. One can generate motions by switching between the vector fields for very short time intervals. Turning on the ith vector field for time interval δt_1, followed by the jth vector field for δt_2, yields, to first order, a displacement $\delta t_1 V_i(\vec{x}_0) + \delta t_2 V_j(\vec{x}_0 + \delta t_1 V_i(\vec{x}_0)) \simeq \delta t_1 V_i(\vec{x}_0) + \delta t_2 V_j(\vec{x}_0)$. Since δt_1 and δt_2 are arbitrary non-negative small numbers, we can generate small forward motions that lie in the cone generated by $V_i(\vec{x}_0)$ and $V_j(\vec{x}_0)$. The same follows for a collection of six vector fields, instead of two. For STLC however we need to be able generate small motions in any direction. Therefore, the cone generated by the six vector fields must contain all directions, *i.e.*

it must be $\mathbb{R}^2$.

Concerning the equivalent statement, a pair of vectors can be described by an angular separation $\alpha \leq \pi$, so that one vector is an angle α counter-clockwise from the other. The cone generated by this pair includes only vectors with a counter-clockwise angle from the first vector taken in the interval $[0, \alpha]$ and excludes vectors with angles in the interval $(\alpha, 2\pi)$. That is, vectors can't generate other vectors in the sector that has an angle of π or greater. This fact generalizes to a collection of vectors. One can only generate vectors in sectors that have an angle less than π. If one orders the vectors in counter-clockwise order, and there is a sector with an angle larger than π, one cannot generate vectors there. Vectors can be generated in all other sectors. Fig. 5.3 contrasts an example where the generated cone is $\mathbb{R}^2$ with a counter-example. □

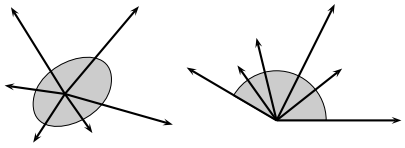

Figure 4.1: The cone generated by the six vectors on the left is $\mathbb{R}^2$, while the cone generated on the right is not.

We will now apply this to find STLC sets. We will first start with the degenerate systems, then proceed to the non-degenerate systems.

4.2 The degenerate cases

First, let us note the following formulas that can be calculated directly from (3.3):

$$tr(A(\vec{w})) = w_{12} + w_{21} + w_{31} + w_{32} + w_{13} + w_{23} \geq 0$$

$$det(A(\vec{w})) = w_{12}w_{13} + w_{21}w_{23} + w_{31}w_{32}$$
$$+ w_{21}w_{13} + w_{31}w_{12} + w_{32}w_{21} + w_{12}w_{23} + w_{13}w_{32} + w_{23}w_{31} \geq 0.$$

Since all w_{ij}'s are non-negative, it follows that the trace and determinant are also non-negative. This means the eigenvalues of $-A(\vec{w})$ must have non-positive real part. This is natural, of course, since otherwise there would be trajectories that go to infinity, escaping T_3^E. Inspecting the determinant formula, one can see there are three cases where the determinant of A_0 fails to be non-zero, ignoring the trivial case where all w_{ij}'s are zero:

· There is only one non-zero w_{ij}.

· There are two non-zero w_{ij}'s, and they share their *second* index (*e.g.* w_{12} and w_{32}).

· There are two non-zero w_{ij}'s whose indices are flipped (*e.g.* w_{12} and w_{21}).

We will examine each of these cases in turn. Without losing generality, we need only consider one sub-case each. For example, in the first case, we only have to consider what happens when w_{12} is non-zero. We can draw conclusions for the other sub-cases by permuting indices. A key property in each case is that while the vector fields vary over T_3^E, they vary only in magnitude and not in direction (although they do reverse direction). This means one can find the STLC by considering where the vector fields change direction.

4.2.1 $w_{12} \neq 0$, but other components of $\vec{w}$ are zero.

In this case, $\vec{b_0} = \begin{pmatrix} \frac{2}{3} \\ 0 \end{pmatrix} w_{12}$ and $A_0 = \begin{pmatrix} 1 & -\frac{1}{\sqrt{3}} \\ 0 & 0 \end{pmatrix} w_{12}$. This vector field is horizontal everywhere, since $\dot{x}_2 = 0$. Furthermore, $\dot{x}_1 = \frac{2}{3} - x_1 + \frac{1}{\sqrt{3}} x_2$, which is zero only along the line passing through the right edge of T_3^E, positive to the left of it, and positive to the right. At $\vec{x} = (0,0)^T$, under the reflections and rotations generated by the symmetric group, the remaining vector fields are equally spaced at angles of $\frac{\pi}{3}$, so the generated cone is clearly $\mathbb{R}^2$. This will remain true until at

least two vector fields reverse direction. However, the images of the right edge of T_3^E under the action of the symmetric group are other edges, so we can conclude that we have STLC everywhere in the interior of T_3^E. The boundary of T_3^E however can never be reached in finite time.

4.2.2 $w_{12} \neq 0$, $w_{32} \neq 0$ but other components of $\vec{w}$ are zero.

In this case, we have

$$\vec{b}_0 = \begin{pmatrix} \frac{2}{3}(w_{12} + \frac{1}{2}w_{32}) \\ -\frac{1}{\sqrt{3}}w_{32} \end{pmatrix}$$

$$A_0 = \begin{pmatrix} w_{12} + \frac{1}{2}w_{32} & -\frac{1}{\sqrt{3}}(w_{12} + \frac{1}{2}w_{32}) \\ -\frac{\sqrt{3}}{2}w_{32} & \frac{1}{2}w_{32} \end{pmatrix}.$$

This can be re-written

$$V_0(\vec{x}) = \begin{pmatrix} \frac{2w_{12}+w_{32}}{3} \\ -\frac{w_{32}}{\sqrt{3}} \end{pmatrix} (1 - \frac{3x_1}{2} + \frac{\sqrt{3}x_2}{2}).$$

Once more the direction does not depend on $\vec{x}$, and the magnitude only becomes zero on the right edge of T_3^E. The only difference here is that the angular separations between the vector fields are not equally spaced, but not that does not affect controllability. As in the previous case, one has STLC in the interior of T_3^E.

4.2.3 $w_{12} \neq 0$, $w_{21} \neq 0$ but other components of $\vec{w}$ are zero.

Assume, without loss of generality, that $w_{12} \geq w_{21}$ (inverting the order is equivalent to reflecting across $x_1 = 0$). In this case,

$$\vec{b}_0 = \begin{pmatrix} \frac{2}{3} \\ 0 \end{pmatrix} (w_{12} - w_{21})$$

$$A_0 = \begin{pmatrix} (w_{12} + w_{21}) & -\frac{1}{\sqrt{3}}(w_{12} - w_{21}) \\ 0 & 0 \end{pmatrix}.$$

Just as in the two previous cases, the direction of the vector field is constant, but this time the magnitude becomes zero *inside* T_3^E, namely at the line $x_2 = -\frac{2}{\sqrt{3}} + \sqrt{3}\left(\frac{w_{12}+w_{21}}{w_{12}-w_{21}}\right)x_1$. This line intersects the bottom vertex of T_3^E but has slope greater than $\sqrt{3}$ (if $w_{12} = w_{21}$, the line is just the x_2 axis). Note also that the vector field is horizontal: this means, as in the first case, that the vector fields have equal angular separation at each point, *i.e.* $\frac{\pi}{3}$ radians.

The line above, and its five cousins under the symmetric group, divide T_3^E into regions, and we can determine STLC in each of them. Figure 4.2 shows an example of how the vector fields reverse direction as we cross these lines. Crossing one line does not destroy STLC, but as soon as we cross another, there is an angular separation of exactly π radians, which forbids STLC. We can conclude that we have STLC in the center region, and the six peripheral regions where only one vector field has reversed direction. Elsewhere, there is no STLC.

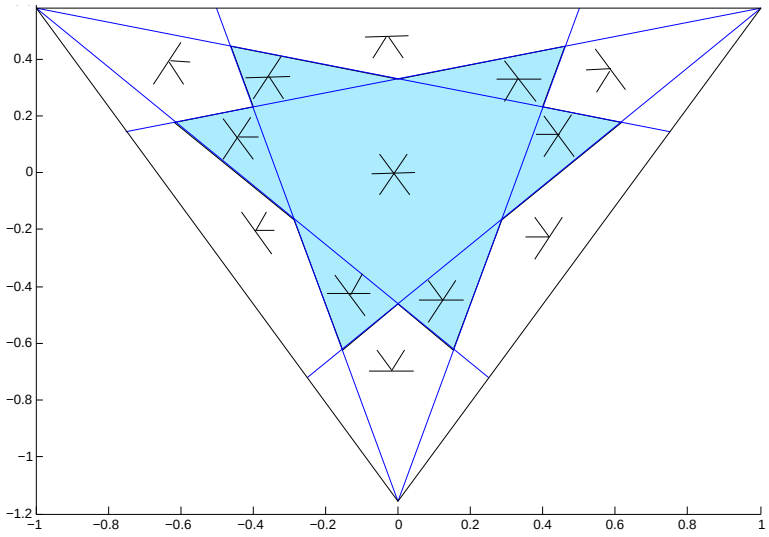

Figure 4.2: The STLC set (light blue) when $w_{12} = 3$, $w_{21} = 1$, $w_{31} = w_{32} = w_{13} = w_{23} = 0$. The blue lines indicate where vector fields reverse direction, and the pictograms show which directions can be generated in each region.

As is turns out, we have global controllability on a larger set (which happens to

be the convex hull of the STLC set). For example, note that in the bottom-most diamond in fig. 4.2, we can still go horizontally in either direction. Therefore we can include all points in between two STLC points that are horizontally separated. This logic extends to the other outer regions in fig. 4.2 that have pictograms: in those regions we can always travels bidirectionally parallel to nearest edge of T_3^E, so we can fill in all points between two STLC points whose separation is parallel to that edge. See figure 4.3 to see the new regions of global controllability. Since all vectors point inward on the boundary of this set, this set is maximally globally controllable (MGC). To be precise, the MGC set is the interior of the set bounded by the lines shown.

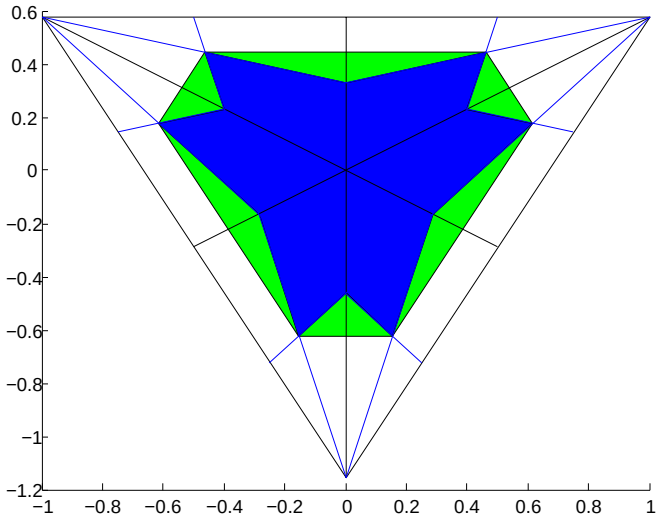

Figure 4.3: The controllable set when $w_{12} = 3$, $w_{21} = 1$, $w_{31} = w_{32} = w_{13} = w_{23} = 0$. The blue region indicates points of STLC. The green region indicates points that are not STLC but within the maximally globally controllable set.

We can specify formulas for the six vertices of the MGC set. The vertex in sextant

I has co-ordinates

$$x_1 = \frac{w_{12}(w_{12} - w_{21})}{w_{12}^2 + w_{12}w_{21} + w_{21}^2}$$
$$x_2 = \frac{x_1}{\sqrt{3}} + \frac{2}{\sqrt{3}} \frac{w_{21}(w_{12} - w_{21})}{w_{12}^2 + w_{12}w_{21} + w_{21}^2}.$$

Note that when $w_{12} = w_{21}$, these formulas give zero. In that case, the STLC and MGC sets vanish.

4.2.4 STLC of non-degenerate systems

It is clear that there is always STLC at the point $\vec{x} = (0, 0)$, since every sextant has a vector field pointing into it (assuming of course that the system isn't unital which would make $V_j(\vec{0}) = \vec{0}$). Furthermore, since the vector fields vary continuously, the boundary of the locally controllable set occurs when two of the six vector fields are anti-parallel, since the largest angular separation must pass from $< \pi$ to $\geq \pi$. The following proposition identifies the set of points where this is true.

Proposition IV.2. *Consider the vector fields $V_j = \vec{b}_j - A_j\vec{x}$ and $V_k = \vec{b}_k - A_k\vec{x}$, $j \neq k$ and $j, k \in \{0, \ldots, 5\}$. These vector fields are collinear, but with non-positive dot product, on the following curve and only on the following curve:*

$$\vec{x}_{jk}(s) = (sA_j + (1-s)A_k)^{-1}(s\vec{b}_j + (1-s)\vec{b}_k) \qquad s \in [0, 1].$$

Proof. Note at the endpoints, this is trivially true since $V_j(\vec{x}_{jk}(1)) = \vec{b}_j - A_j(A_j^{-1}\vec{b}_j) = \vec{0} = V_k(\vec{x}_{jk}(0))$ so the dot product is zero, and any vector is collinear with the zero vector. For $s \in (0, 1)$, $V_j(\vec{x})$ and $V_k(\vec{x})$ are nonzero and collinear with opposite orientation iff there is a linear combination of them, using positive coefficients, that

is zero. Let c_j and c_k be these coefficients. So we have

$$\begin{aligned} c_j V_j(\vec{x}) + c_k V_k(\vec{x}) &= \vec{0} \\ c_j\vec{b}_j + c_k\vec{b}_k &= c_j A_j\vec{x} + c_k A_k\vec{x} \\ c_j\vec{b}_j + c_k\vec{b}_k &= (c_j A_j + c_k A_k)\vec{x} \\ \vec{x} &= (c_j A_j + c_k A_k)^{-1}(c_j\vec{b}_j + c_k\vec{b}_k) \\ &= (\frac{c_j}{c_j+c_k}A_j + \frac{c_j}{c_j+c_k}A_k)^{-1}(\frac{c_j}{c_j+c_k}\vec{b}_j + \frac{c_k}{c_j+c_k}\vec{b}_k). \end{aligned}$$

If we define $s := \frac{c_j}{c_j+c_k}$, we have arrived at the conclusion of the proposition. Note that the positivity of the coefficients requires $s \in (0,1)$. Also note that we've assumed the inverse operation in the fourth step can be done for any c_j, c_k. This is an essential and non-obvious assumption: without it, the curve wouldn't be a continuous bounded arc, a property we will want later. We will prove this fact for a pair separated by a reflection (V_0 and V_1) and a pair separated by a rotation (V_0 and V_4), and from symmetry extend to all other pairs.

First note, for two matrices A and $\bar{A}$ with equal, positive determinant, $\det(sA + (1-s)\bar{A}) = s^2\det(A) + (1-s)^2\det(\bar{A}) + s(1-s)(\det(a_1\bar{a}_2) + \det(\bar{a}_1 a_2))$, where the $\det(a_1\bar{a}_2)$ means the determinant of the matrix formed from the first column of A and the second column of $\bar{A}$. This is a quadratic function in s with critical point $s = \frac{1}{2}$. Since the determinants we are interested in are positive at $s = 0$ and $s = 1$, if we can show they are positive at $s = \frac{1}{2}$, then we can conclude they are positive for all $s \in (0,1)$. In fact, we can show this by brute calculation using Mathematica:

$$\begin{aligned} \det(\frac{1}{2}A_0 + \frac{1}{2}R_1 A_0 R_1^{-1}) &= A_{011}A_{022} \\ \det(\frac{1}{2}A_0 + \frac{1}{2}R_4 A_0 R_4^{-1}) &= \frac{5}{8}\det(A_0) + \frac{3}{16}||A_0||^2. \end{aligned}$$

The first determinant is positive since the diagonal elements of A_0 are positive, and the second is positive since the determinant of A_0 is positive. $\square$

We can use this proposition to construct $\mathcal{A}_3^E$. There are $6 \times 5 = 30$ curves $\vec{x}_{ij}(s) = (sA_j + (1-s)A_k)^{-1}(s\vec{b}_j + (1-s)\vec{b}_k)$ for $i \neq j$, although $\vec{x}_{ji}(s)$ and $\vec{x}_{ij}(s)$ are parametrizations of the same curve, so there are at most 15 unique loci of points. Also, there are six endpoints to these curves: $\vec{x}_{\infty,j} := A_j^{-1}\vec{b}_j$, where the ∞ is used since these points are the asymptotic endstates of each vector field − since the matrix A_j is invertible, all initial states are driven to $\vec{x}_{\infty,j}$ as $t \to \infty$. It is possible for the $\vec{x}_{\infty,j}$'s to coincide, but symmetry dictates they coincide in one of two ways: (1) if the system is unital, they all coincide at $\vec{x} = (0,0)$ or (2) three pairs converge so that each pair lies on one of the three inner legs of T_3^E. We will ignore the first case since it means there is no local or global controllability, and in the second case at least three of the arcs become trivial in that they map to a single point. The following theorem describes how to build $\mathcal{A}_3^E$:

Theorem IV.3. *For a triple of distinct indices (j_1, j_2, j_3), one can form a closed curve with the domain $s \in [0,3]$ (which may not be simple):*

$$\vec{x}_{j_1 j_2 j_3}(s) = \begin{cases} (sA_{j_2} + (1-s)A_{j_1})^{-1}(s\vec{b}_{j_2} + (1-s)\vec{b}_{j_1}) & s \in [0,1] \\ (sA_{j_3} + (1-s)A_{j_2})^{-1}(s\vec{b}_{j_3} + (1-s)\vec{b}_{j_2}) & s \in [1,2] \\ (sA_{j_1} + (1-s)A_{j_3})^{-1}(s\vec{b}_{j_1} + (1-s)\vec{b}_{j_3}) & s \in [2,3]. \end{cases}$$

This closed curve lies entirely within T_3^E, and partitions it into the interior and exterior of the curve (include the curve itself with the exterior). Call the interior region $\mathcal{A}_{(j_1,j_2,j_3)}$. Then $\mathcal{A}_3^E = \left(\bigcup_{j_1 \neq j_2 \neq j_3 \neq j_1} \bar{\mathcal{A}}_{(j_1,j_2,j_3)}\right)^o$, where the bar indicates closure, and the ^{o} indicates interior.

Proof. The system can clearly not be STLC on the boundary of T_3^E, or else we could achieve non-physical states. Similarly, the endpoints $\vec{x}_{\infty,j}$ must lie in T_3^E since we can approach these points asymptotically. It follows that the exterior of $\vec{x}_{j_1 j_2 j_3}(s)$

contains points on the boundary of T_3^E. But since the system can only switch from STLC with controls j_1, j_2 and j_3 to non-STLC after passing through $\vec{x}_{j_1 j_2 j_3}(s)$, it cannot be STLC using those controls anywhere on the exterior.

Furthermore, the system must be STLC on the interior. To see this consider the function $z_{jk}(\vec{x}) = V_j(\vec{x})^T J V_k(\vec{x})$, where $J = \begin{pmatrix} 0 & 1 \\ -1 & 0 \end{pmatrix}$, which gives the cross product of the vector fields at each point. This must be zero where the fields are anti-parallel, but more importantly, $z_{jk}(\vec{x})$ must *change sign* if one gains STLC when crossing curve $\vec{x}_{jk}(s)$. If we were to cross $\vec{x}_{j_1 j_2 j_3}(s)$ from exterior to interior and *not* gain STLC, z_{jk} would have to be zero on the curve, and have the same sign on either side. That is, z would have a one-dimensional locus of local extrema on $\vec{x}_{j_1 j_2 j_3}$. But note that $z_{jk}(\vec{x})$ is a quadric surface, and the only quadric surfaces that have such a feature are degenerate. But since we are assuming A_j and A_k are non-degenerate, $A_j^T J A_k$ is non-degenerate, and therefore z_{jk} is a non-degenerate quadric surface, and can only have isolated local extrema. It follows that it changes sign at almost all points along $\vec{x}_{j_1 j_2 j_3}(s)$. Therefore one has STLC in the interior $\mathcal{A}_{(j_1,j_2,j_3)}$.

Once one has identified the STLC regions for triples of vector fields, we must extend. Clearly, if the system is STLC using just a particular triple of the vector fields, it is STLC using a sextuple. It is technically possible to have STLC with six field without STLC for any triple, and this happens on the arcs $\vec{x}_{j_1 j_2}(s)$ that are on the interior of $\mathcal{A}_3^E$. These line are not part of A_{j_1,j_2,j_3}, which is why the theorem invoked the closure and interior operations. Note that if one starts with a collection of m vectors in $\mathbb{R}^2$ with angular separations $\Delta\theta_j$ so that $\sum \Delta\theta_j = 2\pi$, one can always remove a vector so that the largest angular separation is no more than $\frac{4\pi}{m}$: find the two adjacent angular separations with the smallest sum, which must be less than or

equal to $\frac{4\pi}{m}$, and remove the middle vector. If one does this three successive times starting with six vectors, one can end with a maximum angular separation of $\frac{4\pi}{4} = \pi$ (see the top process in fig. 4.4). Of course, we need it to be strictly less than π, and this is where one can have STLC with six vector fields, without STLC with any triple.

There is only one way for the above procedure to yield a maximum angular separation of π: when the quadruple before the final removal has four angular separations of $\frac{\pi}{4}$ (see the bottom process in fig. 4.4). This only happens however when there are two pairs of vectors that are anti-parallel, *i.e.* we are on the intersection of two of the arcs $\vec{x}_{jk}(s)$. Such points must only occur on the interior of the closure of the union of $\mathcal{A}_{(j_1,j_2,j_3)}$: it is clear that perturbing the quadruple of vectors does not ruin STLC, therefore one has STLC at least in a neighborhood of the intersection point. Therefore, if we close the union, and then take the interior, such points will be included in $\mathcal{A}_3^E$.

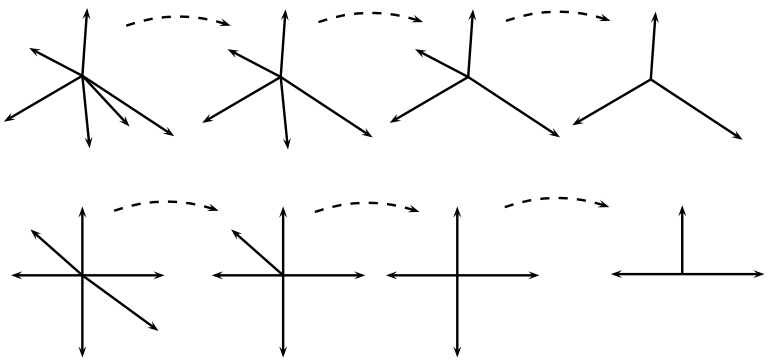

Figure 4.4: Removing vectors from an STLC sextuple to end with an STLC triple. The top row shows the typical case. The bottom row shows the case where the final triple has an angular separation of π.

□

The above theorem pins down the procedure for finding $\mathcal{A}_3^E$. We have written a MATLAB procedure for plotting $\mathcal{A}_3^E$ when the Lindblad operators are of the form

$\sqrt{\gamma}|j\rangle\langle k|$, and Figure 4.5 shows some examples. One can see that we can get qualitatively different regions, and one can ask how this variation depends on the Lindblad operators. We address that question in the next section.

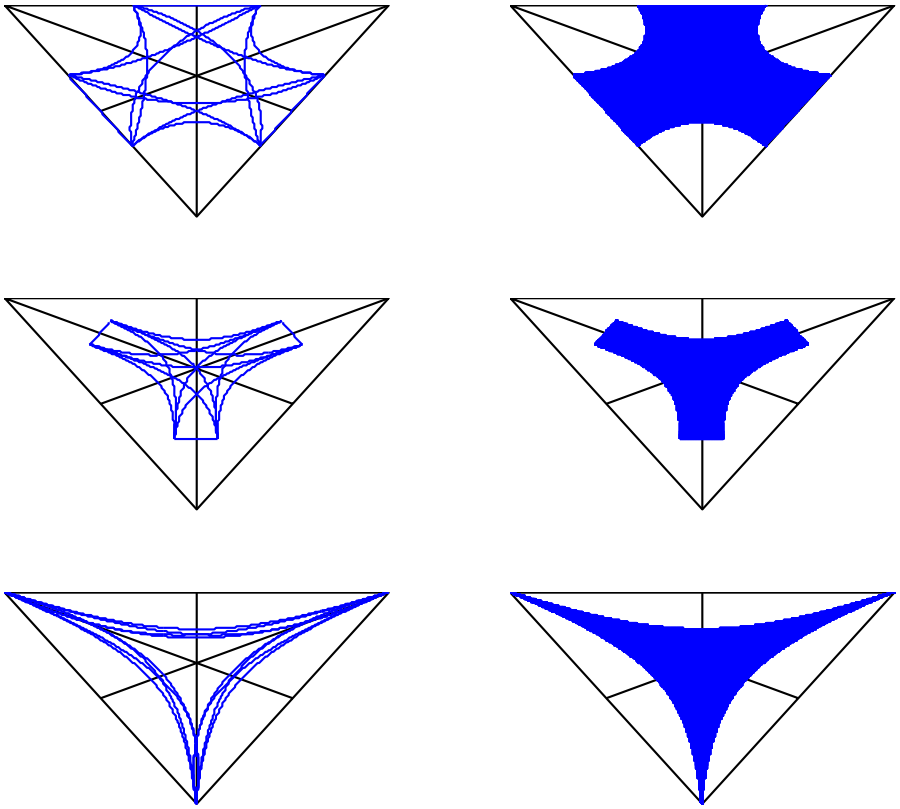

Figure 4.5: $\mathcal{A}_3^E$ for dissipations with the Lindblad operators *(top)*. The figures on the left show the arcs, and the ones the right show $\mathcal{A}_3^E$. The Lindblad operators are: $\sqrt{2}|1\rangle\langle 2|$, $2|2\rangle\langle 1|$, $|3\rangle\langle 1|$ and $\sqrt{5}|3\rangle\langle 2|$ *(middle)*: $|1\rangle\langle 2|$, $\sqrt{2}|2\rangle\langle 1|$, $\sqrt{2}|3\rangle\langle 1|$, $\sqrt{3}|2\rangle\langle 3|$ and $2|3\rangle\langle 2|$ *(bottom)*: $\sqrt{2}|1\rangle\langle 2|$, $\sqrt{5}|1\rangle\langle 3|$, $\sqrt{3}|3\rangle\langle 1|$ and $\sqrt{6}|3\rangle\langle 2|$.

4.3 Characterizing $\mathcal{A}_3^E$

We would like to study the relationship of the shape of $\mathcal{A}_3^E$ with the w_{ij}'s. First, it should be noted that the boundary of $\mathcal{A}_3^E$ is formed from segments of conic sections: the curves $\vec{x}_{jk}(s)$ are parametrizations of the algebraic varieties $z_{jk}(\vec{x}) = 0$, which are quadratic in x_1 and x_2. We claim that there are four parameters that are important to the shape, and one other that may be of interest depending on the system. Since there

are six coefficients in the vector field $V_j(\vec{x}) = \vec{b}_j - A_j\vec{x}$, reducing to six parameters of interest would be natural, but we have yet to identify a sixth. The five parameters are:

- The two co-ordinates that describe the positions of the $\vec{x}_{\infty,j}$'s. While this point is not always the highest-purity point in $\mathcal{A}_3^E$, it gives a good indication of its spatial extent. The co-ordinates that we will use will not be x_1 and x_2, but $z_1 = x_1$ and $z_2 := -\frac{1}{2}x_1 + \frac{\sqrt{3}}{2}x_2 = \lambda_2 - \lambda_3$, for reasons that will make our result simpler. Note that these co-ordinates can be used to define a different measure of purity. Typically, purity-squared is defined to be $tr\rho^2 = \lambda_1^2 + \lambda_2^2 + \lambda_3^2 = \frac{1}{3} + \frac{2}{3}(x_1^2 + x_2^2)$. Instead, we can define purity-squared to be $(\lambda_1 - \lambda_2)^2 + (\lambda_2 - \lambda_3)^2 = z_1^2 + z_2^2$. It is important to note that $\vec{x}_{\infty,j}$ may not fall in the same sextant as $R_j\vec{b}$ does, and in particular, $\vec{x}_{\infty,0} = A_0^{-1}\vec{b}_0$ may not fall in sextant I. However, there is a $\vec{x}_{\infty,j}$ that does − let us call this point $\vec{x}_{\infty,I} = A_I^{-1}\vec{b}_I$, with co-ordinates z_1^I and z_2^I, and let z_j^k refer to the coordinates of its cousin in the kth sextant.

- If one looks at fig. 4.5, one sees that the connecting arcs can "sag" to various degrees. The system at the top has straight arcs when exchanging the leading indices, and significantly curved arcs when exchanging the lagging indices, while it is the reverse for the system in the middle. To measure this, we look at the intercepts of these arcs at the interior axes. While there are fifteen arcs in total, only arcs that are symmetric about a given axis can have a maximal (most positive or negative) intercept. There are three such arcs for any given axis, and because of symmetry, each axis has the same three intercepts. We only need to consider the three intercepts along an axis of our choosing, and we will look at the $x_1 = 0$ axis, where λ_1 and λ_2 cross. As above, we will consider

the intercepts in the z_1, z_2 co-ordinate system, as it conveniently eliminates a multiplicative constant.

$$z_2^{I,II} := (\frac{1}{2}A_I + \frac{1}{2}R_1 A_I R_1)^{-1}(\frac{1}{2}\vec{b}_I + \frac{1}{2}R_1\vec{b}_I)$$
$$z_2^{III,VI} := (\frac{1}{2}R_4 A_I R_5 + \frac{1}{2}R_2 A_I R_2)^{-1}(\frac{1}{2}R_4\vec{b}_I + \frac{1}{2}R_2\vec{b}_I)$$
$$z_2^{IV,V} := (\frac{1}{2}R_3 A_I R_3 + \frac{1}{2}R_5 A_I R_4)^{-1}(\frac{1}{2}R_3\vec{b}_I + \frac{1}{2}R_5\vec{b}_I)$$

The superscripts denote which sextants the arc endpoints lie in. We typically expect only $z_2^{I,II}$ and $z_2^{IV,V}$ to be of interest, since they connect adjacent sextants. However, it is possible for the middle arc to "peek" past one of the others, so that its intercept is either the most negative or positive. Essentially, the spatial extent of $\mathcal{A}_3^E$ along a short leg of a sextant can be quantified by $\sup(z_2^{I,II}, z_2^{III,VI}, z_2^{IV,V})$ and along the long leg by $|\inf(z_2^{I,II}, z_2^{III,VI}, z_2^{IV,V})|$.

Our main result in this section, and in fact the most interesting result in this thesis, connects these parameters to rooted trees. To introduce this connection we recall the expression for the determinant of $A(\vec{w})$ (and its symmetric images):

$$det(A(\vec{w})) = w_{12}w_{13} + w_{21}w_{23} + w_{31}w_{32}$$
$$+ w_{21}w_{13} + w_{31}w_{12} + w_{32}w_{21} + w_{12}w_{23} + w_{13}w_{32} + w_{23}w_{31}.$$

It is the sum of products in the form $w_{ij}w_{kl}$, but not all possibilities are represented. If one excludes w_{ij}'s with repeated indices as well as products with repeated factors, there are fifteen possibilities (six choose two), but only nine appear. One way to describe the ones that do appear are in terms of rooted trees. A tree is a connected graph without closed cycles. A rooted tree is a directed tree where one vertex (the root) has only edges that direct into it, and all other vertices have only one edge that direct away from it. Cayley's formula [13] says that the number of (unrooted) trees

on n vertices is n^{n-2}. Since there are n rooted trees for every tree (one can choose any of the vertices to be the root), there are n^{n-1} of them, and therefore n^{n-2} rooted trees for every choice of root.

For every product $\Pi_{i=1}^{m} w_{j_i k_i}$, associate a directed graph with three vertices and m edges where edge i directs from vertex k_i to vertex j_i. Physically, w_{jk} is the rate at which state $|\psi_k\rangle$ will jump to state $|\psi_j\rangle$. So the product $\Pi_{i=1}^{m} w_{j_i k_i}$ can be thought of as the rate of the mth order process whereby states $|\psi_{k_i}\rangle$ jump to states $|\psi_{j_i}\rangle$. Using Cayley's formula, there are $3^{3-2} = 3$ possible trees on 3 vertices, and $3^{3-1} = 9$ rooted trees. Let Γ^S be the set of all rooted trees with vertices in the set $S \subset \mathbb{N}$, and let Γ_p^S be the set of all such trees with root at vertex $p \in S$. For tree $\bar{t} \in \Gamma^S$, let $E(\bar{t})$ be the $|S|$-tuple of edges (j_i, k_i) corresponding to $\bar{t}$. Then we have the following formula:

$$det(A(\vec{w})) = \sum_{\bar{t} \in \Gamma^{\mathbb{Z}_3}} \prod_{e \in E(\bar{t})} w_e.$$

Note that we don't see a product such as $w_{12}w_{21}$. This product corresponds to a graph with a 2-cycle. Similarly, there are no products such as $w_{13}w_{23}$. If one were to ignore directionality, this product would correspond to a tree. However, it is not a rooted tree since there isn't a unique root. Fig. 4.6 shows some directed graphs that do not correspond to rooted trees.

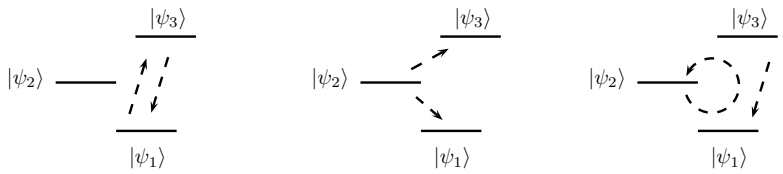

Figure 4.6: Examples of directed graphs that are not rooted trees. On the left, $w_{13}w_{31}$ corresponds to a 2-cycle. In the center, $w_{32}w_{12}$ is a tree but has two roots. On the right, $w_{22}w_{13}$ is both disconnected and has a 1-cycle.

This gives a description of the determinant in terms of trees, but we can extend this to our five shape parameters. If we compute z_1^I and z_2^I, we get the following

formulas:

$$z_1^I = \frac{w_{12}w_{13} + w_{12}w_{23} + w_{13}w_{32} - w_{21}w_{23} - w_{21}w_{13} - w_{23}w_{31}}{det(A_I)}$$
$$z_2^I = \frac{w_{21}w_{23} + w_{21}w_{13} + w_{23}w_{31} - w_{31}w_{32} - w_{31}w_{12} - w_{32}w_{21}}{det(A_I)}.$$

We've already addressed the determinant, but notice the numerators also can be described in terms of trees, although now we need to sort the trees according to their root. Let us define

$$\mathcal{J}_j := \sum_{\bar{t} \in \Gamma_j^{\mathbb{Z}_3}} \prod_{e \in E(\bar{t})} w_e.$$

Essentially, $\mathcal{J}_j$ is the sum of the second order tree processes with root corresponding to $|\psi_j\rangle$. Fig. 4.7 shows the three trees that contribute to $\mathcal{J}_1$.

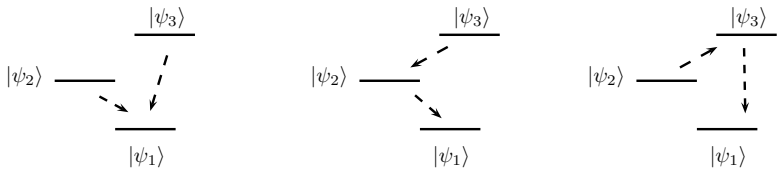

Figure 4.7: The three trees that contribute to $\mathcal{J}_1$.

We can now write down z_1^I and z_2^I:

$$z_1 = \frac{\mathcal{J}_1 - \mathcal{J}_2}{\mathcal{J}_1 + \mathcal{J}_2 + \mathcal{J}_3}$$
$$z_2 = \frac{\mathcal{J}_2 - \mathcal{J}_3}{\mathcal{J}_1 + \mathcal{J}_2 + \mathcal{J}_3}. \tag{4.1}$$

The denominators we have already seen. The numerators show that the relative magnitudes of the second order rates belonging to different vertices affect the position of the $\vec{x}_{\infty,j}$'s.

We can also describe the remaining parameters in terms of trees, but these are two-vertex trees instead of three-vertex trees. Since these trees only have one edge, this description may seem like overkill, but work in higher dimensions suggests this

pattern continues, so we believe it worthwhile. The reason there are only two vertices is because these trees connect equivalence classes induced by the degeneracy $\lambda_1 = \lambda_2$. Instead of vertices $\mathbb{Z}_3 = \{1, 2, 3\}$, we have vertices $\mathbb{Z}_3/\sim := \{[1, 2], [3]\}$. Of course, there is only one such tree and two rooted trees on two vertices. But the trees on two vertices induce graphs on the larger vertex set: an edge directing between equivalence classes of m and n elements induces mn possible directed edges on the elements. In our case, the two rooted trees on $\mathbb{Z}_3/\sim$ induce four directed graphs consisting of one edge: the tree with root $[1, 2]$ induces edges $1 \leftarrow 3$ and $2 \leftarrow 3$, and the tree with root $[3]$ induces edges $3 \leftarrow 1$ and $3 \leftarrow 2$ as seen in fig. 4.8. Note that the induced graphs are not trees because they are disconnected, although the connected components are trees since there are no closed cycles.

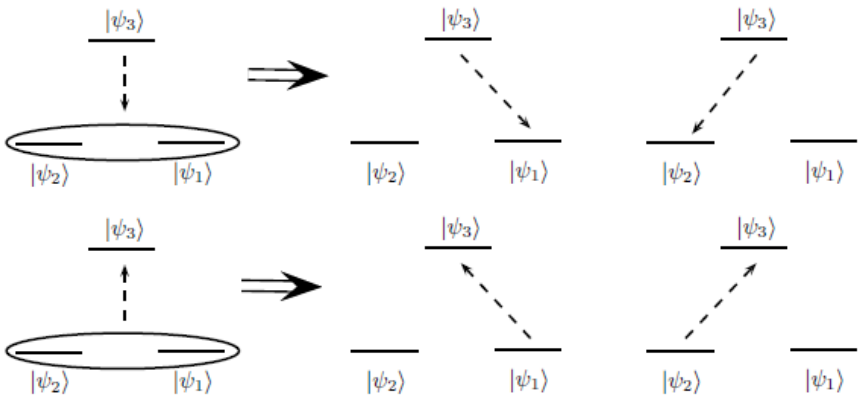

Figure 4.8: The rooted trees on $\mathbb{Z}_3/\sim$ and the directed graphs they induce on $\mathbb{Z}_3$.

The formulas for the parameters are:

$$
\begin{aligned}
z_2^{I,II} &= \frac{w_{13} + w_{23} - w_{31} - w_{32}}{2w_{13} + 2w_{23} + w_{31} + w_{32}} \\
z_2^{III,VI} &= \frac{w_{12} + w_{32} - w_{21} - w_{23}}{2w_{12} + 2w_{32} + w_{21} + w_{23}} \\
z_2^{IV,V} &= \frac{w_{21} + w_{31} - w_{12} - w_{13}}{2w_{21} + 2w_{31} + w_{12} + w_{13}}.
\end{aligned} \tag{4.2}
$$

Each formula contains four first-order rates, corresponding to the four induced directed graphs. The equivalence relation is different in each case: $\sim_{I,II}$ sets $1 \sim_{I,II} 2$, $\sim_{III,VI}$ sets $1 \sim_{III,VI} 3$ and $\sim_{IV,V}$ sets $2 \sim_{IV,V} 3$. This has to do with the fact that the equivalence classes don't refer to the subscripts of degenerate eigenvalues (which are 1 and 2 for all three intercepts), but to the eigenvalues pertaining to the swapped eigenvectors. In each of the three cases, we are swapping $|\psi_1\rangle$ and $|\psi_2\rangle$, but in sextant V for example, these have the eigenvalues of λ_2 and λ_3 respectively (because of the reordering that happens when one crosses an interior leg), and vice versa in sextant IV. So $\sim_{IV,V}$ puts 2 and 3 in the same equivalence class.

Also note the coefficient 2 in the denominator. It turns out that in higher dimensions the terms in the denominator are multiplied by the multiplicity of their root. Since we have a double degeneracy here, trees directing to $[1, 2]$ lead to a coefficient of 2 and those directing to $[3]$ lead to a coefficient of 1.

To rewrite our formulas, let $\bar{\Gamma}^S$ be the set of directed graphs on S with 1 edge, and let the map $Y_{S,\sim} : \bar{\Gamma}^S \to \bar{\Gamma}^{S/\sim}$ map a directed graph on S to its induced graph on $S/\sim$. Similarly, let $y_{S,\sim} : S \to S/\sim$ map $p \in S$ to its equivalence class $[p]_\sim$. Now define

$$
\mathcal{J}^{\sim}_{[j]} := \sum_{\bar{t} \in \Gamma^{\mathbb{Z}_3/\sim}_{[j]}} \sum_{\bar{g} \in Y^{-1}_{\mathbb{Z}_3,\sim}(\bar{t})} \prod_{e \in E(\bar{g})} w_e.
$$

We can now write

$$z_2^{I,II} = \frac{\mathcal{J}_{[1,2]}^{\sim I,II} - \mathcal{J}_{[3]}^{\sim I,II}}{2\mathcal{J}_{[1,2]}^{\sim I,II} + \mathcal{J}_{[3]}^{\sim I,II}}$$
$$z_2^{III,VI} = \frac{\mathcal{J}_{[1,3]}^{\sim III,VI} - \mathcal{J}_{[2]}^{\sim III,VI}}{2\mathcal{J}_{[1,3]}^{\sim III,VI} + \mathcal{J}_{[2]}^{\sim III,VI}}$$
$$z_2^{IV,V} = \frac{\mathcal{J}_{[2,3]}^{\sim IV,V} - \mathcal{J}_{[1]}^{\sim IV,V}}{2\mathcal{J}_{[2,3]}^{\sim IV,V} + \mathcal{J}_{[1]}^{\sim IV,V}}.$$

We will deal with how to generalize these formulas in the following chapter.

We now want to design STLC sets by playing around with our w_{ij}'s. We start with a proposition regarding purifiable STLC sets.

Proposition IV.4. *The boundary of $\mathcal{A}_3^E$ contains the pure orbit $(z_1^I, z_2^I) = (1, 0)$ iff w_{21} and $w_{31} = 0$. Furthermore, $\mathcal{A}_3^E = T_3^{Eo}$ iff w_{21}, w_{31} and either w_{23} or w_{32} is zero. A complementary case where $(z_1^I, z_2^I) = (1, 0)$ but $\sup(z_2^{I,II}, z_2^{III,VI}, z_2^{IV,II}) \ll \frac{1}{2}$ occurs when w_{12}, w_{13} and $|w_{23} - w_{32}|$ are much less than $w_{23} + w_{32}$.*

Proof. $z_1^I = 1$ implies that $-2\mathcal{J}_2 = \mathcal{J}_3$, and $z_2^I = 0$ implies that $\mathcal{J}_2 = \mathcal{J}_3$. Both conditions demand that $\mathcal{J}_2, \mathcal{J}_3 = 0$. For $\mathcal{J}_2 = 0$, one of the following must be true:

1. $w_{21}, w_{31} = 0$ 2. $w_{21}, w_{23} = 0$ 3. $w_{23}, w_{13} = 0$.

In the first case, $\mathcal{J}_3$ will automatically vanish. In the second case, for $\mathcal{J}_3 = 0$, we need one of the following:

A. $w_{31} = 0$ B. $w_{12}, w_{32} = 0$.

In the third case, for $\mathcal{J}_3 = 0$, we need one of the following:

A. $w_{21}, w_{31} = 0$ B. $w_{31}, w_{32} = 0$ C. $w_{12}, w_{32} = 0$.

This gives us six cases, but note that cases 2A and 3A are subsumed by case 1, so only cases 1, 2B, 3B and 3C remain. Since we are assuming that $\mathcal{J}_1 + \mathcal{J}_2 + \mathcal{J}_3 \neq 0$,

however, we need that $\mathcal{J}_1 > 0$. Cases 2B, 3B and 3C violate this condition, so only case 1 remains, which proves the first statement in the proposition.

To prove the second statement, we need $w_{21}, w_{31} = 0$ so that $\mathcal{A}_3^E$ contains the pure orbit. If this is the case, note we have $\vec{x}_{\infty,I} = \vec{x}_{\infty,VI}$, so that the arcs connecting sextants I and II, and sextants III and VI have coincident endpoints. For $\mathcal{A}_3^E = T_3^{Eo}$ we need one of these arcs to coincide with the straight top edge of T_3^E. Since the arcs are quadratic curves, which do not have inflection points, it suffices to show that one of $z_2^{I,II}, z_2^{III,VI} = 1$. Since $w_{21}, w_{31} = 0$, we have

$$z_2^{I,II} = \frac{w_{13} + w_{23} - w_{32}}{2w_{13} + 2w_{23} + w_{32}}$$
$$z_2^{III,VI} = \frac{w_{12} + w_{32} - w_{23}}{2w_{12} + 2w_{32} + w_{23}}.$$

The top expression becomes one if $w_{32} = 0$ and the bottom is one if $w_{23} = 0$.

To prove the third part of the proposition, we need both of these expressions to become arbitrarily small (note that we don't have to worry about the intercept, since $z_2^{IV,V} = -1$ if w_{21} and $w_{31} = 0$). We can't make them both zero, since this requires that w_{12} and w_{13} be zero, which makes the system degenerate. If we set both expressions $\ll \frac{1}{2}$, we can re-arrange to get

$$4w_{13} + 3(w_{23} - w_{32}) \ll 4w_{13} + 3(w_{23} + w_{32})$$
$$4w_{12} + 3(w_{32} - w_{23}) \ll 4w_{12} + 3(w_{32} + w_{23}).$$

Both of these are true if and only if w_{13}, w_{12} and $|w_{23} - w_{32}|$ are $\ll w_{23} + w_{32}$. □

Figure 4.9 shows examples of purifiable systems, contrasting various extents of controllability along the short leg. The example in the center has $\mathcal{A}_3^E = T_3^{Eo}$. The figure on the right shows an example of the third part of the proposition. What is remarkable about these types of systems is that one can achieve the completely mixed

state and the pure states, but one cannot reach states that are completely mixed in only two directions. The next proposition concerns systems where this type of state is the endstate.

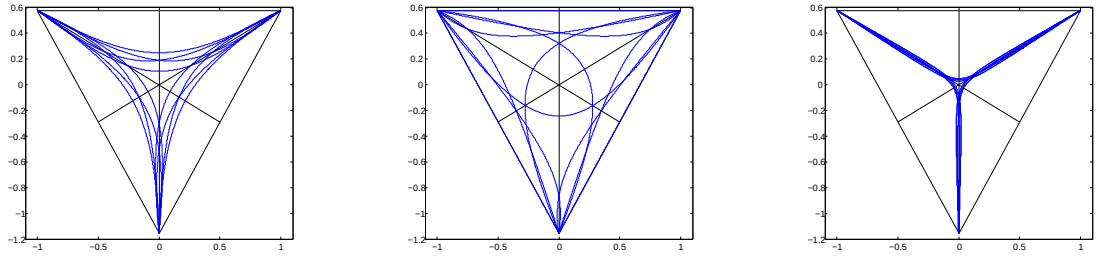

(a) $w_{23} = 9$ and $w_{32} = 7$ (b) $w_{23} = 9$ and $w_{32} = 0$ (c) $w_{23} = 51$ and $w_{32} = 50$

Figure 4.9: Examples of $\mathcal{A}_3^E$ for purifiable systems. $w_{21} = w_{31} = 0$ in all three cases. Additionally, $w_{12} = 5$ and $w_{13} = 6$, chosen arbitrarily.

Proposition IV.5. $(z_1^I, z_2^I) = (0, \frac{1}{2})$ *iff* $w_{31} = w_{32} = 0$ *and* $w_{12} = w_{21}$. *Given this,* $\sup(-z_2^{IV,V}, -z_2^{III,VI}) \to 1$ *if either* $\frac{2w_{12}+w_{21}}{w_{23}} \to 0$ *or* $\frac{2w_{21}+w_{12}}{w_{13}} \to 0$. *Conversely,* $\sup(-z_2^{IV,V}, -z_2^{III,VI}) \to 0$ *if* both *of those fractions go to infinity.*

Proof. $z_1^I = 0$ iff $\mathcal{J}_1 = \mathcal{J}_2$ and $\mathcal{J}_1 > 0$. Given this, $z_2 = \frac{1}{2}$ iff $\mathcal{J}_3 = 0$ and $\mathcal{J}_2 > 0$. Now, $\mathcal{J}_3 = 0$ iff one of the following are true:

1. $w_{31}, w_{32} = 0$ 2. $w_{31}, w_{21} = 0$ 3. $w_{32}, w_{12} = 0$.

However, case 2 implies $\mathcal{J}_2 = 0$, and case 3 implies $\mathcal{J}_1 = 0$. So we are left with only case 1, which implies

$$\mathcal{J}_1 - \mathcal{J}_2 = w_{12}w_{13} + w_{12}w_{23} - w_{21}w_{23} - w_{21}w_{13} = (w_{12} - w_{21})(w_{13} + w_{23}).$$

The second factor cannot be zero, since that would imply $\mathcal{J}_1$, so we require $w_{12} = w_{21}$, which proves the first part of the proposition. The second and third parts of the

proposition follow from the expressions

$$z_2^{I,II} = \frac{w_{13} + w_{23}}{2w_{13} + 2w_{23}} = \frac{1}{2}$$
$$z_2^{III,VI} = \frac{-w_{23}}{2w_{12} + w_{21} + w_{23}}$$
$$z_2^{IV,V} = \frac{-w_{13}}{2w_{21} + w_{12} + w_{13}}.$$

□

Figure 4.10 shows examples, contrasting various extents of controllability along the long leg. The example in the center is notable because $\mathcal{A}_3^E$ occupies most of T_3^E, even though the endstate is completely mixed in two directions. The example on the right complements that in the last set of examples: one can achieve the states that have no population in one component, yet one cannot separate the two leading directions.

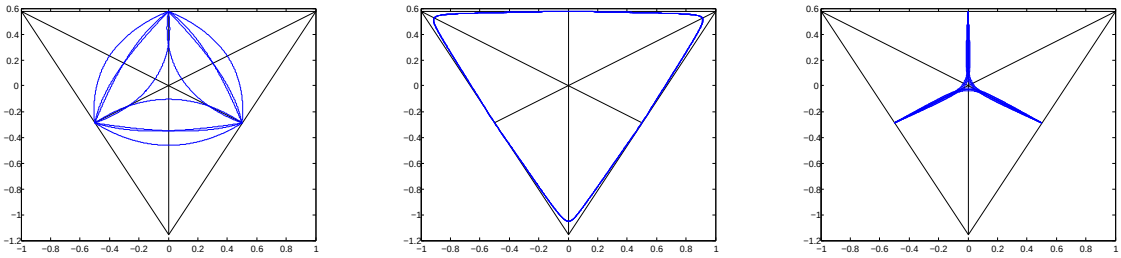

(a) $w_{13} = 0.3$ and $w_{23} = 2$ (b) $w_{13} = 31$ and $w_{23} = 30$ (c) $w_{13} = 0.05$ and $w_{23} = 0.1$

Figure 4.10: Examples of $\mathcal{A}_3^E$ for systems where $(z_1^I, z_2^I) = (0, \frac{1}{2})$. $w_{31} = w_{32} = 0$ and $w_{12} = w_{21} = 1$ in all three cases.

Our final proposition concerns the concavity of the connecting arcs.

Proposition IV.6. *The arc connecting sextants I and II is straight iff* $w_{31} = w_{32}$*, convex if* $w_{31} > w_{32}$ *and concave* $w_{31} < w_{32}$*. The same statements extend to the arc connecting sextants I and VI if* w_{31} *and* w_{32} *are replaced by* w_{13} *and* w_{12} *respectively.*

The intermediate arc connecting sextants III and VI peeks above that between I and II iff $\frac{w_{31}+w_{32}}{w_{13}+w_{23}} > \frac{w_{21}+w_{23}}{w_{12}+w_{32}}$. *It peeks below the arc between IV and V iff* $\frac{w_{31}+w_{32}}{w_{13}+w_{23}} > \frac{w_{21}+w_{23}}{w_{12}+w_{32}}$.

Proof. The arc connecting sextants I and II is straight if the x_2 component of the intercepts equals that of the endstate. That is, $\frac{2}{\sqrt{3}} z_2^{I,II} = \frac{2}{\sqrt{3}} z_2^I + \frac{1}{\sqrt{3}} z_1^I$. Moreover, the arc in question is convex (concave) if the left-hand side is greater (less) than the right. If we insert the relevant formulas, we obtain

$$\frac{(w_{31} - w_{32})(\mathcal{J}_1 - \mathcal{J}_2)}{(2\widetilde{\mathcal{J}_{[1,2]}^{I,II}} + \widetilde{\mathcal{J}_{[3]}^{I,II}})(\mathcal{J}_1 + \mathcal{J}_2 + \mathcal{J}_3)} = 0.$$

Since, the other factors in question must be positive, this is only zero (positive / negative) if w_{31} is equal to (greater than / less than) w_{32}. A similar calculation holds for the second part of the proposition.

To see how the intermediate arc crosses the arc crossing the short leg, we set $z_2^{III,VI} \geq z_2^{IV,V}$, which gives

$$\frac{w_{13} + w_{23} - w_{31} - w_{32}}{2w_{13} + 2w_{23} + w_{31} + w_{32}} \geq \frac{w_{12} + w_{32} - w_{21} - w_{23}}{2w_{12} + 2w_{32} + w_{21} + w_{23}}$$

$$3w_{13}w_{21} + 3w_{13}w_{23} + 3w_{21}w_{23} + 3w_{23}^2 \geq 3w_{12}w_{31} + 3w_{12}w_{32} + 3w_{31}w_{32} + 3w_{32}^2$$

$$(w_{13} + w_{23})(w_{21} + w_{23}) \geq (w_{12} + w_{32})(w_{31} + w_{32})$$

$$\frac{w_{13} + w_{23}}{w_{31} + w_{32}} \geq \frac{w_{12} + w_{32}}{w_{21} + w_{23}}.$$

A similar calculation gives the remaining case. □

Fig. 4.11 shows examples of various concavity. In the leftmost example, $w_{31} = w_{32}, w_{12} = w_{13}$ and $w_{21} = w_{23}$, and one sees that in fact all fifteen arcs are straight. In the other examples, we make the external arcs convex and concave, respectively, by perturbing w_{31}, w_{32}, w_{12} and w_{13}. Fig. 4.12 shows examples of the intermediate arc passing through the other arcs to become part of the boundary.

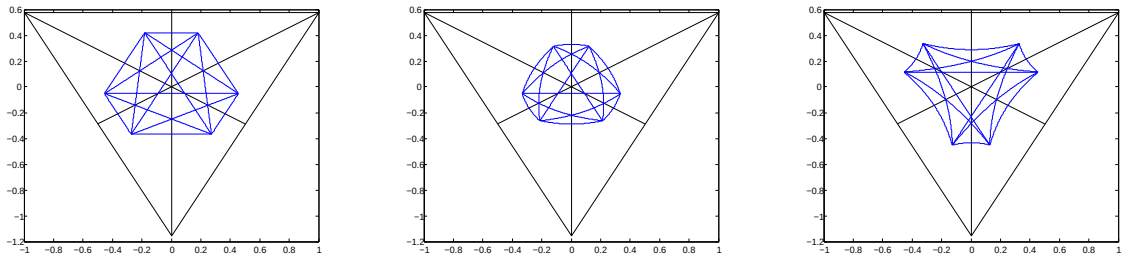

(a) $w_{12}, w_{13} = 6$ and $w_{31}, w_{32} = 1$. (b) $w_{12} = 6, w_{13} = 8$, $w_{31} = 3, w_{32} = 1$. (c) $w_{12} = 8, w_{13} = 6$, $w_{31} = 1, w_{32} = 3$.

Figure 4.11: Examples of different concavity. For all figures, $w_{21} = w_{23} = 4$.

We conclude this section with an example of a feature that escapes our analysis. We have focused on the arcs between sextants separated by a reflection, which accounts for only nine of the fifteen. These arcs necessarily dominate the remaining six at the interior axes, and therefore tend to dominate the shape of $\mathcal{A}_3^E$. However, the arcs connecting rotationally separated arcs may peek past the other nine, and one example where they are particularly prominent is seen in fig. 4.13. Since we are describing systems involving six coefficients using five parameters, it is natural that our analysis would be somehow incomplete. Unfortunately, we have not been able to fit this feature into our description.

4.4 Global controllability of non-degenerate systems

We begin this section by noting that the set of $\vec{x}_{\infty,j}$'s can be connected using trajectories of the vector fields. That is, for any $i \neq j$, there is a solution to $\dot{\vec{x}} = V_j(\vec{x})$ with $\vec{x}_{\infty,i}$ as the initial condition. Call these curves $\vec{x}_{ij}^B(t)$, where $t \in [0, \infty]$, $\vec{x}_{ij}^B(0) = \vec{x}_{\infty,i}$ and $\vec{x}_{ij}^B(\infty) = \vec{x}_{\infty,j}$. There are thirty such curves, although if pairs of $\vec{x}_{\infty,j}$'s coincide, some curves will be trivial. Also, in some cases, the loci of two curves may be the same. In all cases, however, these thirty curves may be concatenated to

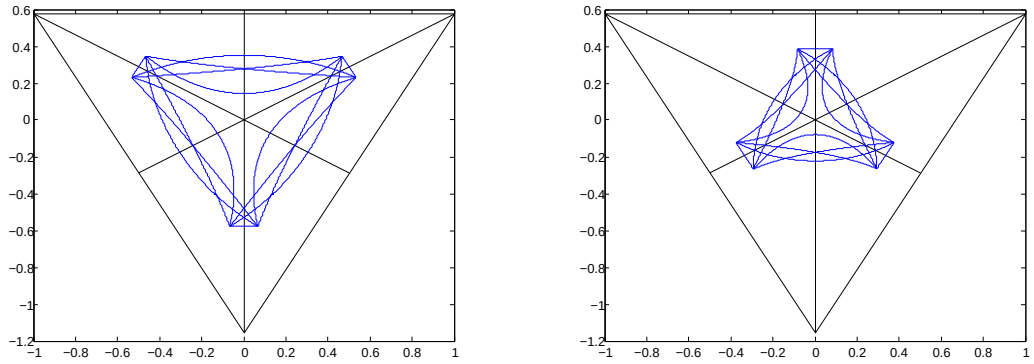

(a) $w_{12} = 6$, $w_{21} = 3$, $w_{13} = 6$, w_{31}, $w_{23} = 0$ and $w_{32} = 4$.(b) $w_{12} = 6$, $w_{21} = 4$, $w_{13} = 0.1$, $w_{31} = 1$, $w_{23} = 8$ and $w_{32} = 1$.

Figure 4.12: Examples of the intermediate arc peeking past the other arcs.

form a closed, non-simple curve that divides T_3^E into two regions, in the same way that $\mathcal{A}_3^E$ is formed. Call the interior region $\mathcal{B}_3^0$.

First, consider the case where $\mathcal{A}_3^E \subseteq \mathcal{B}_3^0$. In this instance, it is often true that $\mathcal{B}_3^0$ and $\mathcal{B}_3^E$ are identical. Define functions on these curves $g_{ij,k}(t) = V_k(\vec{x}_{ij}^B(t))^T J V_j(\vec{x}_{ij}^B(t))$, $k \neq j$, which specify the cross product of the tangent vector fields with remaining vector fields. The following proposition uses these functions to determine when $\mathcal{B}_3^0 = \mathcal{B}_3^E$ are identical.

Proposition IV.7. *For any point on the boundary of $\mathcal{B}_3^0$, belonging to the curve $\vec{x}_{ij}^B(t)$, one can specify the point as clockwise or counter-clockwise, depending on whether $\mathcal{B}_3^0$ lies to the right or left of $\dot{\vec{x}}_{ij}^B(t)$. $\mathcal{B}_3^0 = \mathcal{B}_3^E$ if and only if $g_{ij,k}(t) \leq 0$, $\forall k \neq j$, when $\vec{x}_{ij}^B(t)$ is clockwise, and $g_{ij,k}(t) \geq 0$, $\forall k \neq j$, when $\vec{x}_{ij}^B(t)$ is counter-clockwise.*

Proof. The conditions merely demand that the vector fields that are not tangent point inward. If any vector field were to point outward, one could escape $\mathcal{B}_3^0$, and

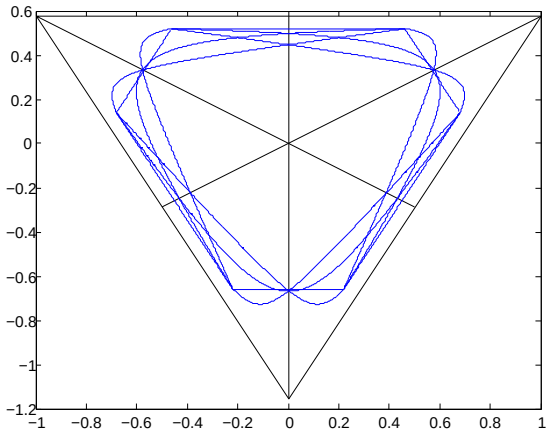

Figure 4.13: An example of the arcs connecting rotationally separated sextants peeking above the reflectionally separated sextants. $w_{12} = 4$, $w_{21} = 0.6$, $w_{13} = 4$, $w_{31} = 1$, $w_{23} = 25$ and $w_{32} = 1$.

therefore one could reach points lying outside from any point within.

It should also be mentioned that if one can reach all points on the boundary, one can reach all points in the interior. Because the vector fields specify non-degenerate affine differential equations, and the relevant eigenvalues have negative real parts, one can evolve any interior point backward in time, with any of the six vector fields, to some point on the boundary. □

Figure 4.14 shows an example of such a system. We see that $\mathcal{A}_3^E$, the blue region, lies within $\mathcal{B}_3^0$, the green region. To show that $\mathcal{B}_3^0 = \mathcal{B}_3^E$, we can look at figures 4.15 and 4.16, which zoom in on the top and bottom of $\mathcal{B}_3^0$ (the remaining parts are covered by symmetry). The top is shown in fig. 4.15, the part between $\vec{x}_{\infty,1}$ and $\vec{x}_{\infty,2}$. There is a counter-clockwise piece and a clockwise piece, as we can see in 4.15a. Figure 4.15b shows the $g_{21,k}(t)$'s, which belong to the counter-clockwise piece, but only the part that is on the boundary. The values are all negative, which means the

vector fields point inward. Figure 4.15c is a magnification of $g_{21,1}(t)$. Similarly, fig. 4.16 shows the bottom part, between $\vec{x}_{\infty,6}$ and $\vec{x}_{\infty,3}$. There are likewise a counter-clockwise and a clockwise piece. We can see from 4.16b, which shows the $g_{63,k}(t)$'s on the boundary portion, that the vector fields point inward.

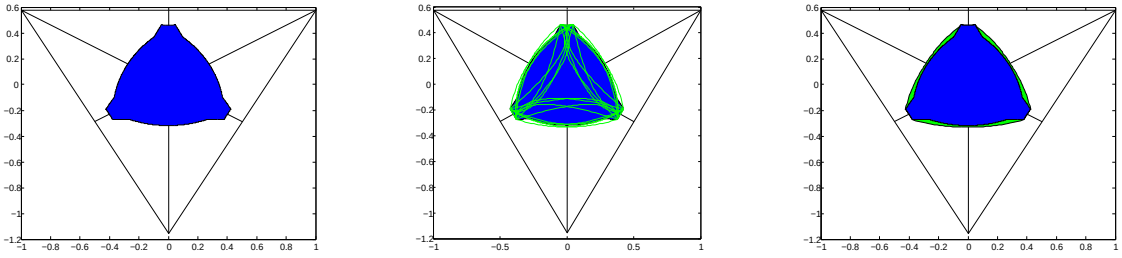

(a) $\mathcal{A}_3^E$ (b) $\mathcal{A}_3^E$ with $\vec{x}_{ij}^B(t)$ in green (c) $\mathcal{A}_3^E$ in blue, $\mathcal{B}_3^0$ in green

Figure 4.14: An example of a system where $\mathcal{B}_3^0 = \mathcal{B}_3^E$. $w_{12} = 1.2$, $w_{21} = 1$, $w_{13} = 0.1$, $w_{31} = 0.1$, $w_{23} = 2$ and $w_{32} = 0.2$.

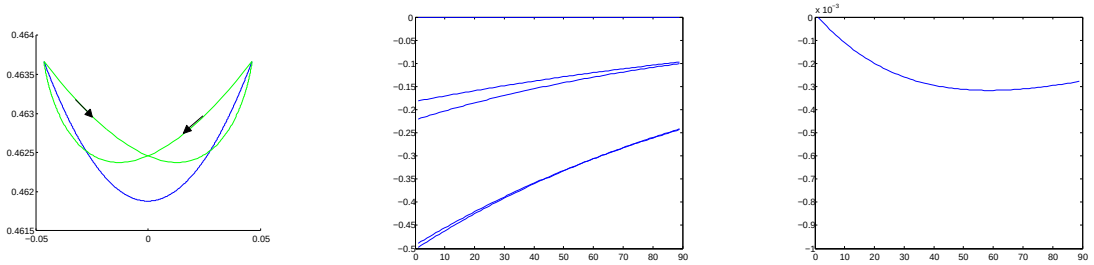

(a) The top edge of $\mathcal{A}_3^E$ with $\vec{x}_{12}^B(t)$ and $\vec{x}_{21}^B(t)$. (b) Values of $g_{21,k}$ (c) Magnification of $g_{21,1}$

Figure 4.15: The top part of $\mathcal{A}_3^E$ and $\mathcal{B}_3^0$ for the system in 4.14, showing that $\mathcal{B}_3^E$ and $\mathcal{B}_3^0$ coincide there.

In some cases, there is no need to distinguish between STLC and global controllability:

Corollary IV.8. *$\mathcal{B}_3^E = \mathcal{A}_3^E$ if and only if V_i and V_j are tangent to $\vec{x}_{ij}(s)$ when $\vec{x}_{ij}(s)$*

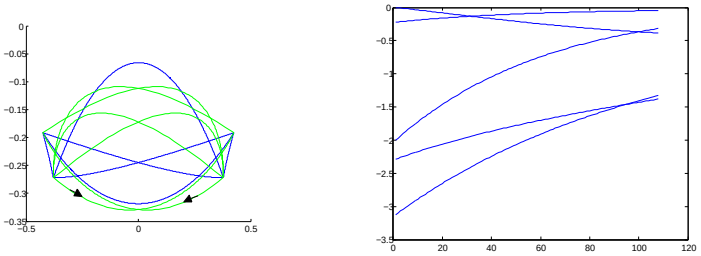

(a) The bottom edge of $\mathcal{A}_3^E$ with nearby $\vec{x}_{ij}^B(t)$'s.

(b) Values of $g_{63,k}$'s.

Figure 4.16: The bottom part of $\mathcal{A}_3^E$ and $\mathcal{B}_3^0$ for the system in 4.14, showing that $\mathcal{B}_3^E$ and $\mathcal{B}_3^0$ coincide there.

is on the boundary of $\mathcal{A}_3^E$.

Proof. If the condition of the corollary is met, $\vec{x}_{ij}^B(t)$, $\vec{x}_{ji}^B(t)$ and $\vec{x}_{ij}(s)$ all have the same loci of points (at least when they form the boundary). Since they form the boundary of $\mathcal{A}_3^E$, the other vector fields must all point inward, and therefore the preceding proposition is satisfied.

Conversely, for $\mathcal{B}_3^E = \mathcal{A}_3^E$, V_i and V_j must be tangent to the boundary of $\mathcal{A}_3^E$, since we know they are anti-parallel, and therefore one will point outward if they are not tangent. □

Figure 4.17 shows a system (the same as 4.11a) to which this corollary applies. The $\vec{x}_{ij}(s)$'s (blue) and $\vec{x}_{ij}^B(t)$'s (green) are both shown, but the former can't be seen as loci of the former are identical to the latter.

The preceding has assumed that $\mathcal{A}_3^E \subseteq \mathcal{B}_3^E$, but this is not always true. In this case, we look for points on the boundary of $\mathcal{A}_3^E$ where the corresponding vector fields are tangent to the boundary. The reason for this is that if the vector fields in question are not tangent, the corresponding trajectories cannot be part of the boundary of $\mathcal{B}_3^E$, since there are trajectories on either side. If the vector fields are

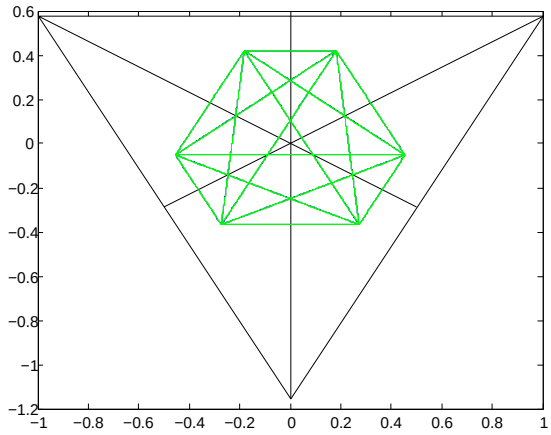

Figure 4.17: An example of when $\mathcal{A}_3^E = \mathcal{B}_3^E$. $\vec{x}_{ij}(s)$ are in blue, but they can't be seen as they coincide with $\vec{x}_{ij}^B(t)$, which are shown in green. $w_{12} = 6$, $w_{21} = 4$, $w_{13} = 6$, $w_{31} = 1$, $w_{23} = 4$ and $w_{32} = 1$.

tangent, however, one of the trajectories may form a part of the boundary, as there are nearby trajectories only on one side. See fig. 4.18 for a depiction.

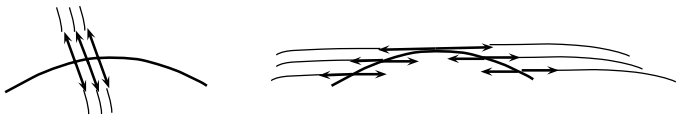

Figure 4.18: Vector fields that are non-tangent (left) and tangent (right) to their corresponding $\vec{x}_{ij}(s)$.

For any arc $\vec{x}_{ij}(s)$, there is a point $\vec{x}_{ij}^M$ (possibly not unique) such that its trajectories (there are two) are maximal, in the sense that any other trajectory starting on the arc is contained within. Let these two trajectories be named $\vec{x}_{ij}^M(t)$ and $\vec{x}_{ji}^M(t)$. If the point $\vec{x}_{ij}^M$ is not unique, we still have only two trajectories, since they must share trajectories. We now have thirty trajectories $\vec{x}_{ij}^M(t)$, which we can concatenate to form a closed curve, whose interior we call $\mathcal{B}_3^1$. If $\mathcal{A}_3^E \subseteq \mathcal{B}_3^0$, then $\mathcal{B}_3^0$ and $\mathcal{B}_3^1$ are identical. But in general, $\mathcal{B}_3^0 \subseteq \mathcal{B}_3^1$.

Proposition IV.9. *Classify points on the boundary of $\mathcal{B}_3^1$ as clockwise or counter-clockwise as before, and let $g_{ij,k}^M$ be defined as $g_{ij,k}(t)$, except using $\vec{x}_{ij}^M(t)$ instead of $\vec{x}_{ij}^B(t)$. The result of the preceding proposition holds for $\mathcal{B}_3^1$.*

Proof. This proposition is true for the same reasons as the preceding proposition. □

It is difficult to find examples of systems where the difference betweem $\mathcal{B}_3^0$ and $\mathcal{B}_3^1$ is visually significant. Figure 4.19 shows an example of a system, where we have shown $\mathcal{B}_3^1$, with $\vec{x}_{ij}(s)$ overlaid in blue. If we zoom in on the top piece, which is shown in 4.20, we can see what is happening. The trajectories that are seeded at $\vec{x}_{\infty,1}$ and $\vec{x}_{\infty,2}$ initially are inside $\mathcal{A}_3^E$, and emerge only on the other side. $\vec{x}_{12}^M$, which lies at the halfway point of $\vec{x}_{12}(s)$, seeds two trajectories that form part of the boundary of $\mathcal{B}_3^1$, as trajectories that are seeded at other points must fall within. We've shown a close-up only of the top piece, as the other pieces are qualitatively the same. Figure 4.20b shows $g_{21,k}^M$ − since they are all negative, the vector fields point inward, and thus $\mathcal{B}_3^1 = \mathcal{B}_3^E$.

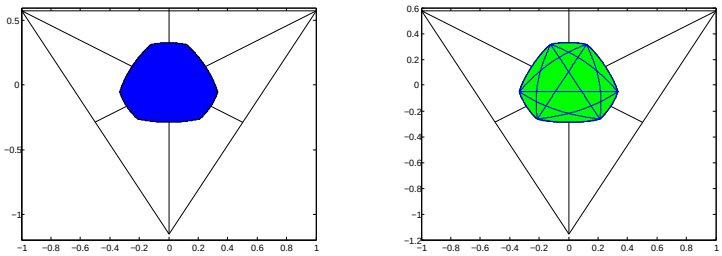

(a) $\mathcal{A}_3^E$ (b) $\mathcal{B}_3^E$ in green with $\vec{x}_{ij}(s)$ in blue

Figure 4.19: An example of a system where $\mathcal{B}_3^1 = \mathcal{B}_3^E$. $w_{12} = 6$, $w_{21} = 4$, $w_{13} = 8$, $w_{31} = 3$, $w_{23} = 4$ and $w_{32} = 1$.

There are systems to which the two preceding propositions do not apply − that is, systems where g_{ij} or g_{ij}^M change sign. In this case, we can use the points where this

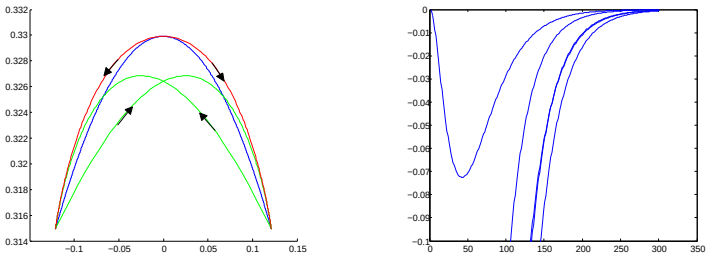

(a) The top edge of $\mathcal{A}_3^E$ (blue) with $\vec{x}_{12}^B(t)$ (green), $\vec{x}_{21}^B(t)$ (green), $\vec{x}_{12}^M(t)$ (red) and $\vec{x}_{21}^M(t)$ (red) .

(b) Values of $g_{21,k}^M$

Figure 4.20: The top part of $\mathcal{A}_3^E$ and $\mathcal{B}_3^0$ for the system in 4.19, showing that $\mathcal{B}_3^E$ and $\mathcal{B}_3^1$ coincide there.

sign change occurs to seed new trajectories. We will not write down a proposition in this case, but instead show an example, shown in figure 4.21. $\mathcal{B}_3^0$ takes up most of $\mathcal{B}_3^E$, but there are pieces, shown in red, of $\mathcal{B}_3^E$ that peek out. As we see in figure 4.22, which show the arcs at the bottom, there are two points at which vector fields V_6 and V_4 take over from V_1 and V_2, respectively. This point can be seen in figure 4.22b − the earliest point at which a $g_{41,k}$ changes sign. In this case, we must take care that there isn't another changeover − the vector fields have been confirmed to point inward on the red trajectories (not shown).

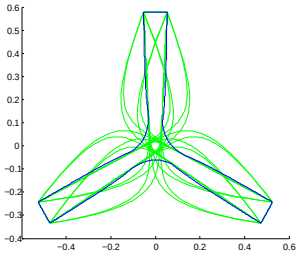

(a) $\vec{x}_{ij}(s)$ and $\vec{x}^B_{ij}(t)$

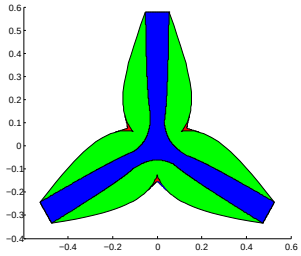

(b) $\mathcal{A}^E_3$ (blue), $\mathcal{B}^0_3$ (green) and$\mathcal{B}^E_3$ (red).

Figure 4.21: An example of a system where $\mathcal{B}^1_3 \neq \mathcal{B}^E_3$. $w_{12} = 100$, $w_{21} = 90$, $w_{13} = 5$, $w_{31} = 0$, $w_{23} = 10$ and $w_{32} = 0$.

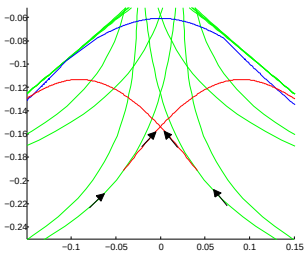

(a) $\vec{x}_{36}(s)$ (blue), selected $\vec{x}^B_{ij}(t)$ (green) and two trajectories that are seeded at points where g_{26} and g_{14} change sign.

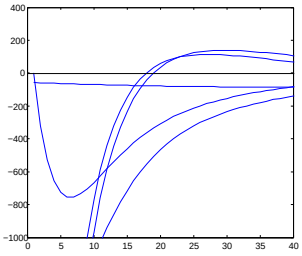

(b) $g_{41,k}(t)$'s.

Figure 4.22: An example of a system where $\mathcal{B}^1_3 \neq \mathcal{B}^E_3$. $w_{12} = 100$, $w_{21} = 90$, $w_{13} = 5$, $w_{31} = 0$, $w_{23} = 10$ and $w_{32} = 0$.

CHAPTER V

n-Dimensional Systems

We would like to know how our results from chapters three and four generalize to higher dimensions. A good portion of them do, and we will present them here. There are three exceptions that have yet to be worked out: results for systems where $A(\vec{w})$ has an eigenvalue with zero real part, a generalization of (4.2), and global controllability results. However, the STLC results for positive stable systems (*i.e.* those having only eigenvalues with positive real part) do carry over.

5.1 Projection of the Lindblad equation

We want to project the Lindblad equation for an n-dimensional Hilbert space onto its space of unitary orbits. The set of orbits is one-to-one with the set of spectra $\{\lambda_1 \geq \lambda_2 \geq \cdots \geq \lambda_n \geq 0\}$. Since $\sum_j \lambda_j = 1$, we want to write them in terms of $(n-1)$ variables. The mapping we've chosen generalizes the mapping in 3 dimensions. $\mathcal{T}_n(\rho) = \vec{x}$ is defined to be

$$x_j = \sqrt{\frac{2}{j(j+1)}} \left(\sum_{i=1}^{j} \lambda_i - j\lambda_{j+1} \right).$$

The pre-image of a particular $\vec{x}$ is the orbit of density matrices with the spectrum given by the recursive equations

$$\lambda_n = \frac{1}{n} - \sqrt{\frac{n-1}{2n}}x_{n-1}$$
$$\lambda_j = \lambda_{j+1} + \sqrt{\frac{j+1}{2j}}x_j - \sqrt{\frac{j-1}{2j}}x_{j-1}$$

which yield

$$\lambda_n = \frac{1}{n} - \sqrt{\frac{n-1}{2n}}x_{n-1}$$
$$\lambda_j = \frac{1}{n} + \sum_{i=j}^{n-1}\sqrt{\frac{1}{2i(i+1)}}x_i - \frac{j-1}{2j}x_{j-1}, \quad j = 2...n-1$$
$$\lambda_1 = \frac{1}{n} + \sum_{i=1}^{n-1}\sqrt{\frac{1}{2i(i+1)}}x_i.$$

Let $T_n \in \mathbb{R}^{n-1}$ be the image of $\mathcal{T}_n$. It is bounded by hyperplanes whose equations can be constructed from the n equations $\lambda_j = \lambda_{j+1}$ (which imposes the ordering of eigenvalues) and $\lambda_n = 0$ (which imposes non-negative eigenvalues). These equations are

$$x_1 = 0$$
$$x_j = \sqrt{\frac{j-1}{j+1}}x_{j-1} \quad j = 2...n-1$$
$$x_n = \sqrt{\frac{2}{n(n-1)}}.$$

Alternatively, we can consider T_n^E, the image of the mapping when we do not impose eigenvalue ordering. In this case, the region is bounded by setting the expressions above for λ_j to zero. Both T_n and T_n^E are regions in $\mathbb{R}^{n-1}$ bounded by n hyperplanes, all mutually oblique. It follows that both regions are n-simplices. Furthermore, T_n^E is highly symmetric, as we shall now prove.

Proposition V.1. *The boundary of T_n^E is a regular polytope. Each pair of its vertices is separated by a distance of 2. There exists a representation of the symmetric group S_n in $\mathbb{R}^n$ that permutes the vertices of the polytope.*

Proof. The vertices are determined by setting a particular $\lambda_k = 1$, and the rest to zero. The coordinates are then $x_j = 0$ for $j < k-1$, $x_{k-1} = -\sqrt{\frac{2(k-1)}{k}}$ (for $k \geq 2$ only) and $x_j = \sqrt{\frac{2}{j(j+1)}}$ for $j > k-1$. If follows that for the k_1th and k_2th vertices, with $k_1 < k_2$, the jth component of the vector between the vertices is 0 for $j < k_1 - 1$ and $j > k_2 - 1$, $\frac{\sqrt{2}(k_1-1)}{\sqrt{k_1(k_1-1)}}$ for $j = k_1 - 1$, $-\sqrt{\frac{2}{j(j-1)}}$ for $k_1 - 1 < j < k_2 - 1$ and $k_2\sqrt{\frac{2}{k_2(k_2-1)}}$ for $j = k_2 - 1$. If we square these and sum, we get

$$\frac{2(k_1-1)}{k_1} + \sum_{k=k_1+1}^{k_2-1} \frac{2}{k(k-1)} + \frac{2k_2}{k_2-1} = \frac{2(k_1-1)}{k_1} + 2\frac{k_2-2}{k_2-1} - 2\frac{k_1-1}{k_1} + \frac{2k_2}{k_2-1} = 4$$

where the sum has been evaluated using the method of telescoping sums. After taking the root, we have a distance of 2.

As for the representation, the symmetric group and its representations can be generated by exchanges of consecutive indices, which here are represented by reflections. For any pair of vertices, there is a $(n-1)$-dimensional hyperplane that passes through the other $(n-2)$ vertices, the origin, and the midpoint of the two vertices. If the pair are vertices 1 and 2, the hyperplane is is just $x_1 = 0$. This hyperplane passes through the origin, as well as vertices 3 through n, as their x_1 coordinate is zero. The x_1 coordinates of vertices 1 and 2 are 1 and -1, and their other coordinates are identical, so their midpoint also lies on the hyperplane $x_1 = 0$.

If the indices are j and $j+1$, the hyperplane is $x_j = \sqrt{\frac{j-2}{j}}x_{j-1}$. This passes through the origin. It passes through vertices $j+1$ through n, as their x_j and x_{j-1} coordinates are zero. It passes through vertices 1 through $j-2$, as their coordinates are $x_j = \frac{1}{\sqrt{2j(j-1)}}$ and $x_{j-1} = \frac{1}{\sqrt{2(j-1)(j-2)}}$. The midpoint of vertices j and $j+1$

has $x_j = \frac{1}{2}\left(\frac{1}{\sqrt{2j(j-1)}} - \frac{j-1}{\sqrt{2j(j-1)}}\right) = \frac{2-j}{2\sqrt{2j(j-1)}}$ and $x_{j-1} = \frac{1}{2}\left(0 - \frac{j-2}{\sqrt{2(j-1)(j-2)}}\right) = \frac{2-j}{2\sqrt{2(j-1)(j-2)}}$, which obeys the equation of the hyperplane.

Since there exists such a hyperplane, there is a reflection matrix that exchanges the pair and fixes the other $n-2$ vertices. Since the symmetric group can be generated by these pairwise exchanges, the rest of the representation can be generated by composition of the reflection matrices. We will denote the elements of the representation as R_σ, where $\sigma \in S_n$. □

Next we want to write down differential equations for the dynamics on T_n and T_n^E. The calculation in (2.12) says that $\dot{\lambda}_j = \langle\psi_j|\mathcal{L}_D(\rho)|\psi_j\rangle$, which means we can write

$$\dot{x}_j = \sqrt{\frac{2}{j(j+1)}}\left(\sum_{k=1}^{j}\langle\psi_k|\mathcal{L}_D(\rho)|\psi_k\rangle - j\langle\psi_{j+1}|\mathcal{L}_D(\rho)|\psi_{j+1}\rangle\right).$$

The density matrix can be written

$$\begin{aligned}\rho &= \sum_{j=1}^{n}\lambda_j|\psi_j\rangle\langle\psi_j| \\ &= \frac{1}{n}I + \sum_{j=1}^{n-1}\frac{x_j}{\sqrt{2j(j+1)}}\left(\sum_{k=1}^{j}|\psi_j\rangle\langle\psi_j| - j|\psi_{j+1}\rangle\langle\psi_{j+1}|\right).\end{aligned}$$

We can substitute that into $\mathcal{L}_D(\rho)$, and write $w_{jk} = |\langle\psi_j|\mathcal{L}_D(\rho)|\psi_k\rangle|^2$ as before. We will omit the details of the calculation, but the result is that, as in three dimensions, we have an affine differential equation $\dot{\vec{x}} = \mathcal{F}(\vec{x},\vec{w}) = \vec{b}(\vec{w}) - A(\vec{w})\vec{x}$, where $\vec{w}$ is the vector of w_{jk}'s with $j \neq k$ (the ones with identical indices do not survive the calculation). The elements of $\vec{b}$ are

$$b_j = \frac{1}{n}\sqrt{\frac{2}{j(j+1)}}\left((j+1)\sum_{k=1}^{j}(w_{k,j+1} - w_{j+1,k}) + j\sum_{k=j+2}^{n}(w_{k,j+1} - w_{j+1,k}) + \sum_{k=1}^{j}\sum_{l=j+2}^{n}(w_{kl} - w_{lk})\right).$$

The diagonal elements of A are

$$A_{jj} = \frac{1}{j(j+1)} \left((j^2+j) \sum_{k=1}^{j} w_{k,j+1} + (j+1) \sum_{k=1}^{j} w_{j+1,k} + j^2 \sum_{k=j+2}^{n} w_{k,j+1} + \sum_{k=j+2}^{n} \sum_{l=1}^{j} w_{kl} \right).$$

The subdiagonal elements of A are

$$A_{jk} = \frac{1}{\sqrt{jk(j+1)(k+1)}} \left((j+1) \sum_{m=1}^{k} w_{j+1,m} + \sum_{l=j+2}^{n} \sum_{m=1}^{k} w_{lm} - (j+1)k w_{j+1,k+1} - k \sum_{l=j+2}^{n} w_{l,k+1} \right).$$

The superdiagonal elements of A are

$$A_{jk} = \frac{1}{\sqrt{jk(j+1)(k+1)}} \left((j+1) \left(\sum_{m=1}^{j} w_{j+1,m} - \sum_{l=1}^{j} w_{l,j+1} \right) + \sum_{l=j+2}^{n} \sum_{m=1}^{j} w_{lm} - \sum_{l=1}^{j} \sum_{m=j+2}^{k} w_{lm} + j \left(\sum_{m=j+2}^{k} w_{j+1,m} - \sum_{l=j+2}^{n} w_{l,j+1} \right) + k \sum_{l=1}^{j} w_{l,k+1} - jk w_{j+1,k+1} \right).$$

Now let us clarify the control aspect. Let $\mathcal{V}_n$ be the set of complete flags on $\mathbb{C}^n$. Any complete flag is specified by a choice of $|\psi_1\rangle$ through $|\psi_n\rangle$. Then we define the map $\mathcal{W}_n$ from $\mathcal{V}_n$ into $\mathbb{R}^{n^2-n}$ given by $w_{jk} = |\langle\psi_j|\mathcal{L}_D(\rho)|\psi_k\rangle|^2$, which means we can view $\dot{\vec{x}} = \vec{b}(\vec{w}) - A(\vec{w})\vec{x}$ as a control equation with $\vec{w}$ as the control, but only if we are free to choose a complete flag. This is only true when the eigenvalues are distinct, but not when there is multiplicity. As we did in three dimensions, we will proceed as in three dimensions: we will look for controllability on sets in T_n^E, with the implicit assumption that we can only infer controllability on the intersection of those sets with T_n^o, the interior of T_n. Theorems III.1 and III.2 have straightforward extensions:

Theorem V.2. *Let $\mathcal{U}$ be a maximally globally controllable open subset of T_n^E, where the control functions are piecewise-differentiable function taking values in $\mathcal{V}_n$. Let $\vec{x}_1$*

and $\vec{x}_2$ be in $\mathcal{U} \cap T_n^o$. The trajectory between them may exit (and re-enter) T_n^o. Then any density matrix $\rho_1 \in \mathcal{T}_n^{-1}(\vec{x}_1)$ may be steered arbitrarily close to $\rho_2 \in \mathcal{T}_n^{-1}(\vec{x}_2)$.

Theorem V.3. *If one has STLC at a point $\vec{x}_0 \in T_n^o$, then one has STLC at any density matrix $\rho_0 \in \mathcal{T}_n^{-1}(\vec{x}_0)$.*

Proof. The proofs proceed just as in the three-dimensional case. □

5.2 Small-time local controllability of the $\mathcal{V}_n^R$ problem

Instead of considering the control problem using $\mathcal{V}_n$ as the control set, we can instead consider the reduced problem using $\mathcal{V}_n^R$, which we will define here. At $\vec{x} = \vec{0}$, the dissipation superoperator reduces to $\mathcal{L}_D(\frac{1}{n}I) = \frac{1}{n}\sum_j [L_j, L_j^\dagger]$.

Proposition V.4. *Let $\{|\Lambda_j\rangle, j = 1...n\}$ be an eigenbasis of the Hermitian operator $\mathcal{L}_D(\frac{1}{n}I)$, with eigenvalues λ_j^{LC}. Then $\mathcal{F}(\vec{0}, W_n)$ is bounded by a polytope with at most $n!$ vertices $\mathcal{F}\left(\vec{0}, \mathcal{W}_n\left(flg(\{|\Lambda_{\sigma(j)}\rangle\})\right)\right)$, where $\sigma(j)$ denotes an element of S_n. The exact number of distinct vertices depends on the quotient of S_n with the equivalence relation induced by the eigenvalue multiplicity.*

Proof. This is essentially the Schur-Horn theorem [46, 21], which says that the set of all Hermitian matrices sharing a common spectrum is the convex hull of a polytope determined by that spectrum. Precisely, if one maps an n by n Hermitian matrix to $\mathbb{R}^n$ by mapping its jth diagonal element to the jth coordinate, then the image is the convex hull of the image of the diagonal matrices in the set (whose coordinates are permutations of the eigenvalues). In our case, the vector in $\mathbb{R}^n$ with elements $\mathcal{L}_D(\frac{1}{n}I)_{jj}$ is inside the convex hull of the $n!$ vectors with elements λ_j^{LC}, in some order. We have to map this into the tangent space of $\vec{x} = \vec{0}$, which is $(n-1)$ dimensional, and we do that in the usual way, by using $\mathcal{T}_n$. Since $\mathcal{T}_n$ is a linear map from $\mathbb{R}^n$ to $\mathbb{R}^{n-1}$, it preserves the convex hull. □

If $\mathcal{L}_D(\frac{1}{n}I)$ has non-distinct eigenvalues, the choice of eigenbasis is not unique. We won't worry about which basis is optimal − henceforth we assume an arbitrary eigenbasis, and define the $\mathcal{V}_n^R$ problem as follows:

Definition V.5. Choose an eigenbasis $\{|\Lambda_j\rangle\}$ of $\mathcal{L}_D(\frac{1}{n}I)$ such that the eigenvalues λ_j^{LC} are in decreasing order. Let $\vec{w}_I = \mathcal{W}_n(flg(\{|\Lambda_j\rangle\}))$, and let $\vec{b}_I = \vec{b}(\vec{w}_I)$, $A_I = A(\vec{w}_I)$ and $V_I(\vec{x}) = \vec{b}_I - A_I\vec{x}$. For any element σ of S_n, let $\vec{b}_\sigma = R_\sigma\vec{b}_I$, $A_\sigma = R_\sigma A_I R_\sigma^{-1}$ and $V_\sigma(\vec{x}) = \vec{b}_\sigma - A_\sigma\vec{x}$. Then the $\mathcal{V}_n^R$ problem is the switching problem where the control is a piecewise constant function $\sigma(t)$ on S_n, and $\dot{\vec{x}} = V_{\sigma(t)}(\vec{x})$.

We now want to determine the regions of STLC for this problem. This has only been worked out for the case when A_I is positive stable. While one can show that A_I must have non-negative real part, there are cases where the real part is zero. Nevertheless, we can state the generalization of theorem IV.3 under this assumption.

Theorem V.6. *Let $\mathcal{A}_n^E$ be the set of all points in T_n^E where one has STLC. For every subset $\bar{S} \subset S_n$ with $(n-1)$ elements, construct the hypersurface $\mathcal{S}_{\bar{S}}$ given by $\vec{x}(s_{\sigma_1}, ..., s_{\sigma_{n-1}}) = (\sum_{\sigma\in\bar{S}} s_\sigma A_\sigma)^{-1}(\sum_{\sigma\in\bar{S}} s_\sigma\vec{b}_\sigma)$, where the parametrization is constrained by $s_\sigma \geq 0$, $\sum_{\sigma\in\bar{S}} s_\sigma = 1$. Let $\mathcal{S}$ be the union of all such hypersurfaces, which is a closed hypersurface. Then $\mathcal{A}_n^E$ is an open set whose closure is equal to the closure of the interior of $\mathcal{S}$.*

Proof. First, we should prove that these surfaces are well-defined, as one must be able to perform the inverse operation. A_I is positive stable, and any of its images under S_n must be positive stable as well (since they are separated by orthogonal transformations, an eigenvector $\vec{v}$ of A_I becomes an eigenvector $R_\sigma\vec{v}$ of A_σ, and they share eigenvalues). Furthermore, $s_\sigma A_\sigma$ is positive stable if $s_\sigma > 0$. Now a sum of two such $s_\sigma A_\sigma$ cannot have a zero eigenvalue: if $(s_{\sigma_1}A_{\sigma_1} + s_{\sigma_2}A_{\sigma_2})\vec{v} = 0$,

then $s_{\sigma_1} A_{\sigma_2}^{-1} A_{\sigma_1} \vec{v} = -s_{\sigma_2} \vec{v}$, but since these are positive stable matrices, this is a contradiction. This extends by induction to the sum of $(n-1)$ such terms, which shows that $\sum_{\sigma \in \bar{S}} s_\sigma A_\sigma$ cannot have a zero eigenvalue and is therefore invertible.

Secondly, we should note that a system is STLC at a point $\vec{x}_0$ if and only if the convex cone generated by the vector fields $\{V_j(\vec{x}_0)\}$ is $\mathbb{R}^{n-1}$. This statement is true for the same reason that proposition IV.1 is true.

Next, we shall prove the following lemma:

Lemma V.7. *$\mathcal{A}_n^E$ consists of points of the form $\vec{x}_0 = (\sum_{\sigma \in S_n} s_\sigma A_\sigma)^{-1} (\sum_{\sigma \in S_n} s_\sigma \vec{b}_\sigma)$ for some choice of $\{s_\sigma > 0 : \sigma \in S_n, \sum_{\sigma \in S_n} s_\sigma = 1\}$.*

Proof. Note that these sums are over all elements of S_n not just subsets of $(n-1)$ elements. Moreover, the inverse operation can be performed for the same reason that the inverse operation in the theorem can be performed.

To prove the lemma, first we show that a set of vectors $\{\vec{v}_j\}$ generates a (closed) convex cone that is identical to its span if and only if there is a linear combination $\sum c_j \vec{v}_j$ of those vectors with $c_j > 0$ that is equal to the zero vector. For the first leg: given any vector in its span $\sum c'_j \vec{v}_j$ with $c'_{min} = \inf\{c'_j\} \leq 0$, one can find a linear combination with positive coefficients by adding $\frac{|c'_{min}|+1}{c_{min}} \sum c_j \vec{v}_j$, where $c_{min} = \inf\{c_j\} > 0$. To prove the second leg, note that to generate the entire span with non-negative coefficients, $-\sum_j \vec{v}_j$ must be generated with some coefficients $\bar{c}_j \geq 0$. Then it follows that $\sum (1 + \bar{c}_j) \vec{v}_j$ is the zero vector, and it has strictly positive coefficients.

For STLC, we need the cone generated by the vector fields to be $\mathbb{R}^{n-1}$, which means there has to be a strictly positive linear combination that is zero:

$$\sum c_\sigma (\vec{b}_\sigma - A_\sigma \vec{x}_0) = 0$$

$$\sum c_\sigma A_\sigma \vec{x}_0 = \sum c_\sigma \vec{b}_\sigma$$

$$\vec{x}_0 = (\sum c_\sigma A_\sigma)^{-1}(\sum c_\sigma \vec{b}_\sigma)$$
$$\vec{x}_0 = (\sum s_\sigma A_\sigma)^{-1}(\sum s_\sigma \vec{b}_\sigma)$$

where $s_\sigma = \frac{c_\sigma}{\sum c_\sigma}$. This proves the lemma. □

Next, we show that $\mathcal{A}_n^E$ must be open. If one has STLC at $\vec{x}_0$, and if one perturbs by $\delta\vec{x}$, then given an arbitrary vector $\vec{v} = \sum c_\sigma(\vec{b}_\sigma - A_\sigma\vec{x}_0)$, $c_\sigma > 0$ [1], we can write it as:

$$\begin{aligned}\vec{v} &= \sum c_\sigma(\vec{b}_\sigma - A_\sigma(\vec{x}_0 + \delta\vec{x})) + \sum c_\sigma A_\sigma \delta\vec{x} \\ &= \sum c_\sigma(\vec{b}_\sigma - A_\sigma(\vec{x}_0 + \delta\vec{x})) + \sum \bar{c}_\sigma(\vec{b}_\sigma - A_\sigma(\vec{x}_0 + \delta\vec{x})) \\ &= \sum (c_\sigma + \bar{c}_\sigma)(\vec{b}_\sigma - A_\sigma(\vec{x}_0 + \delta\vec{x})).\end{aligned}$$

where in the second line, we can assume that we can re-write in terms of the perturbed vector fields because the set of full-rank matrices is open, so a span of vector fields at a point is preserved in a neighborhood of that point. Now the new coefficients can be negative, so $(c_\sigma + \bar{c}_\sigma)$ may be negative. But one can see that the $\bar{c}_\sigma$'s are of order $\delta\vec{x}$, while the c_σ's are fixed and positive, so $\delta\vec{x}$ can be made small enough to ensure $c_\sigma + \bar{c}_\sigma$ is positive for all σ. Since $\vec{v}$ is arbitrary, and $\delta\vec{x}$ has arbitrary direction, we can write all vectors as positive linear combinations in a neighborhood of $\vec{x}_0$. So $\mathcal{A}_n^E$ is open, and furthermore is connected, since continous maps preserve connectedness (but not necessarily simple connectedness).

The only thing left to show is that its boundary is made of points on the hypersurfaces described in the theorem. We will use the closed map lemma [34], which says that any continuous map from a compact space to a Hausdorff space is closed (closed sets map to closed sets) and proper (preimages of compact sets are com-

[1] We can always re-write a non-negative linear combination as a positive combination if the convex cone is the entire vector space, because as noted above, we can write the zero vector as a strictly positive linear combination.

pact). As in the theorem, let $s_\sigma \geq 0$ and $\sum s_\sigma = 1$, although this time let σ range over the entire S_n, not a subset. Note that this is a compact set. Now the map $\{s_\sigma\} \to (\sum s_{\sigma \in S_n} A_\sigma)^{-1}(\sum s_{\sigma \in S_n} \vec{b}_\sigma)$ is continuous on its domain as it is a rational polynomial (the inverse operation can't be perform when all $s_\sigma = 0$, but that is not in the domain). And since it maps into $\mathbb{R}^{n-1}$, which is Hausdorff, the mapping must be closed.

We already know that the image of the open set $\{s_\sigma > 0 : \sigma \in S_n, \sum s_\sigma = 1\}$ is open. It follows that any point on the boundary of $\mathcal{A}_n^E$ must have at least one $s_\sigma = 0$. The hypersurfaces, however, require that at most $(n-1)$ s_σ's be nonzero, and we can use Carathéodory's theorem [12] to show that. Carathéodory's theorem says that any point in the convex hull of a set of a points in $\mathbb{R}^d$ is in the convex hull of a subset of $d+1$ points. Take an arbitrary subset with n elements $S' \subset S_n$. Let $\mathcal{A}_{S'}$ be the set of points $(\sum_{\sigma \in S'} s_\sigma A_\sigma)^{-1}(\sum_{\sigma \in S'} s_\sigma \vec{b}_\sigma)$, where all s_σ represented are strictly positive and sum to one. Carthéodory's theorem implies that $\mathcal{A}_n^E$ is the union of all such sets. Furthermore, the closure of $\mathcal{A}_n^E$ must be the union of the closures of the $\mathcal{A}_{S'}$'s, and therefore its boundary consists of points on the boundaries of the $\mathcal{A}_{S'}$'s. But these boundaries are the hypersurfaces described in the theorem: $\mathcal{A}_{S'}$ is open, so its boundary must consist of points on the boundary of $\{s_\sigma : \sigma \in S_{S'}, s_\sigma > 0, \sum s_\sigma = 1\}$. This boundary consists of one or more s_σ becoming zero, which means we are now on one of the hypersurfaces $\mathcal{S}_{S'}$, and so we are done. □

5.3 Characterizing $\mathcal{A}_n^E$

Now we would like to generalize the combinatorial formulas for points in the closure of $\mathcal{A}_n^E$. Let $\vec{x}_{\infty,\sigma} = A_\sigma^{-1}\vec{b}_\sigma$. As in the three-dimensional case, we will use

different coordinates:

$$z_j = \lambda_j - \lambda_{j+1} = \begin{cases} x_j & j = 1 \\ \sqrt{\frac{j+1}{2j}} x_j - \sqrt{\frac{j-1}{2j}} x_{j-1} & j = 2...n-1. \end{cases}$$

As before, let Γ_j^S be the set of rooted trees on the set S with its root at vertex $j \in S$, and let $E(\bar{t})$ be the set of edges of a rooted tree $\bar{t}$ (an edge being represented by an ordered pair of elements in S). Then define:

$$\mathcal{J}_j := \sum_{\bar{t} \in \Gamma_j^{\mathbb{Z}_n}} \prod_{e \in E(\bar{t})} w_e.$$

We can now state the following theorem:

Theorem V.8. *The coordinates of $A_I^{-1}\vec{b}_I$ in the z-coordinate system are:*

$$z_{\infty,j} = \frac{\mathcal{J}_j - \mathcal{J}_{j+1}}{\det A_I}$$
$$\det A_I = \sum_{k=1}^{n} \mathcal{J}_j.$$

Proof. Because $A_I^{-1}\vec{b}_I$ is unique up to permutations of the vertices, it suffices to show that the density matrix corresponding to $\vec{z}_\infty$ is both an admissible density matrix and stationary under $\mathcal{L}_D(\cdot)$. Of course, the eigenvectors of this density matrix must be $|\Lambda_j\rangle$, and because $z_j = \lambda_j - \lambda_{j+1}$, the formula implies that the eigenvalues of the density matrix are $\frac{\mathcal{J}_j}{\sum_{j=1}^n \mathcal{J}_j}$, and therefore the stationary density matrix we want is $\rho_s = \frac{\mathcal{J}_j}{\sum_{j=1}^n \mathcal{J}_j} |\Lambda_j\rangle\langle\Lambda_j|$. Note that the eigenvalues are non-negative and sum to one, so this density matrix is admissible. To show that this density matrix is stationary, we must show that for some appropriate collection of Lindblad operators, $\mathcal{L}_D(\sum_{j=1}^n \mathcal{J}_j |\Lambda_j\rangle\langle\Lambda_j|) = 0$.

We will use the operators $L_{j_1 j_2} = c_{j_1 j_2} |\Lambda_{j_1}\rangle\langle\Lambda_{j_2}|$, since this satisfies the fact that $|\Lambda_j\rangle$ is an eigenvector of $\sum [L_{j_1 j_2}, L_{j_3 j_4}^\dagger]$. The $c_{j_1 j_2}$'s are real and otherwise arbitrary.

Note that under these Lindblad operators $w_{j_1 j_2} = c^2_{j_1 j_2}$. Also note that

$$L_{j_1 j_2}|\Lambda_{j_3}\rangle\langle\Lambda_{j_3}|L^\dagger_{j_1 j_2} - \frac{1}{2}\{L^\dagger_{j_1 j_2}L_{j_1 j_2}, |\Lambda_{j_3}\rangle\langle\Lambda_{j_3}|\} = c^2_{j_1 j_3}\left(|\Lambda_{j_1}\rangle\langle\Lambda_{j_1}| - |\Lambda_{j_3}\rangle\langle\Lambda_{j_3}|\right).$$

So we have

$$\begin{aligned}
\mathcal{L}_D(\rho_s) &= \mathcal{L}_D\left(\sum_{j=1}^{n} \mathcal{J}_j|\Lambda_j\rangle\langle\Lambda_j|\right) \\
&= \sum_{j=1}^{n} \mathcal{J}_j\mathcal{L}_D\left(|\Lambda_j\rangle\langle\Lambda_j|\right) \\
&= \sum_{j=1}^{n}\sum_{j_1=1}^{n} \mathcal{J}_j w_{j_1 j}\left(|\Lambda_{j_1}\rangle\langle\Lambda_{j_1}| - |\Lambda_j\rangle\langle\Lambda_j|\right) \\
&= \sum_{j=1}^{n}\sum_{j_1=1}^{n}\sum_{\bar{t}\in\Gamma_j^{\mathbb{Z}_n}}\prod_{e\in\bar{t}} w_e w_{j_1 j}\left(|\Lambda_{j_1}\rangle\langle\Lambda_{j_1}| - |\Lambda_j\rangle\langle\Lambda_j|\right).
\end{aligned}$$

Our coefficients are $(\prod_{e\in\bar{t}} w_e)w_{j_1 j}$. They are products corresponding to graphs of n edges on n vertices. These graphs are obtained by taking a rooted tree and adding one edge pointing outward from the root vertex, so that every single vertex has precisely one outgoing edge. The new graphs have precisely one cycle, and those cycles are unidirectional. We can describe such a graph as the union of a unidirectional cycle on a subset $S \subset \mathbb{Z}_3$, with $n' \leq n$ elements, and n' rooted trees, so that each vertex in the cycle is a root, and all vertices in $\mathbb{Z}_n$ lie in one tree. Let $\Gamma_{\bar{c}}^{\mathbb{Z}_n}$ represent all such graphs where the cycle is $\bar{c}$, and let $\bar{C}^{\mathbb{Z}_n}$ represent all unidirectional cycles on subsets of $\mathbb{Z}_n$. Note that if one removes any edge from the cycle, one obtains a rooted tree (if one removes edge jk, then vertex j is now the root vertex). Since we are summing over all rooted trees and all vertices j_1, every one of these graphs is represented in the expression above. So we can re-write:

$$\begin{aligned}
\mathcal{L}_D(\rho_s) &= \sum_{\bar{c}\in\bar{C}^{\mathbb{Z}_n}}\sum_{\bar{g}\in\Gamma_{\bar{c}}^{\mathbb{Z}_n}}\prod_{e\in\bar{g}} w_e\left(\sum_{j_1\in\bar{c}}|\Lambda_{j_1}\rangle\langle\Lambda_{j_1}| - \sum_{j\in\bar{c}}|\Lambda_j\rangle\langle\Lambda_j|\right) \\
&= 0.
\end{aligned}$$

which concludes the proof. □

Work on formulas for the intercepts is ongoing, and as mentioned in the previous chapter, it is believed that there is a generalization in terms of rooted trees inducing graphs with fewer than $(n-1)$ edges. A precise formulation remains elusive, so we will not provide a conjecture.

We will however provide a sufficient condition for a purifiable system assuming A_I is positive stable.

Proposition V.9. *A Lindblad system on a Hilbert space with positive stable A_I is purifiable using $\mathcal{V}_n^R$ if there exists a k such that $w_{jk} = 0$ for all j.*

Proof. Since we have positive stability, we have enough Lindblad operators to generate at least one rooted tree, as $\det A_I$ must be positive. The condition $w_{jk} = 0$ essentially says that there can be no outgoing edges from vertex k, meaning $\mathcal{J}_j = 0$ for all $j \neq k$. In this case, $z_{\infty,k} = 1$, and if $k > 1$, $z_{\infty,k-1} = -1$. This implies that $\lambda_k = 1$, and all other λ_j's are zero. □

We will conclude by showing some examples for $n = 4$. The first two examples are governed by the previous proposition: $w_{j1} = 0$ for all j. The first has all other w_{jk}'s being nonzero, and the shape is such that it hugs the $z_2 = z_3$ axis. Meaning that while the system can be purified, and it can be well-mixed in all four directions, one cannot choose two or three directions to mix. The faces of the tetrahedron correspond to one of the eigenvalues being zero, and $\mathcal{A}_4^E$ only approaches these faces at the pure orbit.

The second example, on the other hand, fills T_n^E. We can purify, but we can also attain all orbits where only one eigenvalue is zero (the faces), or two eigenvalues are zero (the outer edges).

The third example take the second example and impose $w_{21} = 3$. This breaks the condition of the proposition, so we can't purify. Interestingly, there is still a set of orbits where we can eliminate one or two of the eigenvalues: part of the boundary of $\mathcal{A}_4^E$ intersects the faces and the edges. This is where it would be nice to have a well-fleshed out theory for the intercepts, so work in this direction will likely continue.

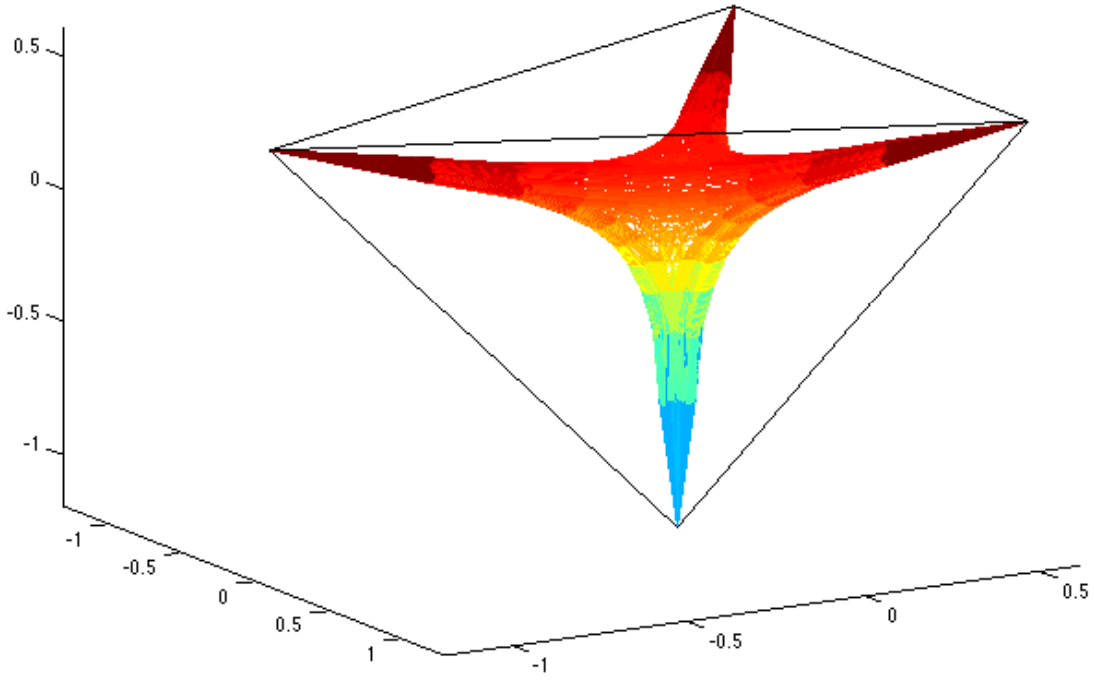

Figure 5.1: $\mathcal{A}_4^E$ for $w_{12} = 5$, $w_{21} = 0$, $w_{13} = 3$, $w_{31} = 0$, $w_{23} = 5$, $w_{32} = 6$, $w_{14} = 1$, $w_{41} = 0$, $w_{24} = 4$, $w_{42} = 5$, $w_{34} = 7$, $w_{43} = 5$

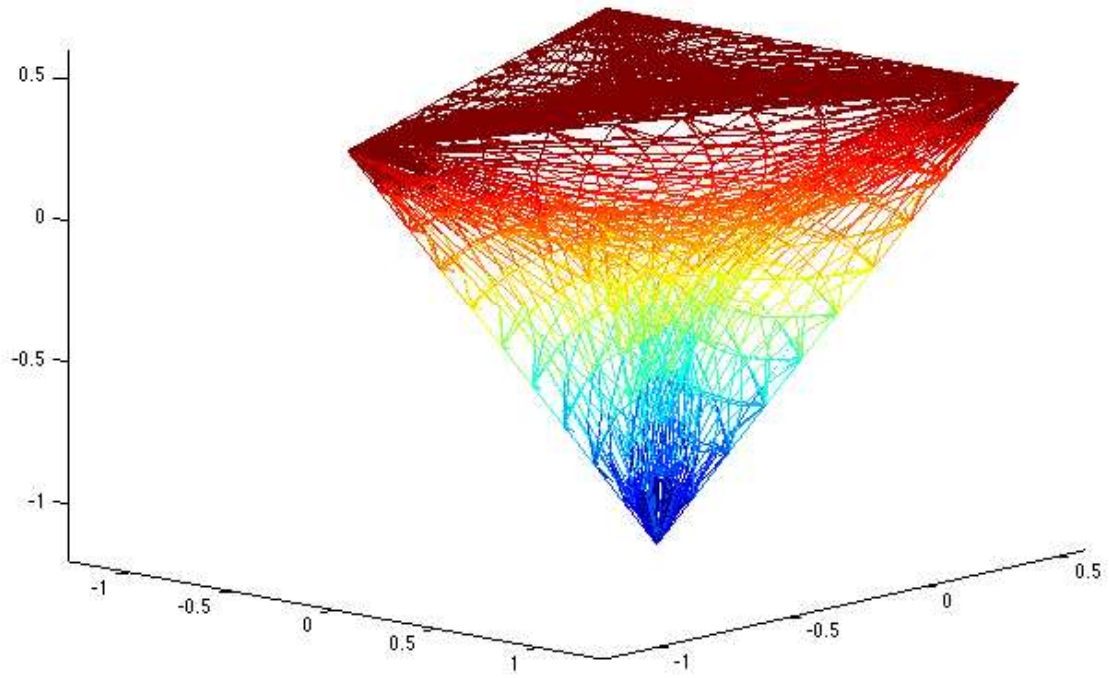

Figure 5.2: $\mathcal{A}_4^E$ for $w_{12} = 5$, $w_{21} = 0$, $w_{13} = 0$, $w_{31} = 0$, $w_{23} = 4$, $w_{32} = 0$, $w_{14} = 0$, $w_{41} = 0$, $w_{24} = 0$, $w_{42} = 0$, $w_{34} = 3$, $w_{43} = 0$

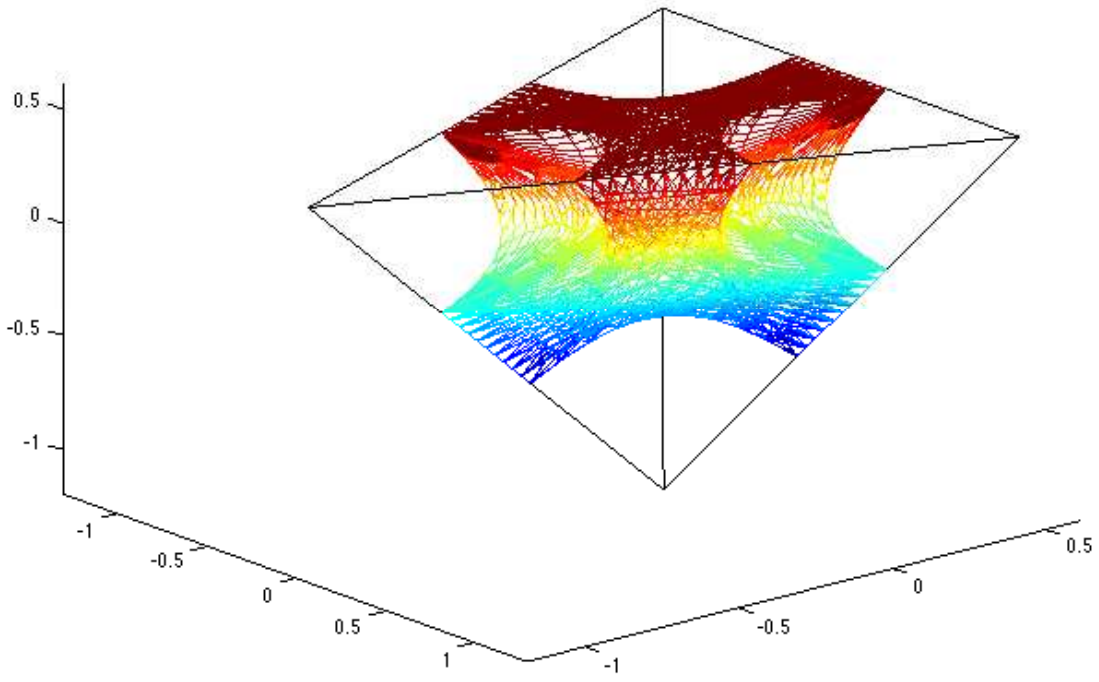

Figure 5.3: $\mathcal{A}_4^E$ for $w_{12} = 5$, $w_{21} = 3$, $w_{13} = 0$, $w_{31} = 0$, $w_{23} = 4$, $w_{32} = 0$, $w_{14} = 0$, $w_{41} = 0$, $w_{24} = 0$, $w_{42} = 0$, $w_{34} = 3$, $w_{43} = 0$

CHAPTER VI

Conclusions

The primary insight of this thesis is the notion that we can project the Lindblad equation onto a dynamical equation over its set of unitary orbits. Under uncontrolled evolution, different initial points on an orbit will evolve differently through the space of orbits. If we have sufficient Hamiltonian control, however, we can consider each orbit as a point in a dynamical space, and watch how orbits evolve depending on where the original system is on the orbit at a given time. This projection is a delicate process, however. The orbits corresponding to density matrices with eigenvalue multiplicity are lower dimensional, which means that our differential equations are not valid there.

We have provided a thorough analysis of what happens for the two-dimensional case. After the projection, our new control variable is a point $\vec{n}$ on the Bloch sphere, and our dynamical variable r takes values in $[0, 1]$. On the subinterval $(0, 1)$, r is governed by the affine differential equation:

$$\frac{dr}{dt} = \sum_{j=1}^{3} b_j n_j - r \sum_{j=1}^{3} a_j (1 - n_j^2) \tag{6.1}$$

where b_j's and a_j's are determined by the dissipation superoperator. At the orbit $r = 0$, the two eigenvalues cross, and so trajectories that pass through this point must be treated with care.

We have performed a controllability analysis on an arbitrary two-dimensional system. Using the method of Lagrange multipliers, we can select controls that maximize and minimize $\dot{r}$ at each r. In general, there is a trap radius r_T inside of which one has small-time local controllability. However, one cannot achieve orbits outside the trap radius when starting inside. We also detailed a theorem classifying purifiable systems, and provided an intuitive physical framework for understanding such systems.

Three-dimensional systems are more challenging. We are able to specifiy the projection procedure and to write down a control system on T_3, the space of orbits. The differential equations however are only valid on the interior, T_3^o. We have given a theorem that says that if we have controllability (global or STLC) on a set in T_3^E, which is the set of ordered eigenvalue triples, then we can infer controllability on the intersection of this set with T_3^o. To analyze controllability, we note that considering all possible controls in the projected problem is not very tractable, so we consider a reduced problem with a discrete control set of six controls $\mathcal{V}_3^R$. At the completely mixed state, these controls correspond to tangent vectors whose convex hull comprises all possible tangent vectors at that state, so we consider this reduced problem to be a good first-order approximation of what can be accomplished.

After making the connection between STLC and convex cones generated by our controls, we describe the controllability sets (global and STLC) for degenerate three-dimensional systems. We then proceed to describe the STLC sets for non-degenerate systems, which are obtained by concatenating fifteen arcs in T_3^E, and taking the interior of the resulting closed curve. These sets can form interesting shapes, so we then attempt to capture these shapes with certain parameters. Two parameters describe the asymptotic states of the $\mathcal{V}_3^R$ controls, and it turns out there is a combinatorial

formula for these pararmeters in terms of rooted trees. There are also three secondary parameters that describe how "fat" or "skinny" the STLC sets are, and we can also describe these parameters in terms of ordered trees (that are of lower order). We conclude our analysis of the $\mathcal{V}_3^R$ problem by analyzing global controllability.

We are able to generalize some of our results to arbitrary dimensions. We are able to describe the set of orbits and write down differential equations. We proved a theorem that assures our controllability results on T_n^E, the set of spectra that does not enforce ordering, can be safely applied to T_n^o, the interior of the set of orbits. We've detailed the reduced problem, using $\mathcal{V}_n^R$ as the control set. We've also provided a construction theorem for $\mathcal{A}_n^E$, the region of STLC, in the case of positive stable systems. This theorem prescribes hypersurfaces that, when concatenated, bound $\mathcal{A}_n^E$. Finally, we have conjectured that our combinatorial formula for the asymptotic states of $\mathcal{V}_n^R$ holds for arbitrary dimension.

BIBLIOGRAPHY

BIBLIOGRAPHY

[1] F. Albertini and D. D'Alessandro. Notions of controllability for bilinear multilevel quantum systems. *IEEE Trans. Automatic Control*, 48(8):1399, 2003.

[2] D. Bacon et al. Universal simulation of Markovian quantum dynamics. *Phys. Rev. A*, 64:062302, 2001.

[3] J.T. Barreiro et al. An open-system quantum simulator with trapped ions. *Nature*, 470:486, 2011.

[4] A. M. Bloch, R. W. Brockett, and C. Rangan. Finite controllability of infinite-dimensional quantum systems. *IEEE Trans. Automatic Control.*, 55(8):1797, 2010.

[5] A. M. Bloch, R. W. Brockett, and T.S. Ratiu. Completely integrable gradient flows. *Comm. Math. Phys.*, 147:57, 1992.

[6] A. M. Bloch, P.S. Krishnaprasad, J.E. Marsden, and T.S. Ratiu. The Euler-Poincaré equations and double bracket dissipation. *Comm. Math. Phys.*, 175:1, 1996.

[7] A. M. Bloch and A. G. Rojo. Control of squeezed states. In *Proceedings of the American Control Conference*, page 3924, 2000.

[8] L. Bouten, R. Van Handel, and M. R. James. An introduction to quantum filtering. 2006. arXiv: quant-ph/0601741v1.

[9] H.-P. Breuer and F. Petruccione. *The Theory of Open Quantum Systems.* Oxford University Press, 2007.

[10] R. W. Brockett. System theory on group manifolds and coset spaces. *SIAM J. Control*, 10(2):265, 1972.

[11] R. W. Brockett. Lie theory and control systems defined on spheres. *SIAM Journal on Applied Mathematics*, 25(2):213, 1973.

[12] C. Carathéodory. Über den Variabilitätsbereich der Fourierschen Konstanten von positiven harmonischen Funktionen. *Rendiconti del Circolo Matematico di Palermo*, 32:193, 1911.

[13] A. Cayley. A theorem on trees. *Quart. J, Math*, 23:376, 1889.

[14] J.I. Cirac and P. Zoller. Quantum computations with cold trapped ions. *Phys. Rev. Lett.*, 74:4091, 1995.

[15] D. D'Alessandro. *Introduction to Quantum Control and Dynamics.* Chapman & Hall/CRC, 2008.

[16] G. Dirr, U. Helmke, I. Kurniawan, and T. Schulte-Herbrüggen. Lie-semigroup structures for reachability and control of open quantum systems: Kossakowski-Lindblad generators form Lie wedge to Markovian channels. *Rep. Math. Phys.*, 64:93, 2009.

[17] D.L. Elliott. *Bilinear Control Systems.* Springer, 2009.

[18] R. P. Feynman. Simulating physics with computers. *Int. J. Theo. Phys.*, 26(6):467, 1982.

[19] V. Gorini and A. Kossakowski. N-level system in contact with a reservoir. *J. Math. Phys.*, 17(7):1305, 1976.

[20] V. Gorini, A. Kossakowski, and E.C.G. Sudarshan. Completely positive dynamical semigroups of N-level systems. *J. Math. Phys.*, 17(5):821, 1976.

[21] A. Horn. Doubly stochastic matrices and the diagonal of a rotation matrix. *Am. J. Math.*, 76:620, 1954.

[22] V. Jurdjevic and H.J. Sussmann. Control systems on Lie groups. *J. Diff. Eq.*, 12:313, 1972.

[23] N. Khaneja, R. Brockett, and S. J. Glaser. Time optimal control in spin systems. *Phys. Rev. A*, 63:032308, 2001.

[24] N. Khaneja, S. J. Glaser, and R. Brockett. Sub-Riemannian geometry and time optimal control of three spin systems: Quantum gates and coherence transfer. *Phys. Rev. A*, 65:032301, 2002.

[25] B. Kneer and C. K. Law. Preparation of arbitrary entangled quantum states of a trapped ion. *Phys. Rev. Lett.*, 57(3):2096, 1998.

[26] C. K. Law and H. Eberly. Arbitrary control of a quantum electromagnetic field. *Phys. Rev. Lett.*, 76(7):1055, 1996.

[27] D. Leibfried et al. Quantum dynamics of single trapped ions. *Rev. Mod. Phys.*, 75:281, 2003.

[28] J.-S. Li and N. Khaneja. Control of inhomogeneous quantum ensembles. *Phys. Rev. A*, 73:030302, 2006.

[29] J.-S. Li and N. Khaneja. Ensemble control of Bloch ensembles. *IEEE Trans. Automatic Control*, 54(3):528, 2009.

[30] G. Lindblad. On the generators of quantum dynamical semigroups. *Comm. Math. Phys.*, 48:119, 1976.

[31] S. Lloyd and L. Viola. Engineering quantum dynamics. *Phys. Rev. A*, 65:010101, 2001.

[32] M. Mirrahimi and R. van Handel. Stabilizing feedback controls for quantum systems. *SIAM J. Control Optim.*, 46(2):445, 2007.

[33] C. Monroe, D. Leibfried, et al. Simplified quantum logic with trapped ions. *Phys. Rev. A*, 55(4):55, 1997.

[34] J.R. Munkres. *Topology, 2nd edition*. Prentice Hall, 2000.

[35] M. A. Nielsen and I. L. Chuang. *Quantum Computation and Quantum Information*. Cambridge University Press, 2000.

[36] J. P. Palao and R. Kosloff. Quantum computing by an optimal control algorithm for unitary transformations. *Phys. Rev. Lett.*, 89(18):188301, 2002.

[37] A. P. Peirce, M. A. Dahleh, and H. Rabitz. Optimal control of quantum-mechanical systems: Existence, numerical approximation, and applications. *Phys. Rev. A*, 37(12):030302, 1988.

[38] J. Preskill. Lecture notes on quantum computation. `http://www.theory.caltech.edu/people/preskill/ph229/notes/chap3.pdf`.

[39] V. Ramakrishna, M. V. Salapaka, M. Dahleh, H. Rabitz, and A. Peirce. Controllability of molecular systems. *Phys. Rev. A*, 51(2):960, 1995.

[40] C. Rangan, A. M. Bloch, C. Monroe, and P. H. Bucksbaum. Control of trapped-ion quantum states with optical pulses. *Phys. Rev. Lett.*, 92(11):113004, 2004.

[41] C. Rangan and P. H. Bucksbaum. Optimally shaped terahertz pulses for phase retrieval in a Rydberg-atom data register. *Phys. Rev. A*, 64:033417, 2001.

[42] S. A. Rice and M. Zhao. *Optical Control of Molecular Dynamics*. Wiley, 2000.

[43] P. Rooney, A.M. Bloch, and C. Rangan. Decoherence control and purification of two-dimensional quantum density matrices under Lindblad dissipation. *submitted to Phys. Rev. A*, 2012. arXiv:1201.0399v1 [quant-ph].

[44] S. G. Schirmer, T. Zhang, and J.V. Leahy. Orbits of quantum states and geometry of Bloch vectors for N-level systems. *J. Phys. A*, 37:1389, 2004.

[45] W. P. Schleich. Engineering decoherence. *Nature*, 403:256, 2000.

[46] I. Schur. Über eine Klasse von Mittelbildungen mit Anwendungen auf die Determinantentheorie. *Sitzungsber. Berl. Math. Ges.*, 22:9, 1923.

[47] M. Shapiro and P. Brumer. Laser control of product quantum state populations in unimolecular reactions. *J. Phys. Chem.*, 84(7):4103, 1986.

[48] M. Shapiro and P. Brumer. *Principles of the Quantum Control of Molecular Processes*. Wiley, 2003.

[49] S. E. Sklarz, D. J. Tannor, and N. Khaneja. Optimal control of quantum dissipative dynamics: Analytic solution for cooling the three-level Λ system. *Phys. Rev. A*, 69:053408, 2004.

[50] A. I. Solomon and S. G. Schirmer. Dissipative 'groups' and the Bloch ball. 2002. arXiv: quant-ph/0211027v1.

[51] A. I. Solomon and S. G. Schirmer. Dissipative effects in multilevel systems. *J. Phys.: Conference Series*, 87:012015, 2007.

[52] D. Sugny et al. Control of mixed-state quantum systems by a train of short pulses. *Phys. Rev. A*, 72:032704, 2005.

[53] D. Sugny et al. Laser control for the optimal evolution of pure quantum states. *Phys. Rev. A*, 71:063402, 2005.

[54] D. Sugny, C. Kontz, and H. R. Jauslin. Time-optimal control of a two-level dissipative quantum system. *Phys. Rev. A*, 76:023419, 2007.

[55] D. J. Tannor and A. Bartana. On the interplay of control fields and spontaneous emission in laser cooling. *J. Phys. Chem. A*, 103:10359, 1999.

[56] D. J. Tannor, V. Kazakov, and V. Orlov. Control of photochemical branching: Novel procedures for finding optimal pulses and global upper bounds. In *Time-dependent Quantum Molecular Dynamics*, page 47, 1992.

[57] D. J. Tannor and S. A. Rice. Control of selectivity of chemical reaction via control of wave packet evolution. *J. Chem. Phys.*, 83(10):5013, 1985.

[58] D. J. Wineland et al. Experimental issues in coherent quantum-state manipulation of trapped atomic ions. *J. Res. Natl. Inst. Stand. Technol.*, 103:259, 1998.

[59] R. Xu, Y. Yan, Y. Ohtsuki, Y. Fujimura, and H. Rabitz. Optimal control of quantum non-Markovian dissipation: Reduced Liouville-space theory. *J. Chem. Phys.*, 120(14):6600, 2004.

[60] H. Yuan and S. Lloyd. Controllability of the coupled spin-$\frac{1}{2}$ harmonic oscillator system. *Phys. Rev. A*, 75:052331, 2007.

[61] W. Zhu and H. Rabitz. A rapid monotonically convergent iteration algorithm for quantum optimal control over the expectation value of a positive definite operator. *J. Chem. Phys.*, 109(2):385, 1998.